NEUTRON DIFFUSION FROM POINT AND PLANE SOURCES

By

LEMUEL CARTER ALLISON

Bachelor of Science

Oklahoma State University of Agriculture and Applied Science

Stillwater, Oklahoma

1960

Submitted to the faculty of the Graduate College
of the Oklahoma State University of
Agriculture and Applied Science
in partial fulfillment of the
requirements for the degree
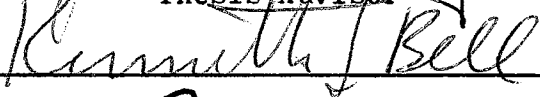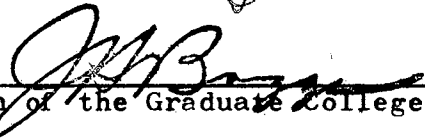of
MASTER OF SCIENCE
May, 1965

DIFFUSION OF NEUTRONS FROM POINT AND PLANE SOURCES

Thesis Approved:

_____
Thesis Advisor

_____

_____
Dean of the Graduate College

587430

ii

PREFACE

The purpose of this study was to determine the relationship
between the neutron flux from a point source and that from a plane
source. In many cases, it may be desirable to determine the
neutron flux within a thermal column of a reactor or in a sub-
critical assembly using a reactor as a source of neutrons prior
to actually using the reactor.

If the flux can be determined without actually using the
reactor, considerable savings may be made if design changes are
required. Thus if a Pu-Be neutron source can be used and the data
extrapolated to a plane source of neutrons, the reactor need not
be used.

In the research carried out in this study, a relationship
between a point and plane source of neutrons was determined.

I thank Dr. John B. West for his assistance in carrying out
the research and the presentation of the results in this thesis.
I thank the Computing Center for use of the IBM 650 digital com-
puter for use during the research.

To my wife, Barbara Ann, who has given encouragement and
understanding throughout this work, I dedicate this thesis.

TABLE OF CONTENTS

LIST OF TABLES

LIST OF TABLES

LIST OF ILLUSTRATIONS

NOMENCLATURE

A - Area, $cm.^2$

A_n - Fourier Constant

B_r - Constant

C - Constant

CR - Cadmium Ratio

D - Diffusion Coefficient

D' - Constant

D'_i - Constant

E - Energy

E_i - Exponential Integral

F - Intercalibration Factor of the Foils

J - Neutron Current, $neutrons/cm.^2 sec.$

J_o - Bessel Function

J_1 - Bessel Function

K - Constant

K_i - Fourier Constant

L - Diffusion Length, cm.

N - Density, nuclei/cc

R - Extrapolated Radius of Cylinder, cm.

S - Source Strength, neutrons

V - Dummy Function

X - Function of x alone

Z - Function of z alone

c - Extrapolated Height of Cylinder, cm.

f_i - Fraction of Neutrons in the i'th Range

g - Gaussian Range, cm.^{2}

j_n - Zero of Bessel Function, J_o

n - Neutron Density, neutrons/cc

q - Slowing-Down Density

r - Radius, cm.

$\bar{r}$ - Vector Locating a Point in Space

t - Time, sec.

u - Lethargy

v - Velocity, cm./sec.

x - Distance in x Direction, cm.

y - Distance in y Direction, cm.

z - Distance in z Direction, cm.

ϕ - Flux, neutrons/cm.^{2} sec

Σ_a - Macroscopic Absorption Cross Section, cm.$^{-1}$

τ - Fermi Age, cm.^{2}

γ - Constant

σ_a - Microscopic Absorption Cross Section, cm.^{2}

β^- - Beta Decay

α - Absorption Coefficient

λ_{tr} - Transport Mean-Free Path, cm.

ρ - Direct Distance from a Point, cm.

δ - Dirac Delta Function

Θ - Function of τ Alone

INTRODUCTION

In addition to the process of production of neutrons, the processes of slowing-down, transport and absorption of the neutrons completely describe the neutron cycle in a nuclear reactor. A mathematical model which describes this cycle would be very useful in designing nuclear reactors. Diffusion theory is such a model which lends itself easily to preliminary design application.

Certain limitations are inherent in neutron diffusion theory due to an assumed model which does not completely describe the neutron cycle in a reactor. Diffusion theory can be used only for mono-energetic neutrons and then only at two or three mean-free paths from strong sources. In addition to several other limitations, it also is not applicable near strong absorbers nor near boundaries between dissimilar materials.

In most diffusion experiments where diffusional properties of a moderator are measured, external sources of neutrons are used. Usually, in applying the diffusion equation, the sources are assumed to emit only thermal neutrons. In most cases, however, the external sources emit fast neutrons. Therefore, near the source the assumption of thermal sources inadequately describes the actual case.

If the neutron sources are treated as emitting neutrons of energies above thermal, a more exact expression for the source term

of the diffusion equation can be calculated. In such a case, the source term may be determined for space and energy by the Fermi age equation for neutron slowing-down.

Anselone (2) and Glasstone, et al., (10) describe the mathematical coupling of the Fermi age equation and the thermal diffusion equation. Glasstone, et al., use the "kernel method" in developing the mathematics; whereas, Anselone uses the diffusion equation directly. Anselone's method appears to be more easily handled due to the fact that the type of source does not appreciably change the derivation, whereas Glasstone, et al., use a different "kernel" for each type of source.

Previous work indicates that the coupled equation is preferable to the thermal diffusion equation alone. Davenport, et al., (7) found that only with a single fast source assumption did the solution differ significantly from that determined from the thermal source assumption. L. R. Foulke (9) indicated that the flux distribution from a Pu-Be neutron source is not adequately described by a thermal source assumption.

Scope and Specific Objectives of the Thesis

The thesis project was divided into two main considerations. These were the following:

1. Theoretical consideration of diffusion of neutrons for three neutron source conditions, i.e., a thermal source case, a mono-energetic fast source case and a multi-energetic fast source case.

2. Experimental analysis of neutron diffusion by measurement of the thermal neutron flux distribution in graphite.

In the theoretical considerations, the relationship between the flux distribution from a point and plane source of neutrons was predicted for each of the source cases.

The experimental analysis consisted of experimentally verifying the theoretically predicted relationship between a point and plane source of neutrons. The Pu-Be neutron source was used to approximate the point source of neutrons. Data recorded in the literature were used in the plane source case.

CHAPTER I

REVIEW OF DIFFUSION THEORY

One-Group Diffusion Model

In a nuclear reactor, neutrons are continually being produced and lost. The general diffusion equation is used to describe this process of production and loss of neutrons throughout the reactor. The diffusion equation is also applicable, within the limitations of diffusion theory, in a reflector or in a pure moderator as well as in the core of a reactor. In a reflector or moderator, the production rate of neutrons is zero.

In a volume element of the reactor, the change in neutron density is due to the following processes:

1. The diffusion of neutrons across the boundaries of the volume element.

2. The absorption of neutrons by the nuclei within the element.

3. The production of neutrons by fission or by external sources within the volume element.

If n is the number of neutrons of velocity, v, (which is assumed to be constant) present in the unit element at any time, t, the rate of change of neutron density is given by the equation of continuity, i.e.,

$$\frac{\partial n}{\partial t} = \text{Production} - \text{Leakage} - \text{Absorption} \qquad (1)$$

If Fick's first law is assumed to be valid for the neutron diffusion, the neutron current can be expressed by the following equation:

$$J = -D\nabla\phi \qquad (2)$$

where the neutron current, J, is defined as the number of neutrons passing through a unit area normal to the direction of flow per second. Then, the net number of neutrons diffusing into the volume element is given by the divergence of the neutron current or:

$$-\text{div}(J) = \nabla\cdot(D\nabla\phi) \qquad (3)$$

where D is the diffusion coefficient.

If D is independent of position, the divergence of the neutron current is given as:

$$-\text{div}(J) = D\nabla^2\phi \qquad (4)$$

For a reactor with a macroscopic absorption cross section, Σ_a (the total target area per cc), the rate of absorption of neutrons per unit volume will be:

$$\phi\Sigma_a = \text{Rate of Absorption} \qquad (5)$$

where $\phi = nv$.

If S is the rate of production of neutrons within the unit volume element, the equation of continuity becomes:

$$D\nabla^2\phi - \Sigma_a\phi + S = \frac{\partial n}{\partial t} \qquad (6)$$

For steady state, the change in neutron density with time is zero. Thus, the one-velocity general diffusion equation becomes:

$$D\nabla^2\phi - \Sigma_a\phi + S = 0 \tag{7}$$

The application of this equation is dependent upon the particular source condition. For the one-group diffusion equation only neutrons of thermal energies are considered. It also is assumed that the neutrons from the source are born at thermal energies. This is perhaps the most widely used model in diffusion experiments.

With the assumption of a one-group model, the source term in a pure moderator is seen to be zero. Then the diffusion equation becomes:

$$D\nabla^2\phi - \Sigma_a\phi = 0 \tag{8}$$

Defining K^2 as Σ_a/D, the diffusion equation becomes:

$$\nabla^2\phi - K^2\phi = 0 \tag{9}$$

This is the equation for the thermal diffusion model.

Age-Diffusion Model

In the one-group thermal diffusion model, the assumption was made, although incorrect, that the source neutrons were of thermal energies. However, in the actual case, the sources emit neutrons of energies considerably above thermal energies. The neutrons diffuse from the source and lose energy by colliding with the nuclei of the moderator. The source term in the equation of continuity

for thermal neutrons then is not zero but is a function of position and energy. The source term is due to the neutrons that slow sown from energies above thermal to thermal energies.

To develop a spatial expression for the source term due to slowing-down, it was assumed that the flux is a function of two variables, lethargy and a spatial position, $\bar{r}$, where $\bar{r}$ represents a vector coordinate locating a point in space. Lethargy is a function of energy defined by Murray (15) and Glasstone, et al., (10) by the differential equation:

$$-du = \frac{dE}{E} \tag{10}$$

Thus, as the neutrons slow down, their lethargy increases.

A unit element is now chosen in the position of $\bar{r}$. In addition, the neutrons between lethargy u and u + du are chosen. The number of neutrons in this range and position is denoted by $n(u,\bar{r})du$ and the neutron flux due to these neutrons by $\phi(u,\bar{r})du$. Applying the diffusion equation for non-multiplying media, the flux is given by:

$$-D(u,\bar{r})\nabla^2\phi(u,\bar{r})du + \phi(u,\bar{r})\Sigma_a(u,\bar{r})du = S(u,\bar{r})du \tag{11}$$

where all the diffusion properties are for neutrons at a lethargy, u. For slowing-down in a non-hydrogeneous moderator, the continuous slowing-down model of Fermi age furnishes a means for calculating the diffusion of fast neutrons.

A plot of lethargy as a function of time for a neutron will consist of a series of vertical steps. The vertical lines represent

the change in lethargy of a collision and the horizontal lines rep-
resent the time interval between collisions. As the lethargy in-
creases, the velocity decreases and hence the time between collisions
increases. The following is a schematic plot of the above processes
in slowing-down:
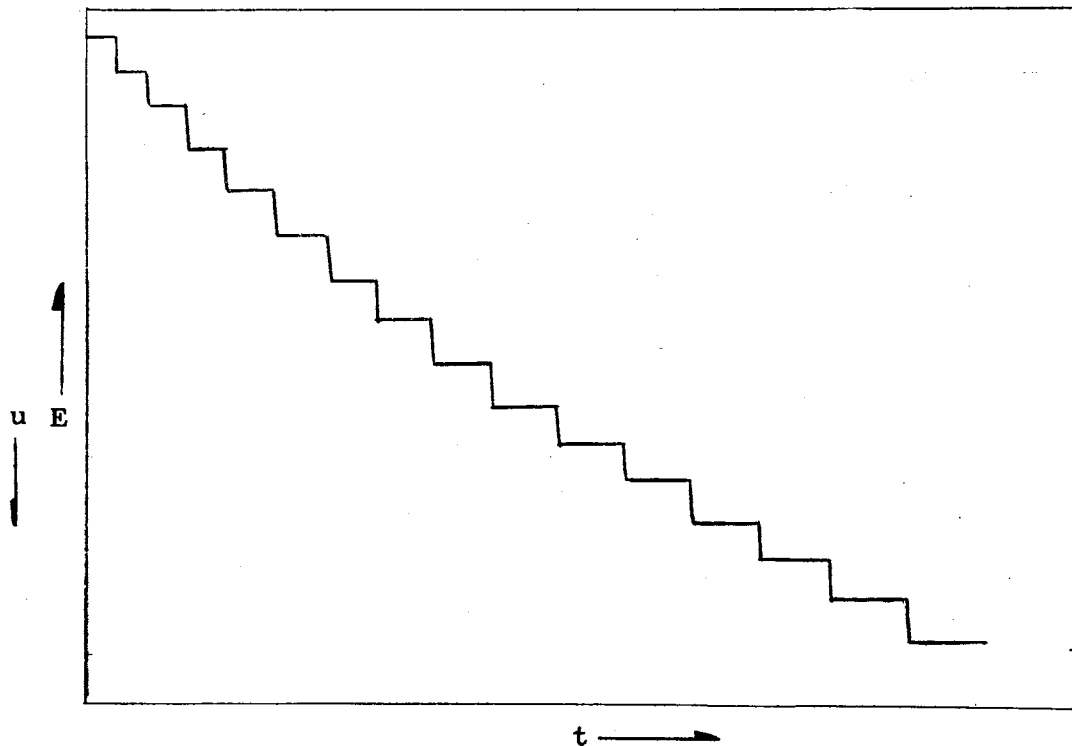
This plot is for a single neutron and there will be some
deviation for other neutrons. But for a moderator such as graph-
ite, the change in lethargy per collision is small. In this case
the individual neutrons will not deviate greatly from the average
behavior. Since the lethargy change per collision is small, the
series of steps can be approximated by a continuous slowing-down
model where it is assumed that the neutrons lose energy continuously

rather than by discrete energy changes.

With the assumption of a continuous slowing-down model, the source term, S(u), in Equation 11 for a non-multiplying medium is the net flux of neutrons slowing-down from a lower lethargy to a higher lethargy over the differential lethargy, du.

The net flux of neutrons is then defined in terms of a slowing-down density, $q(u,\bar{r})$, where $q(u,\bar{r})$ is defined as the number of neutrons crossing a lethargy, u, per cc. per second. Thus, combining these definitions with the diffusion equation and using Fermi-age theory, the following equation can be derived:

$$\nabla^2 q = \frac{\partial q}{\partial \tau} \tag{12}$$

For a complete derivation see Murray (15) or Glasstone, et al., (10).

Where u is the lethargy of thermal neutrons, the slowing-down density becomes the source term for thermal neutrons in the General Diffusion Equation.

The General Diffusion Equation incorporating slowing-down and diffusion becomes:

$$D\nabla^2 - \Sigma_a \phi + q = 0 \tag{13}$$

Criteria for Justification of Diffusion Theory

Foulke (9) gives a very complete list of the criteria for justification of the diffusion equation. These criteria which arise from the assumptions in the derivation of the diffusion equation are:

1. Collisions between neutrons are neglected, making the probability of collision with the nuclei of the diffusion media proportional to the flux. This results in linear equations

describing the neutron diffusion.

2. The neutrons are assumed to be mono-energetic. The neutrons collide elastically with the diffusion media and do not lose energy upon collision. This allows the diffusion equation to be independent of energy.

3. The moderator is assumed to be homogeneous. It also is assumed that the moderator nuclei are at rest and of such a large mass with respect to a neutron that they do not recoil appreciably under the impact of neutrons.

4. The fractional change in the neutron flux over a distance of two or three mean-free paths is small. In a region near a concentrated source, strong absorber of boundary, the flux may change rapidly. In this region the neutron current cannot be represented as being proportional to the gradient of the flux.

5. The diffusion medium is assumed to be a weak absorber so that the scattering cross section can represent the total cross section.

6. The neutron scattering is spherically symmetric or isotropic. This assumption places a limitation on the diffusion equation near sources, boundaries and absorbers where the scattering is not isotropic.

7. The general dimensions of the moderator are much larger than the characteristic lengths, such as the diffusion length in diffusion theory and the slowing-down length in Fermi age theory.

8. The diffusion coefficient is independent of position. This allows the diffusion coefficient, D, to be factored out of the term for the divergence of the neutron current in the equation

of continuity.

Weinberg and Wigner (19) point out that condition one is the most important mathematical property of the diffusion equation. Since the equations are linear, superposition of solutions is possible.

Weinberg and Wigner also state that the diffusion equation is usually derived with the assumption that the scattering is spherically symmetric. They, however, show that the diffusion equation can be derived without this assumption.

Foulke (9) states that without condition four, Fick's first law of diffusion is not valid in describing the neutron diffusion.

CHAPTER II

SOLUTIONS OF THE DIFFUSION EQUATION FOR

PLANE AND POINT NEUTRON SOURCES

The derivation of the flux distribution in a finite cyclindrical moderator, neglecting the source term due to slowing-down of fast neutrons, is presented in Appendix B. The boundary conditions are such that the radial flux is zero at r = R, the extrapolated radius, and the axial flux is zero at z = c, the extrapolated height. The flux distribution was found to be:

$$\phi(r,z) = \sum_{n=1}^{\infty} A_n \, \text{Sinh} \, \gamma_n(c-z) \, J_o(j_n \frac{r}{R}) \tag{14}$$

Where A_n is a Fourier constant, j_n is the argument of the zeros of the Bessel Function, J_o, and γ_n is the relaxation length defined by the following equation:

$$\gamma_n^2 = K^2 + (\frac{j_n}{R})^2 \tag{15}$$

The symbols are as previously defined for Equation 14.

The above flux equation represents the flux distribution for both point and plane sources of thermal neutrons. The Fourier constant, A_n, differs for the different types of sources. For a point source of thermal neutrons, A_n was found to be given by the

following equation:

$$A_n = \frac{1}{2} \; \frac{S}{R^2 J_1^2 (j_n)D} \; \tanh (\gamma_n c) \qquad (16)$$

For a plane source, A_n was found to be given by:

$$A_n = \frac{2S}{j_n J_1 (j_n) D_n} \; \tanh (\gamma_n' c) \qquad (17)$$

From this it is seen that the ratio of the Fourier constants is given by the following equation:

$$\frac{A_n(\text{point})}{A_n(\text{plane})} = K \frac{j_n}{J_1(j_n)} \qquad (18)$$

where K is a constant determined from the ratio of source strengths.

In Appendix C, the solution of the Fermi age equation is presented for both plane and point sources emitting neutrons of a Fermi age, . For a cyclindrical moderator the slowing-down density is given by:

$$q(r,z,\tau) = \sum_{n=1}^{\infty} K_n \; \exp \frac{-z^2}{4\tau} \left[J_0 (j_n \frac{r}{R}) \right] \qquad (19)$$

where K_n is a Fourier constant which is a function of τ. K_n is also dependent on the type of source, point or plane source of neutrons.

Using the slowing-down density from Fermi age theory with the diffusion equation, the thermal neutron flux was also derived in Appendix C. The result is given here as:

$$\phi(r,z) = \sum_{n=1}^{\infty} A_n \, e^{\gamma^2 \tau} \left\{ e^{-\gamma_{nz}} \left[1 + \text{erf}\left(\frac{z}{2\sqrt{\tau}} - \gamma_n \sqrt{\tau} \right) \right] \right.$$

$$\left. + e^{\gamma_{nz}} \left[1 - \text{erf}\left(\frac{z}{2\sqrt{\tau}} + \gamma_n \sqrt{\tau} \right) \right] \right\} J_0\left(j_n \frac{r}{R} \right) \quad (20)$$

The flux distribution reduces to:

$$\phi(r,z) = \sum_{n=1}^{\infty} F_{nz} A_n J_0\left(j_n \frac{r}{R} \right) \quad (21)$$

where F_{nz} was defined as:

$$e^{\gamma \tau} \left\{ e^{-\gamma_{nz}^2} \left[1 + \text{erf}\left(\frac{z}{2\tau} - \gamma_n \tau \right) \right] + \right.$$

$$\left. e^{\gamma_{nz}} \left[1 - \text{erf}\left(\frac{z}{2\tau} + \gamma_n \tau \right) \right] \right\} \quad (22)$$

Comparing the flux from the fast source with the flux from the source emitting only thermal neutrons, it was seen that the factor $F_{nz}/\text{Sinh} \, \gamma_n \, (c - z)$ is used to correct the flux due to the emission of fast neutrons.

The Pu-Be neutron source can not be considered rigorously to be a mono-energetic source. Fermi age treatment does not completely describe the neutron slowing-down. This explains any curvature of a plot of the natural logarithm of the slowing-down density against z^2.

It is noted that $\sqrt{\tau}$ is the slowing-down length of neutrons from a mono-energetic source. The quantity, $2\sqrt{\tau}$, is referred to

as the Gaussian range and denoted by g. For a multienergetic source, g_i is referred to as the Gaussian range of the i'th group of neutrons.

The slowing-down density for an infinite number of Gaussian ranges of neutrons is given by the following equation:

$$q(z, \mathcal{T}) = \sum_{i=1}^{\infty} f_i \; K_i \; e^{\frac{-z^2}{g_i^2}} \tag{23}$$

where f_i is the fraction of the neutrons in the Gaussian range g_i. The solution for each range is super positioned onto the solution of the other ranges.

W. R. Kimel (13) has found excellent agreement with experimental results when three ranges are used to describe the spectrum from the Pu-Be neutron source. He gives the following equation for the slowing-down density to indium resonance using three ranges as:

$$\frac{q(z, \mathcal{T})res}{Q_o} = 1.314 \; \exp \; -(\frac{z}{27.31})^2 \; +$$

$$2.572 \; \exp \; - (\frac{z}{36.94})^2 \; + \; 0.824 \; \exp \; - (\frac{z}{65.44})^2 \tag{24}$$

where $q(z, \mathcal{T})res$ is the slowing-down density to the indium resonance.

The following equation was used to find the slowing-down density from the resonance energy to thermal energies.

$$\mathcal{T}_{th} = \mathcal{T}_{res} + \mathcal{T}_{res-th} \tag{25}$$

or

$$\frac{q^2_{th}}{4} = \frac{q^2_{res}}{4} + \frac{q^2_{res-th}}{4} \tag{26}$$

A value of 49.6 for τ_{res-th}, the age from the indium resonance to thermal energies, was used. This figure was an average of four reported values of the age from the indium resonances to thermal energies (13), (15), (6), (10).

Using the slowing-down density incorporating N Gaussian ranges, the flux equation was derived in Appendix C and is given below.

$$\phi(r,z,q) = \sum_{i=1}^{N} \sum_{n=1}^{\infty} f_i \quad A_n e^{\gamma^2 \tau} \left\{ e^{-\gamma_n z} \right.$$

$$\left[1 + erf\left(\frac{z}{g_i} - \frac{\gamma_n g_i}{2} \right) \right] + e^{\gamma_n z} \left[1 - erf \right.$$

$$\left. \left(\frac{z}{g_i} + \gamma_n \frac{g_i}{2} \right) \right] \right\} J_o \left(j_n \frac{r}{R} \right) \tag{27}$$

Defining F_{niz} for each range as F_{nz} was done for the Fermi age, the flux equation becomes:

$$\phi(r,z,q) = \sum_{i=1}^{N} \sum_{n=1}^{\infty} f_i F_{niz} A_n J_o \left(j_n \frac{r}{R} \right) \tag{28}$$

CHAPTER III

MEASUREMENT OF THERMAL NEUTRON FLUXES

Neutrons are electrically neutral particles. Therefore, neutrons can not be detected by any other means than by secondary processes. The secondary processes are the release of charged particles as the neutron passes through matter, and the production of ionizing radiation upon the passage of the neutron.

For practical efficiencies in neutron detection, the secondary process must produce ionizations which can be conveniently detected by detectors. The energy of the ionizations must be above the threshold energy of the detector.

Foil Activation Method of Thermal Neutron Detection

A number of elements have a large cross section for the neutron-gamma (n,γ) reaction. If the product of this reaction is in itself unstable and decays by the emission of beta particles with a convenient half-life, this element can be used to detect thermal neutrons.

In most applications, the detector element used must be a thin foil and need not be more than three or four cm^2 in area. With such small areas, the foils can be used to determine the thermal neutron flux at known localized areas. For most detector elements, the use of these foils is not affected by the presence

-17-

of gamma rays of less than six MEV. Another desirable, if not
mandatory, characteristic is the absence of resonance absorptions
with unusually large cross section for neutrons at energies near
the thermal region.

From the definition of activation cross section, it is evident that for a foil having an area of A, cm^2, a density of N,
nuclei per cc and a thickness, x, that the rate of neutron capture,
R, is given by:

$$R = nv\,\sigma_{act}NAX \qquad (29)$$

Since $\phi = nv$, ϕ is then given by:

$$\phi = \frac{R}{\sigma_{act}NA_x} \qquad (30)$$

The radioactive product will decay with a characteristic
half-life, $T^{1/2}$. In application of this decay to activity measurements, it is convenient to count the activity with an over-all
efficiency of the counter ϵ . C_s is defined as the counting rate
which would be observed if the irradiation was continued until no
further increased in activity is produced. C_s is referred to as
the saturation activity. Thus it is seen that R, the rate of capture of neutrons as previously defined, is C_s/ϵ .

The counting rate for any irradiation time less than that required for saturation is given by Lapp and Andrews (14) as C =
$C_s (1 - e^{-\lambda t})$, where t is the irradiation time. In most cases,
it is impossible to count the activities immediately after irra-

diation is terminated. The activity will decay in a time, t_1, beginning at the termination of the irradiation and ending at the time the counting is started. The counting rate, at the time the counter is started, is given by $C_1 = Ce^{-\lambda t}$ (14).

It is also usual to count the number of emitted particles from the foil in an interval of time starting at t_1 and stopping at t_2. If C_1 is the number of counts measured in the interval t_2-t_1 per cm^2 of the foil, the saturation activity count rate, C_s, is given by:

$$C_s = \frac{C_1}{(e^{-\lambda t_1} - e^{-\lambda t_2})(1 - e^{-\lambda t})} \qquad (31)$$

In the actual measurement, several precautions and corrections are required in the use of the above outline for determination of the thermal neutron flux.

Indium foils are used widely to measure the neutron flux. This use incorporates the activation of indium-115 according to the following nuclear transformation equation:

$$In^{115} \xrightarrow{\ n\ } In^{116} \xrightarrow{\ \beta^-\ } Sn^{116} \qquad (32)$$

In measuring neutron fluxes, the thickness of the foil must be considered. Increasing the thickness of the foil should increase the sensitivity of detection due to the increase in the number of target nuclei. This expected increase in the sensitivity, however, is obtained only up to a thickness which could be called the optimum thickness.

After the optimum thickness is reached, the sensitivity

decreases. The decrease is due to the combination of two effects.

1. The increased thickness of the foil increases the self absorp-

   tion of beta particles.

2. The increased thickness increases the effect of absorption of

   neutrons by the indium and reduces the neutron flux.

It is sometimes very difficult to determine the correction for

internal absorption of the beta particles in the foil. Foils thin

enough that the effect of self absorption is negligible should be

used.

Bothe (4) suggests a method by which the correction due to

the depression of the neutron flux can be determined. Bothe as-

sumed that a circular foil of radius R would have the same effect

on the neutron flux as a spherical shell of a radius $2R/3$. This

assumption was made since the spherical shell lent itself easily to

theoretical analysis. It, however, has been found from experimental

data that the radius of the shell must be taken as equal to the

radius of the circular foil. This radius gives much better agree-

ment with observations (6).

Bothe computed a factor by which the observed counting rate

was to be multiplied to obtain the actual neutron flux. He gave

the general formula as:

$$F = 1 + \frac{\alpha}{2} \; \frac{3}{2} \frac{R}{\lambda_{tr}} \frac{L}{R + L} - 1 \tag{33}$$

It is noted that if $L << R << \lambda_{tr}$, the case for a nonabsorbing

medium, F becomes:

$$F = 1 + \frac{3}{4} \alpha \frac{R}{\lambda tr} \tag{34}$$

In both equations α is given by the following equation:

$$\alpha = 1 - e^{-\sigma x}(1 - x) + \sigma^2 x^2 E_i(-\sigma x) \tag{35}$$

in which x is the foil thickness, σ is the absorption coefficient in the foil, and $E_i(-\sigma x)$ is the exponential integral function taken from mathematical tables, Jahnke and Emde (11). Curtis (6) defines α as representing the average probability that a neutron will be absorbed in an isotropic flux of neutrons in a layer of material of thickness x and having a neutron absorption coefficient of σ. Curtis also presents a plot of α as a function of σx. Similarly plots can be found in several references (6,13,15,19). Ritchie, et al., (16) present several of the methods by which the foil data can be corrected for flux depression. One of the methods which appears most applicable is that by Skyrme (17). Skyrme computed the factor F from transport theory. This factor is:

$$F = 1 - T(\frac{3}{4} - \frac{1}{2} \ln \sigma T) - T(D' - D_i') \tag{36}$$

where $T = \Sigma_a t$ and D' and D_i' are dependent on the thickness and properties of the foils.

Ritchie, et al., also present the factor F computed by Tittle (18). Tittle gives F as:

$$F = \frac{\frac{1}{2} - E_i(\tau)}{1 + \frac{1}{2} - E_i(\tau) \frac{3\alpha}{2\lambda_{tr}} \frac{L}{\alpha + L} - 1} \tag{37}$$

where the symbols are as previously defined for the Bothe equation.

In all cases:

$$\phi_o = \frac{\phi_m}{F(\tau)} \tag{38}$$

ϕ_o is the undisturbed flux, and ϕ_m is the measured flux. F is seen also to be a function of the thickness and other properties of the foil and not the flux for all cases. Therefore, by comparing the activities of each foil irradiated in the same flux, intercalibration factors can be found to correct the measured activity to that which would have been measured using only one foil.

In measurements of relative activities, F can be combined with the constant of the following equation:

$$\phi_m = \phi_r C \tag{39}$$

ϕ_r is the relative flux, and C is the constant needed to transform the relative flux into an actual flux. Thus:

$$\phi_o = C' \phi_r \tag{40}$$

where $C' = C/F$.

When cadmium covers are used, another important factor must be considered. Cadmium has a very large resonance absorption cross section for neutrons. The counting rate obtained from cadmium covered foils then must be corrected for both flux depression due to

the indium absorption and that due to the resonance absorption of the cadmium. This correction varies with the thickness of the cadmium cover and also with the thickness of the indium foil.

The correction factor F_{cd} is most reliably determined by measurement of the activities induced in foils of equal thicknesses. These foils are placed into identical fluxes with a different thickness of cadmium covers surrounding each foil. An extrapolation of the data to zero cadium thickness will give F_{cd}. This method for indium foils of various thicknesses produces similar curves for each thickness. Using values of F_{cd} calculated in the above manner, F_{cd} can be plotted vs indium thickness for different thicknesses of cadmium.

Where both thermal and epithermal neutrons are present in the neutron flux, the thermal activity is given by the following equation:

$$A_{th}(x) = R(x) \, A(x) \tag{41}$$

where $R(x)$ is the fraction of the activity of the indium foil due to thermal neutrons and is obtained from measurements with cadmium covered foils. The cadmium covered foils will cause variations in the epithermal neutron flux by absorption. The activity of the cadmium covered foils is not rigorously the activity due to the neutrons of an energy above thermal. This activity, however, is given by the following equation:

$$A_{epi} = A_{cd} \, F_{cd} \tag{42}$$

where A_{epi} is the actual activity of the foil due to the epithermal neutrons, and A_{cd} is the measured activity of the cadmium covered

foil.

The activity of the bare indium foil is the sum of the activity due to the thermal and epithermal neutrons or:

$$A_{th} = A(x) - A_{epi} \tag{43}$$

where A_{th} is the thermal activity and $A(x)$ is the activity of the bare foil.

Defining the cadmium ratio $CR(x)$ as:

$$CR(x) = \frac{A(x)}{A_{cd}} \tag{44}$$

the activity due to the thermal neutrons alone is then given by the following equation:

$$A_{th} = A(x) \ \frac{1 - F_{cd}}{CR(x)} \tag{45}$$

CHAPTER IV

EXPERIMENTAL FACILITIES

All neutron flux measurements were made in the graphite pile, shown in Figure 1. The pile consisted of a rectangular parallelepiped section, forty-eight inches square and twenty-eight inches high, and a cylindrical section, thirty-four inches in diameter and twenty-four inches high. The two sections were constructed by stacking layers of machined reactor grade graphite (AGOT) blocks, approximately four inches in cross section. All layers in each section were identical.

Five vertical stringers ran the entire length of the pile. The position of these stringers can be seen in Figure 3. One of these stringers was placed at the central axis of the pile, while the other four were placed along two perpendicular radii. Each of the stringers along one direction was equidistant from the central axis as a stringer along the other direction (see Figure 3). In the center of each stringer was a one-inch hole machined the entire length of the stringer.

Graphite rods were placed into the holes in the stringers to make the moderator homogeneous by eliminating the air gaps. In addition to eliminating the air gaps, the rods served as holders for the indium detection foils. These rods were fifteen-sixteenths

-25
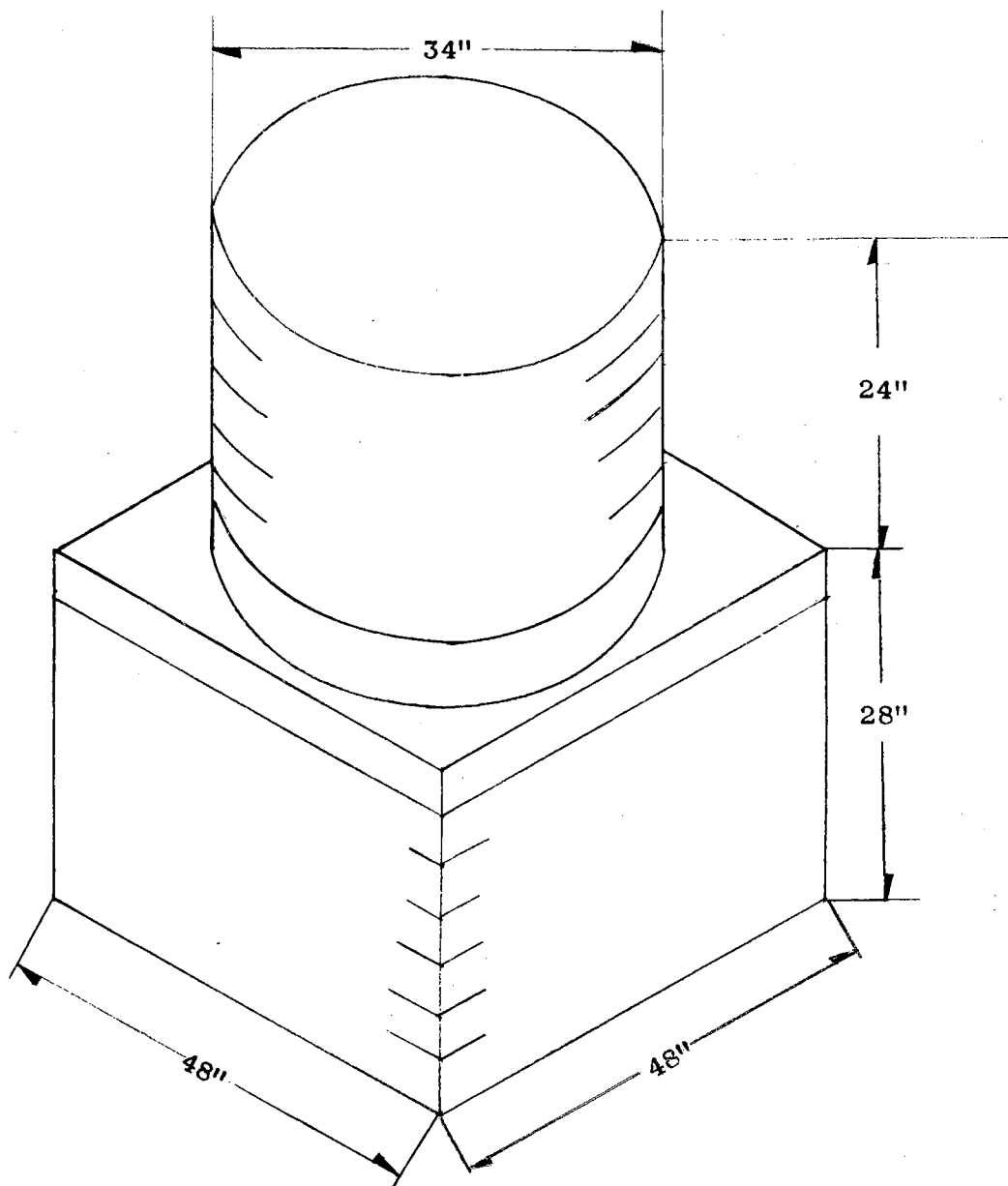
Figure 1.   Schematic of the Graphite Pile.

SHIELD

GRAPHITE POSITIONING
BLOCK

4"

4"

10"

20"

GRAPHITE CYLINDER

24"
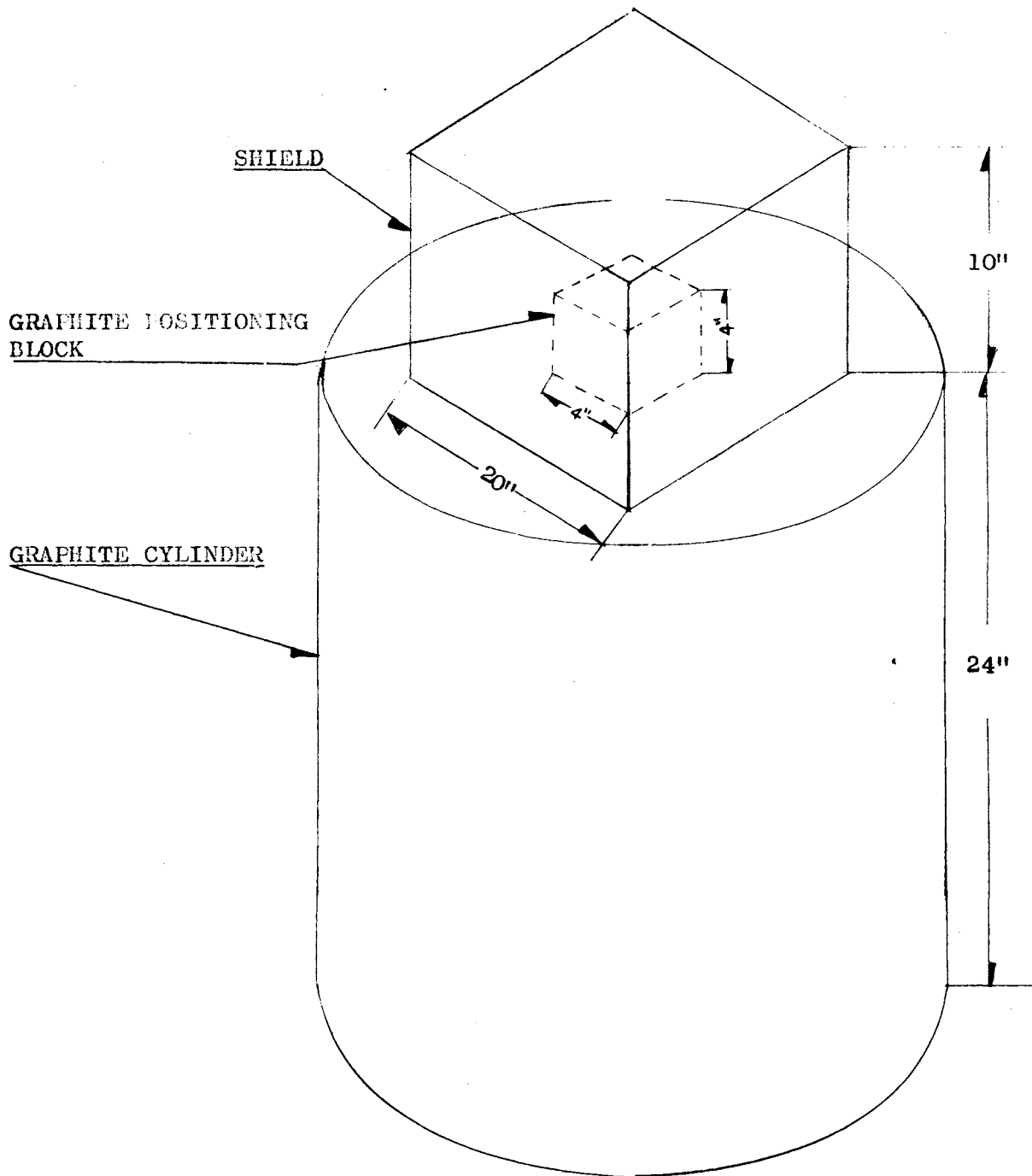
Figure 2. Schematic of the Graphite Cylinder,
Positioning Block and Shield
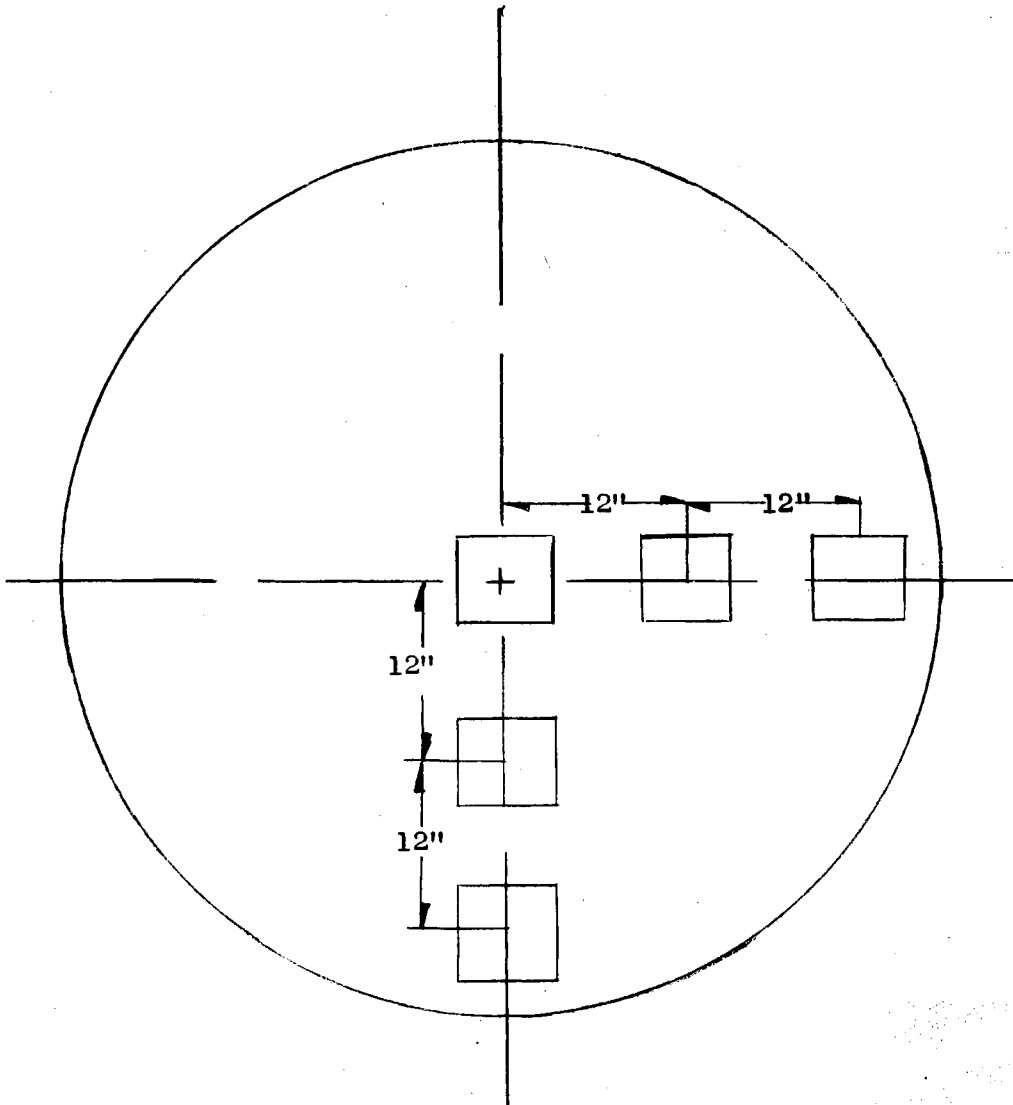
Figure 3. Schematic of the Graphite Cylinder Viewed
From Above.

inch in diameter and fifty-two inches long. Nine-sixteenth inch
holes were milled along the length of the graphite rods to pro-
vide places for the indium foils. The foil holes in the rod for
the center stringer were milled to the center of the rod so that
the foils would be placed exactly on the central axis of the pile.
The foil holes in the other rods were milled to a depth of one-
fourth inch. The spacing of the foil holes along the rods was
three cm. between centers. The first foil hole on each rod was two
cm. from the end of the rod. The center rod had these foil holes
along its entire length; whereas the other rods had foil holes a-
long half their lengths.

The Pu-Be source was held in position with a graphite block
four inches square by about three inches high. A cylindrical hole
was machined through the center of the block. This hole was of
such a size as to allow the source to be easily inserted and re-
moved but still allow positioning of the source accurately. This
positioning block was placed on top of the center stringer as
shown in Figure 2.

Polyethylene was used for a shield around the Pu-Be neutron
source. The polyethylene was in the form of rectangular blocks
stacked around the source to a sufficient thickness to reduce the
fast neutron flux around the source to below the maximum permis-
sible limit in the working area.

Foil Counting Facilities

Twelve indium foils were used in the irradiation. Nine of
the foils had thicknesses of approximately 0.006 inch and a dia-

meter of five-sixteenth inch. This gives a thickness of approximately 96 mg/cm^2. The other three foils had thicknesses of 0.010 inch and a diameter of about seven-sixteenth inch, giving a thickness of approximately 150 mg/cm^2.

The cadmium covers used had an inside diameter of slightly more that seven-sixteenth inch and a wall thickness between 0.0196 inch and 0.0205 inch. In addition to the covers, cadmium caps were used to cover the opposite side of the indium foils. These caps had a diameter of about seven-sixteenth inch and a thickness between 0.021 inch and 0.023 inch. This gave an over-all average cadmium thickness of about 300 mg/cm^2.

A two π gas flow proportional counter was used to measure the activity of the foils. This counter was an NMC model P-10-A proportional counter. The foil counting system consisted of the flow counter, a Nuclear Chicago scaler and a timer. The counting gas was Nuclear Chicago P-10, a mixture of methane and argon.

The background in the counting room was about sixty-three counts per minute. No lead shielding was used to shield the proportional counter. A 0.040 inch aluminum disc provided with the counter was used to facilitate handling and positioning of the foil in the counting chamber.

CHAPTER V

EXPERIMENTAL PROCEDURE

All measurements of the neutron fluxes were made with either bare or cadmium covered indium foils. The bare foils were used to measure the total neutron flux due to fast, epithermal and thermal neutrons. The cadmium covered foils were used to give a measure of the epithermal and fast neutrons.

The foils were placed into the foil stringers of the graphite pile for irradiation. The foils were irradiated for about six hours until they had reached about ninety-nine per cent of the saturation activities of the 54.1 minute half-life indium isotope. In some cases, however, this time was decreased to as low as one hour. To limit flux depression, only twelve foils were irradiated each time. When cadmium covered foils were used, this number was reduced to nine. This was done since the cadmium affects the flux much more than does indium.

After irradiation all the foils were removed from the pile. the foils farthest from the source were counted first. This gave as high a count rate as possible for the points of low flux. About three minuted were allowed to elapse after irradiation before counting began. This allowed the very short half-life (seven seconds) isotope of indium to decay away.

The background count was taken each day only after all foils were counted. This was due to the fact that with the neutron source in position on the pile there was a significant increase in the background measured by the proportional counter.

After completion of the flux measurements with the foils, an intercalibration of the foils was made. Each foil was placed into the same foil position one at a time. The saturation activity of each foil was used to determine intercalibration factors.

Measurement of any residual activity in the foils was made from time to time. After completion of the flux measurements, each foil was again checked to see if there were any residual activity that had accumulated over the period of flux measurements. Also a check was made to see if any impurity with a medium half-life affected the measurements. This was done by measuring the activity of the foils at different time intervals and checking to see if the decay followed exactly the decay curve of pure indium.

The proportional counter was operated at 1750 volts. This voltage is the middle of the beta plateau as determined by measuring the count rate at the different voltages for the Ra DEF standard source . A plot of this count rate vs voltage is presented in Appendix A.

For counting, the foils were placed into the sample chamber of the gas flow counter. The counter was then purged for thirty seconds by allowing the gas to flow rapidly through the chamber. The gas flow rate was then reduced to about two bubbles per second. At this rate the consumption of gas was quite small and the count-

ing rate was not affected by increasing the gas flow rate.

The same counting procedure as above was used to determine the background count, except that the sample chamber was empty except for the aluminum positioning disc.

A foil irradiated each time in the same position was used to establish the stability of the counter and the reproducibility of the flux in the pile.

CHAPTER VI

PRESENTATION AND DISCUSSION OF RESULTS

Flux plots of the total activities of the foils are presented in Figure 4. These activities are due to fast, epithermal and thermal neutrons and were obtained from the activities of the bare foils. The flux plots of the corrected saturation activities of the cadmium covered foils are presented in Figure 5. The flux plots of the thermal neutrons are presented in Figure 6. The curve for the thermal neutron fluxes was obtained by subtracting the curve of the corrected activities of the cadmium covered foils from the curve of the activities of the bare foils. This curve was used in subsequent figures and analysis.

The experimental thermal neutron flux was analyzed by determining the diffusion length that gave the best fit to the experimental data. The method used for determining the diffusion length was to find the best straight line through the experimental data. This straight line was the fundamental solution of the diffusion equation with a particular diffusion length.

The value of the straight line slope is $-\alpha$. α is given by the following equation:

$$\alpha^2 = (\frac{r}{R})^2 + \frac{1}{L^2} \tag{46}$$

The slope was found to be -0.0332. Substituting this value
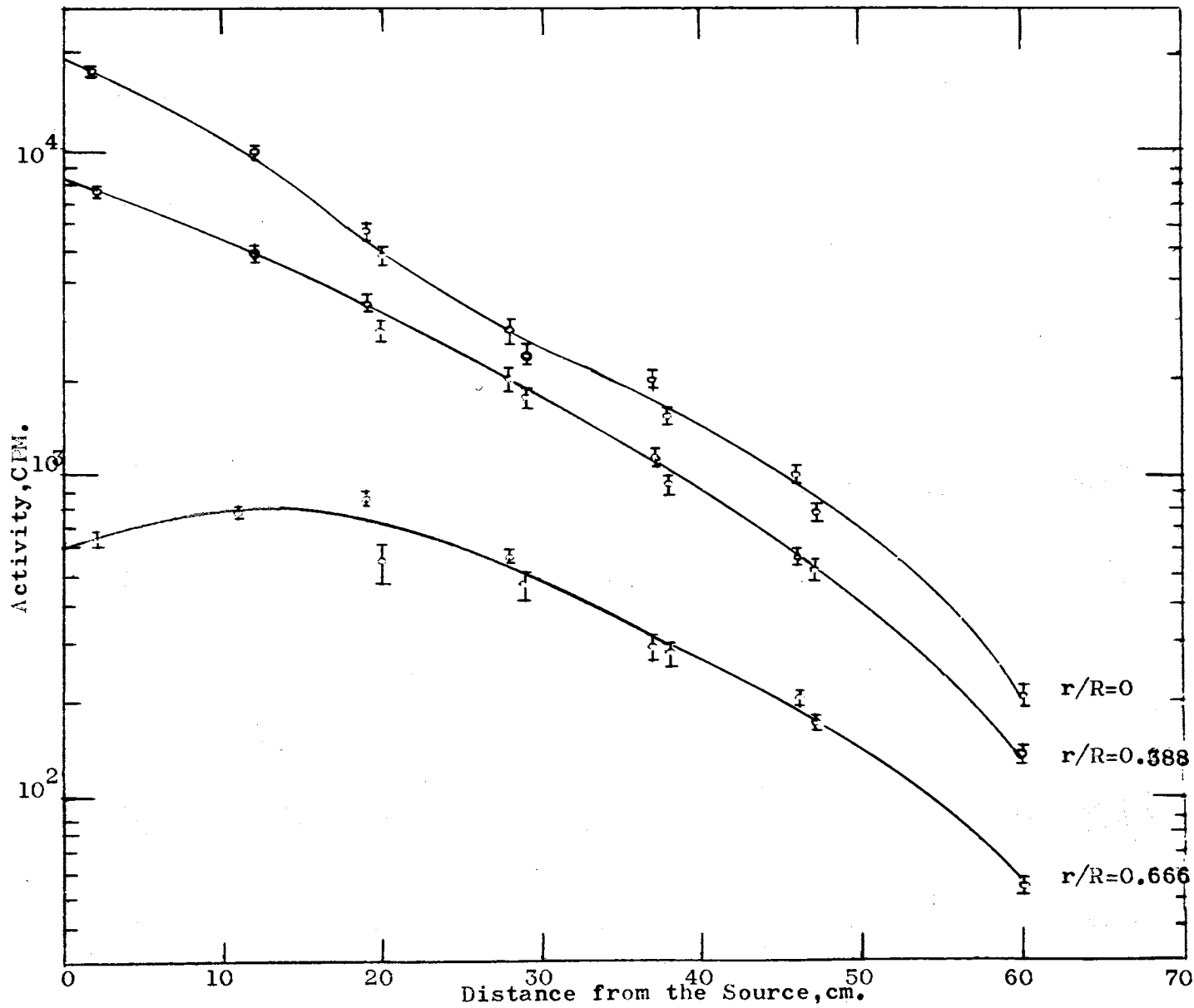
Figure 4. Experimental Activities of the Bare Indium Foils Irradiated in the Graphite Cylinder.
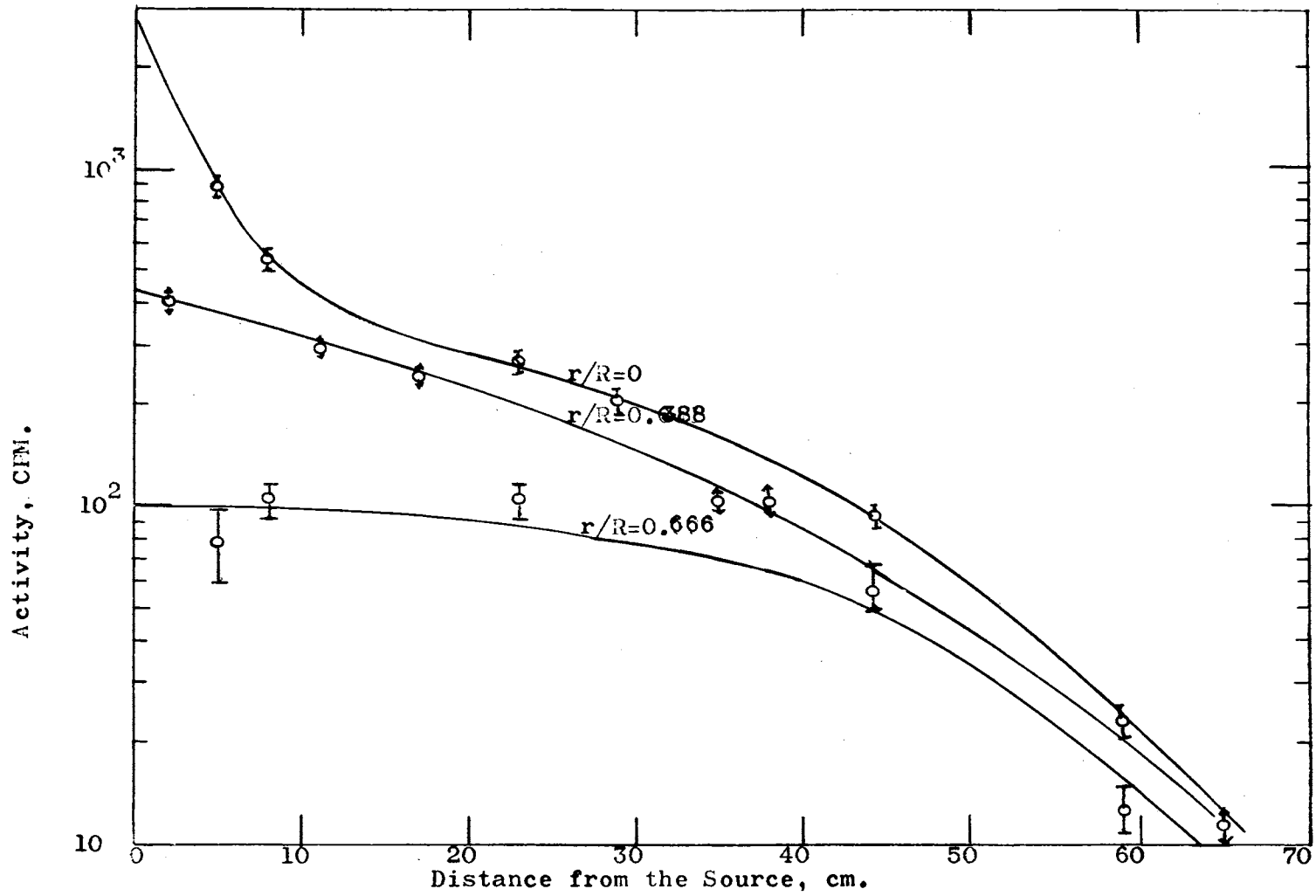
Figure 5.   Corrected Saturation Activities of the Cd Covered Foils
Irradiated in the Graphite Cylinder.
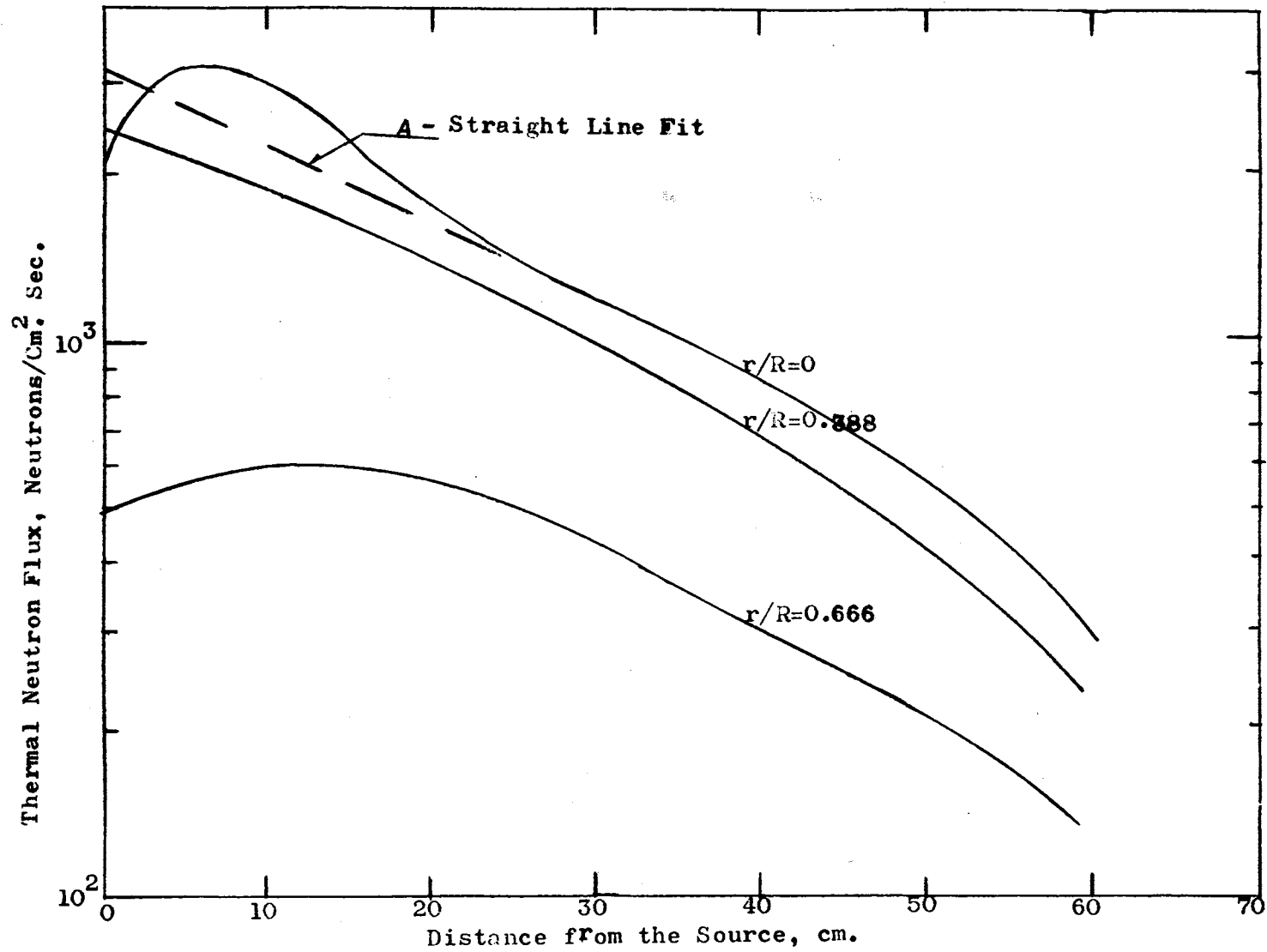
Figure 6.   Thermal Neutron Fluxes in the Graphite Cylinder.

into Equation 46, it is seen that $1/L^2$ is equal to -1.72×10^{-4}.
From physical considerations, it is impossible for the diffusion
length to be imaginary. The straight line fit is curve A of Figure
6.

Problems Arising From Physical Approximations of the Theoretical Source Conditions

If the theoretical conditions could be reproduced physically,
there would be no problem in verifying the theoretical relation-
ship between a point and plane source of neutrons in Equation 18.
The Pu-Be neutron source, however, is not a point neutron source.
This in itself prevented a rigorous application of the theoret-
ically derived relationship in predicting the flux from a plane
source of neutrons by measuring the flux from the Pu-Be neutron
source.

In addition to the above problem of geometry, there is the
problem of the difference in the spectrum of the neutrons from the
Pu-Be source and from the AGN-201 reactor. The reactor is a thermal
reactor wherein there is a very large thermal component to the neu-
tron spectrum; whereas the neutrons from the Pu-Be source spectrum
are almost entirely composed of epithermal and fast neutrons.
Figures 7 and 8 present graphs of the spectrums for the Pu-Be neu-
trons and fission neutrons respectively.

The presence of a large number of fast neutrons from the Pu-Be
source necessitated shielding of the source for safety purposes.
In addition to shielding personnel from possible exposure to large
doses of radiation, the shield provided a hydrogeneous medium in
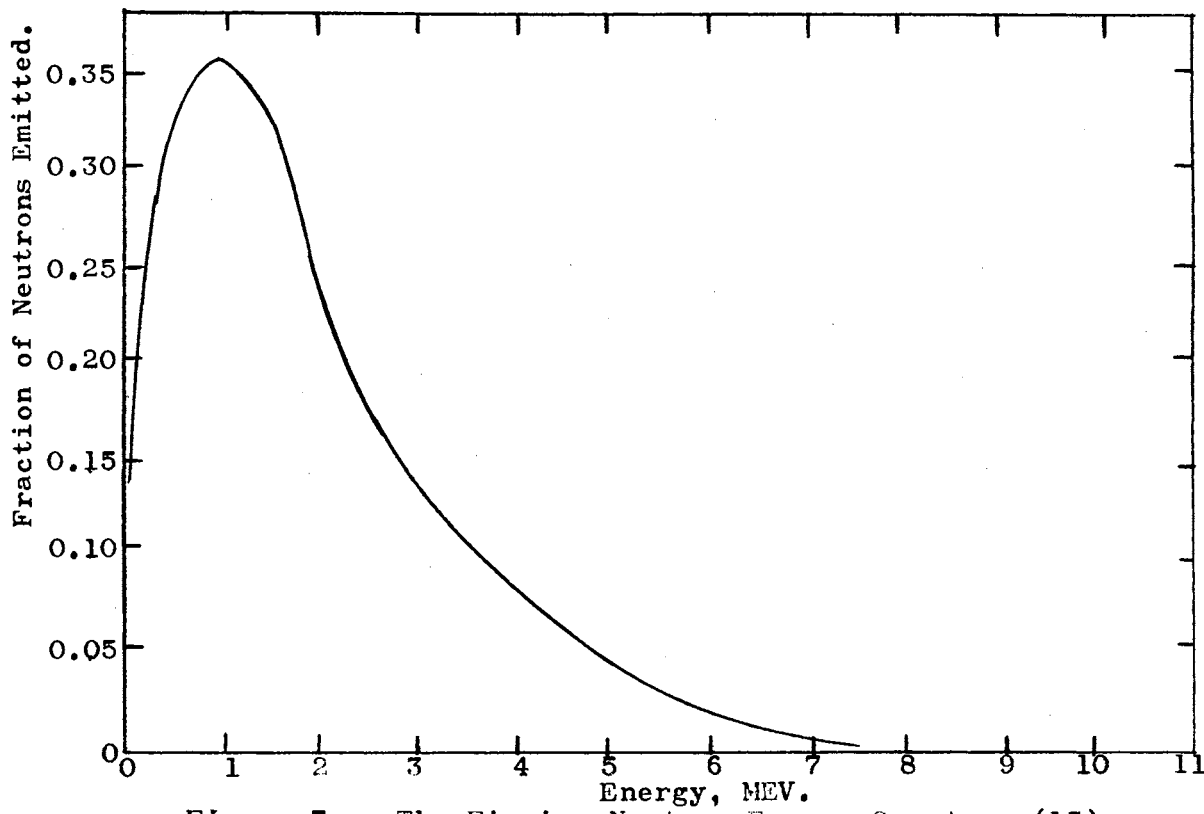
Figure 7.   The Fission Neutron Energy Spectrum (15)
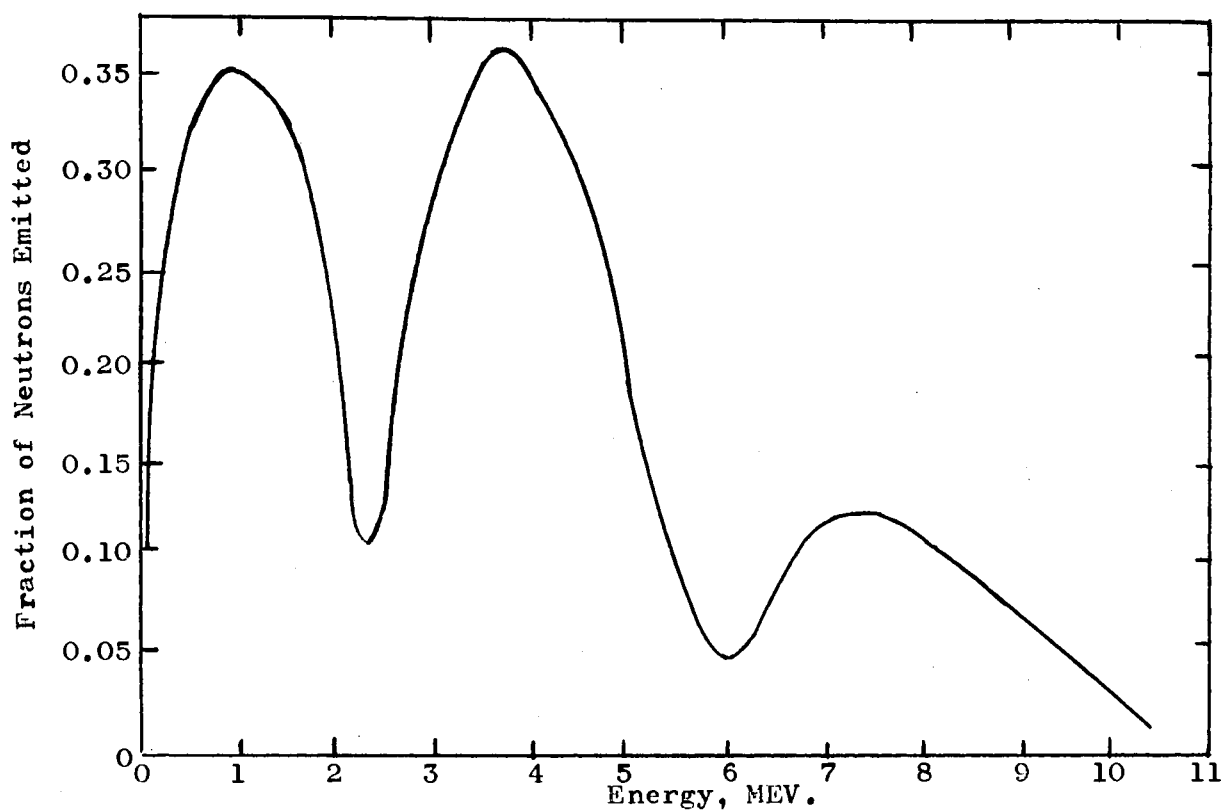
Figure 8.   Pu-Be Neutron Source Energy Spectrum (13)

which the fast neutrons are essentially thermalized upon the first collision with the hydrogen nucleus.

With the above problems, it became necessary to analyze the flux from the Pu-Be neutron source by comparing it with the flux from several theoretical models. If a satisfactory model could be found for the flux from the Pu-Be neutron source, it was postulated that the same model with modification could be used to predict the flux from the AGN-201 reactor.

Thermal Diffusion Model

The flux for a pure thermal point source of neutrons was calculated from Equation 14. The thermal diffusion length was taken to be 52.4 cm. This value for the thermal diffusion length appears to be the most reliable value available in literature (15). The theoretical flux from the thermal point source was calculated using the fundamental harmonic in one case and the first twenty harmonics in the second case.

As can be seen from Figure 9, the fundamental solution is a simple exponential which gives a straight line plot on semi-logarithm paper. It can also be noted that near the source the solution using twenty harmonics is divergent and at large distances from the source it approaches the fundamental harmonic solution as predicted in several references (6, 10, 15, 19).

The flux calculated from the thermal point source model has also been fitted to the experimental data in Figure 9. Figure 9 shows that the flux from a thermal point source model cannot be fitted to the experimental flux except at large distances from
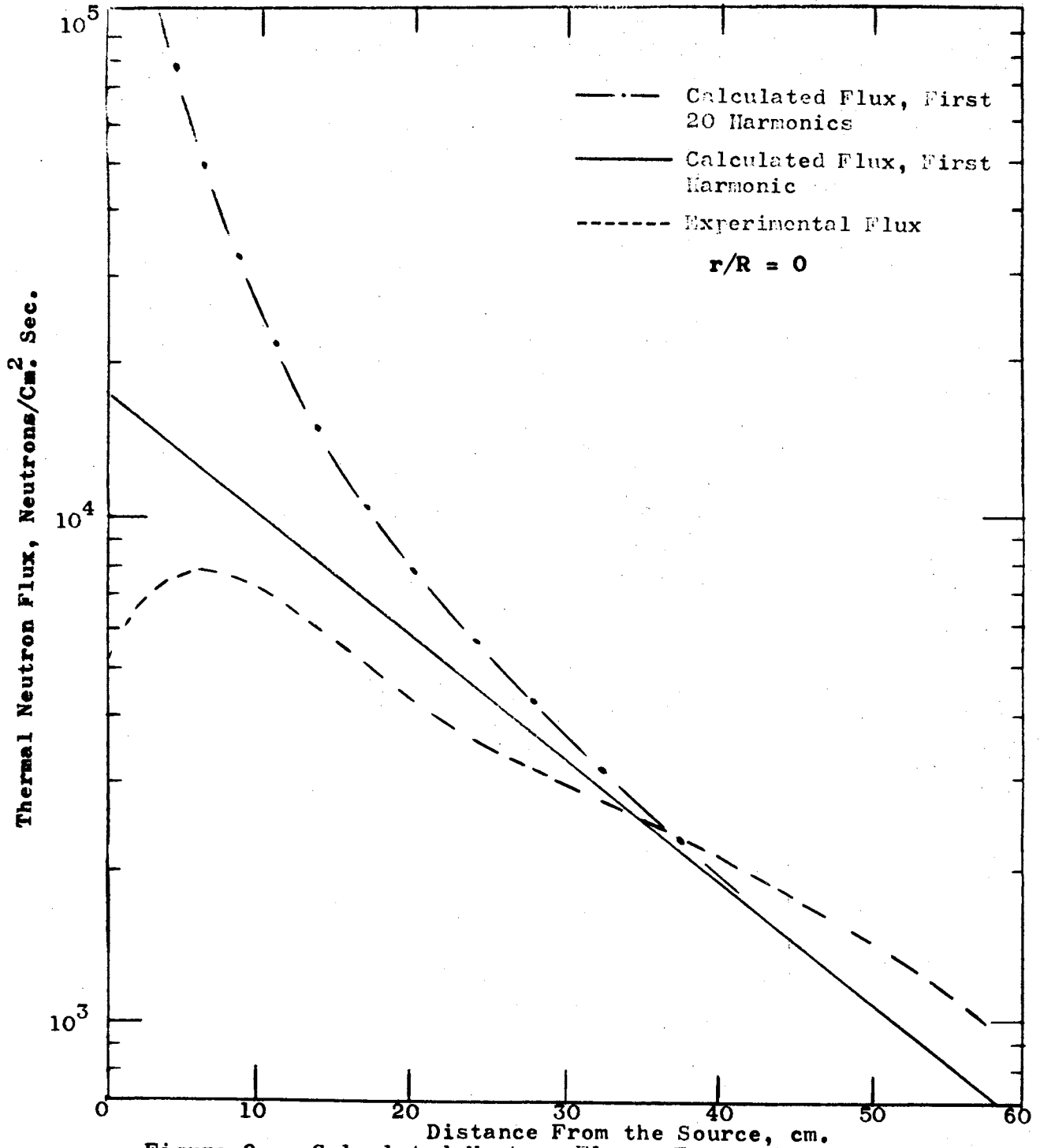
Figure 9. Calculated Neutron Fluxes From Point Thermal Sources.
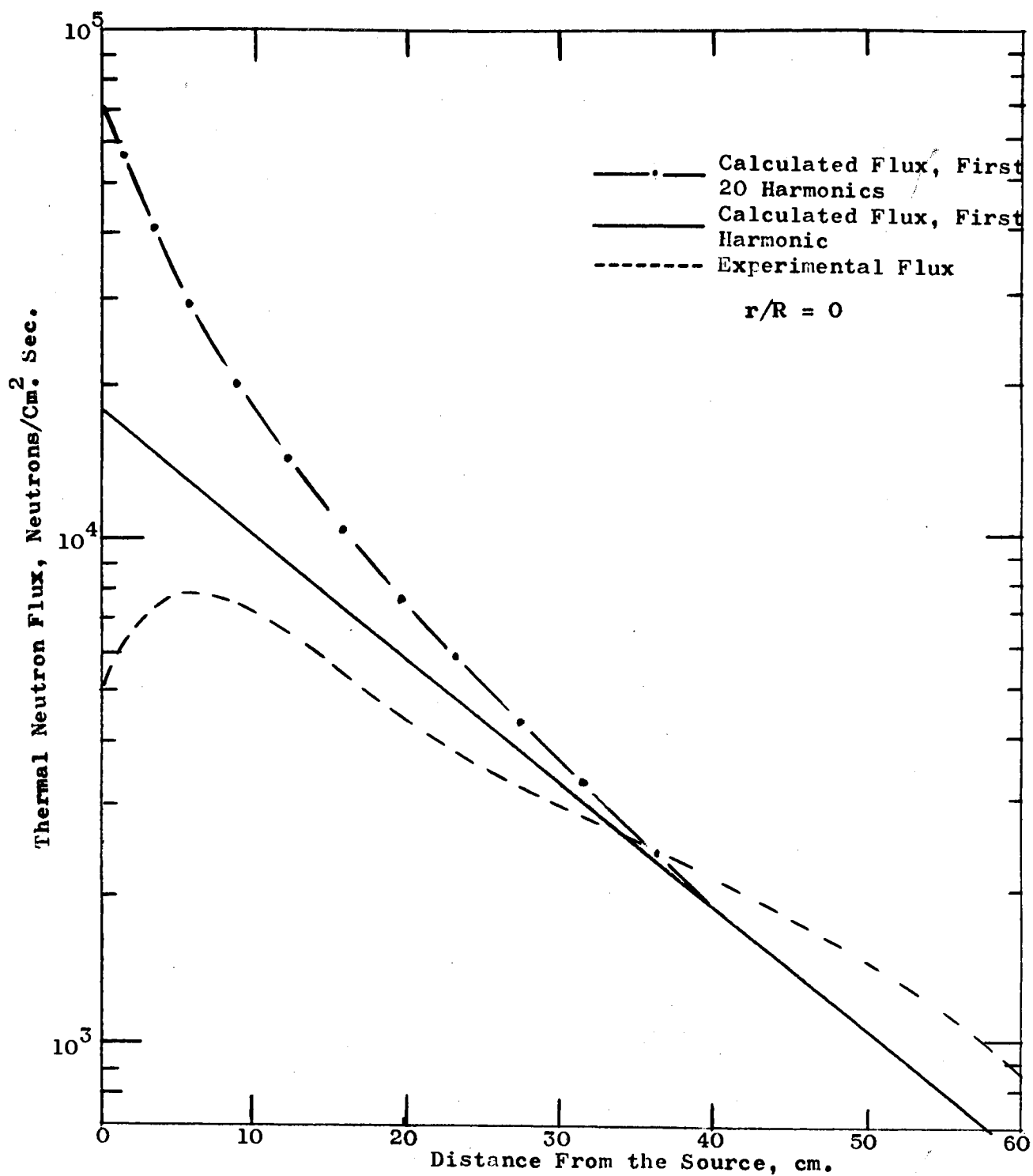
Figure 10.   Calculated Non-diverging Neutron Fluxes From
Point Thermal Sources.

the source.

Since the Pu-Be neutron source is essentially a fast source, it was expected that the thermal point source would be inadequate near the source. At large distances from the source, the contri- bution to the thermal neutron flux by slowing-down is small. Thus at large distances from the source, the neutrons are expected to diffuse as if they had come from a thermal source.

It is noted that very near the source, the flux from the thermal point source model diverges. The experimental flux in this area is significantly lower. This may be explained by the fact that the Pu-Be neutron source is not a point neutron source. There- fore, by extrapolating the theoretically predicted curve for the case of a thermal point source of neutrons from a point some dis- tance from the source, the theoretical flux can be found at zero for the case where the flux does not diverge at the source. Since physically the thermal neutron flux cannot diverge, the extrapola- tion should give a better fit to the experimental data. This is shown to be true by comparing Figures 9 and 10. Figure 10 uses the extrapolated value for the flux; whereas Figure 9 does not.

The thermal point source model is good at large distances from the source. However, even with the correction due to the physical impossibility of a point source of neutrons, this model fails grossly to provide an adequate model.

Age-Diffusion Model with a Mono-energetic Fast Source

The theoretical flux from a source emitting fast neutrons of a Fermi age equal to 421 cm^2 was calculated from Equation 19.
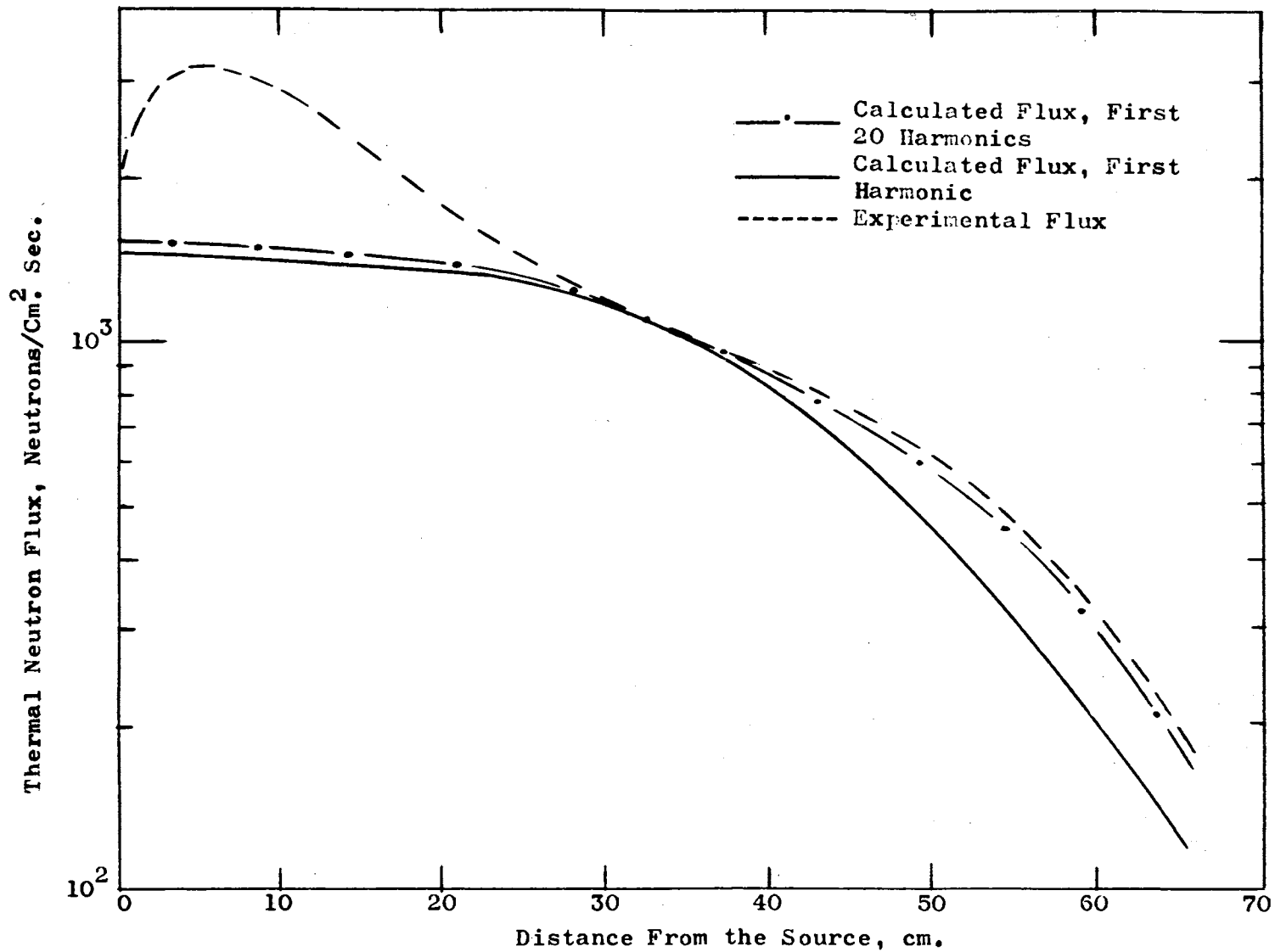
Figure 11.   Calculated Neutron Fluxes From Mono-energetic Fast
Sources of Neutrons.

The value for the Fermi age was taken from studies made at Kansas State University as reported by Kimel (13), Foulke (9) and Kaiser (12). The theoretical flux was calculated for both the fundamental harmonic and a combination of the first twenty harmonics. As can be seen from Figure 11, the solution for the fundamental harmonic is essentially equal to the solution using all the first twenty harmonics.

Figure 11 also gives the fit of the experimental data with the theoretical flux from the mono-energetic fast point source of neutrons. This apparently is a good model at distances above thirty cm from the source. However, closer to the source, the fit is only slightly better than the fit from the thermal source model. It had been anticipated that the combination of slowing-down and diffusion should predict the flux more accurately near the source than the thermal diffusion model. In this area the processes of slowing-down are significant.

Even above thirty cm from the source where the fit is fair, the calculated flux deviates from the experimental data. Figure 12 shows that the slowing-down density from Fermi age treatment does, in fact, deviate from the experimental plot of the slowing-down density. The deviation in the theoretical flux from the experimental flux may then be due to the limitations on Fermi age theory.

The mono-energetic fast source model is a much improved model over the thermal source model. The flux calculated from the mono-energetic fast source model in the volume greater than thirty cm from the source was still inaccurate.

No correction for the source not being physically a point

source was made since the theoretical model of the flux does not

diverge near the source.

Age-Diffusion Model with a Multi-energetic Fast Source

In Figure 12 the slowing-down density does not follow the ex-

perimental points at large distances from the source for a Fermi

age equal to 421 cm^2. Three Gaussian ranges of neutrons were in-

troduced to account for the deviation from a straight line plot on

semi-logarithm paper of the experimental data. The values for

these Gaussian ranges were obtained from values reported by Kimel

at Kansas State (13). For verification of these values, a plot

of the slowing-down density as predicted by Kimel at Kansas State,

using the three Gaussian ranges together with our experimental

data is presented in Figure 13. It is seen that the predicted

curve using three ranges is in very good agreement with the exper-

imental data.

The value of the calculated flux using the three Gaussian

ranges was calcuted from Equation 28 and is presented in Figure

14. It is seen, as was the case for the mono-energetic fast source,

that the fundamental solution does not differ significantly from

the solution using twenty harmonics. Here also the two are al-

most identical.

Figure 14 also gives the fit of the theoretical flux from the

multi-energetic fast neutron source fitted to the experimental data.

Here, as in the case for the mono-energetic source, the fit is

grossly inadequate at small distances from the source. However,
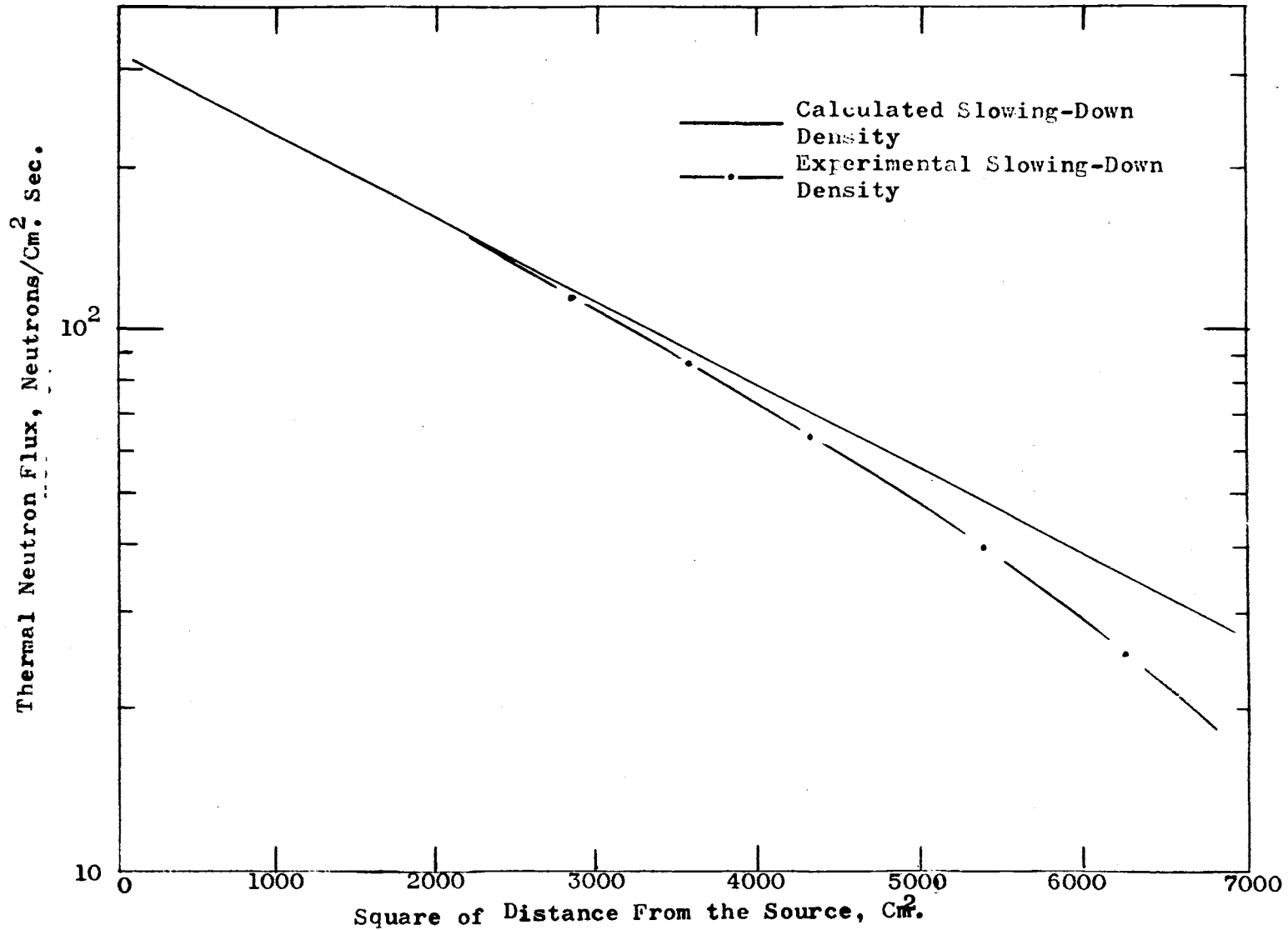
Figure 12.   Slowing-down Density From Mono-energetic Fast Sources
of Neutrons.
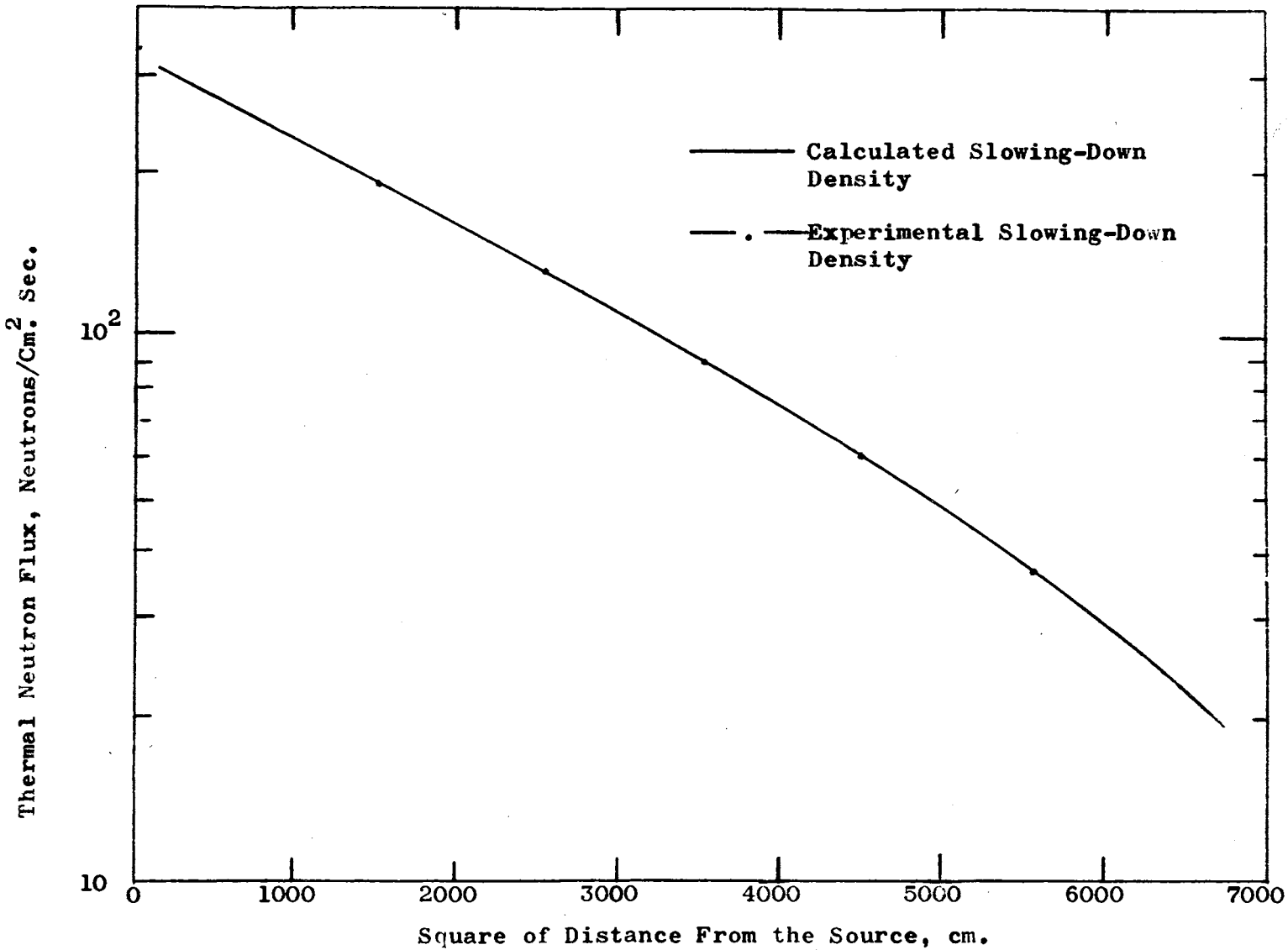
Figure 13. Slowing-down Density From Multi-energetic Fast Sources
of Neutrons.
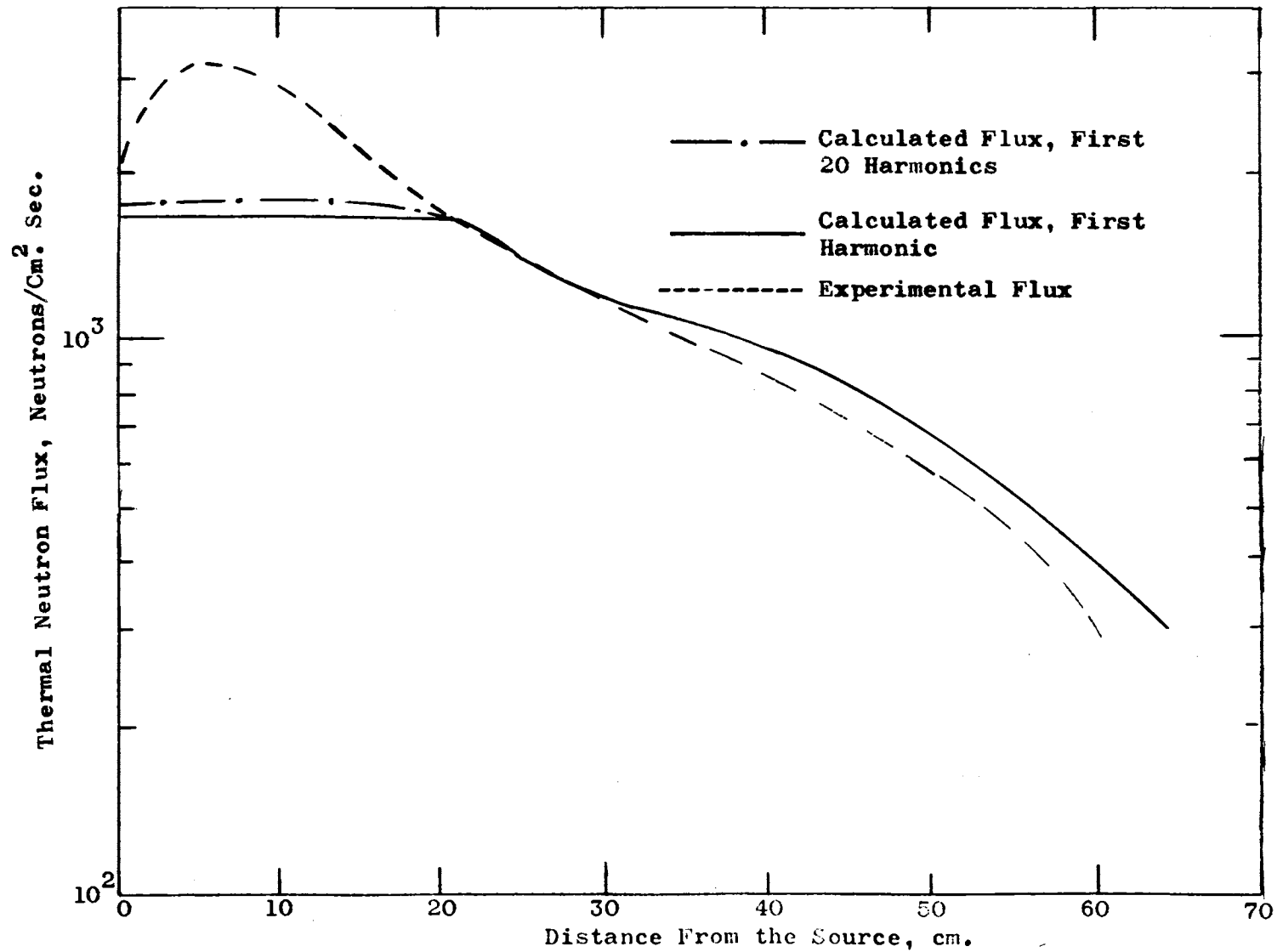
Figure 14. Calculated Neutron Fluxes From Multi-energetic Fast Sources.

the multi-energetic source model predicts the flux much closer

to the actual experimental data in both areas above and below

thirty cm from the source. Above twenty cm from the source the

fit is very good. The fit below twenty cm is grossly inadequate.

Of the three general source models, the multi-energetic source

model more accurately predicts the flux from the Pu-Be neutron

source. Here also an extension to measurements with the AGN-201

reactor would meet with some uncertainty below twenty cm from the

source.

Within two or three mean free paths from strong sources, it

can be expected that no source model using diffusion theory will

be adequate. However, this does not explain the discrepancy at

thirty cm or even twenty cm from the source which is approximately

eleven or nine mean free paths respectively.

Combination of Thermal Diffusion Model and Age-Diffusion Model

Anselone (2) added to his solution for a fast source model a

solution due entirely to a thermal source model. This suggested a

means to fit the experimental data with the theoretically predicted

fluxes. An attempt was made to superimpose the thermal point source

solution on to that of the solutions for the fast source models.

The relative contribution to the flux by each model was found by

determining the best fit to the experimental data. The fit of the

theoretical combination of the thermal model and the mono-energetic

fast source model is presented in Figure 15. The thermal model in

combination with the multi-energetic source model is presented in

Figure 16.
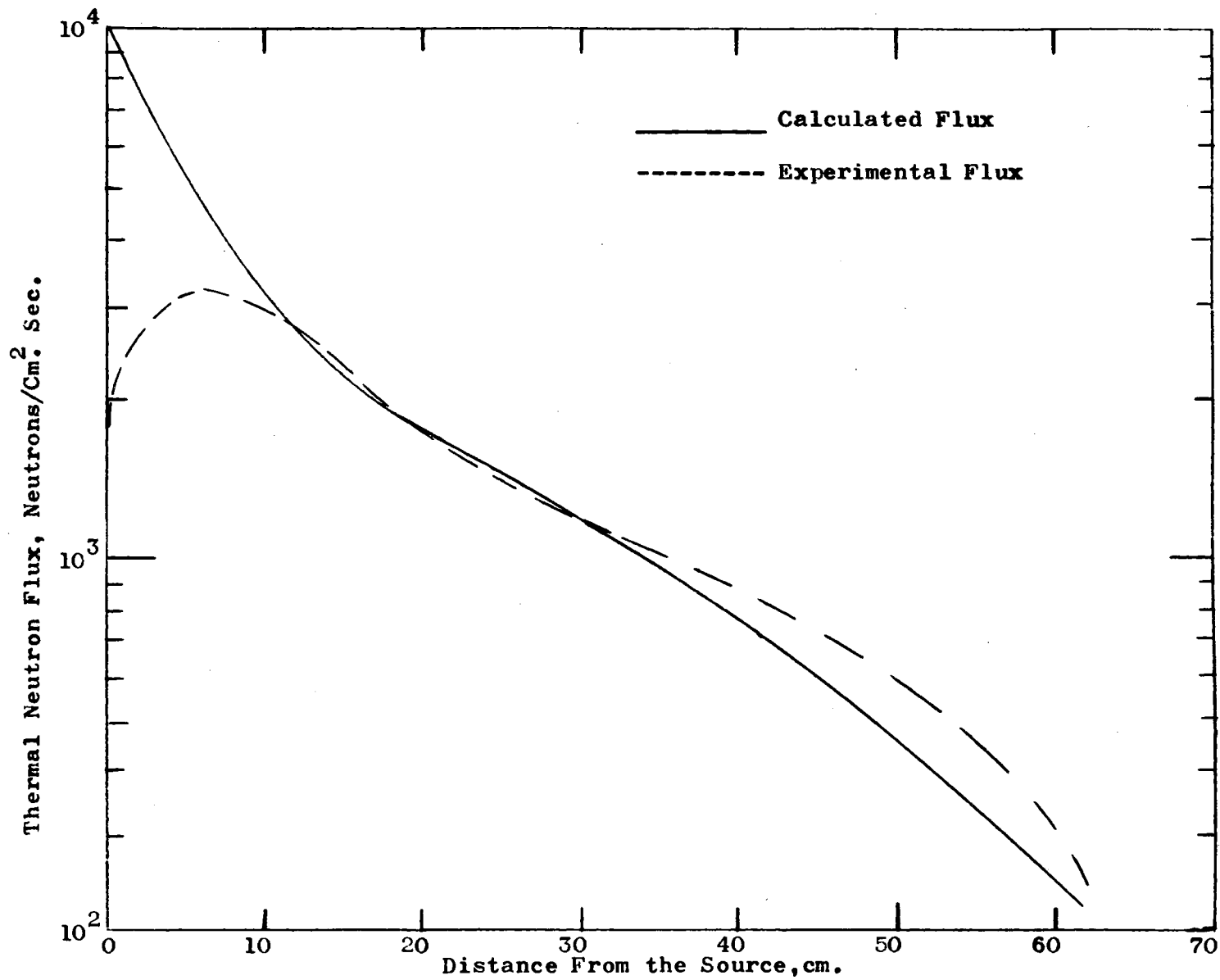
Figure 15. Calculated Neutron Fluxes From a Combination of a Thermal Source Model and a Mono-energetic Source Model.
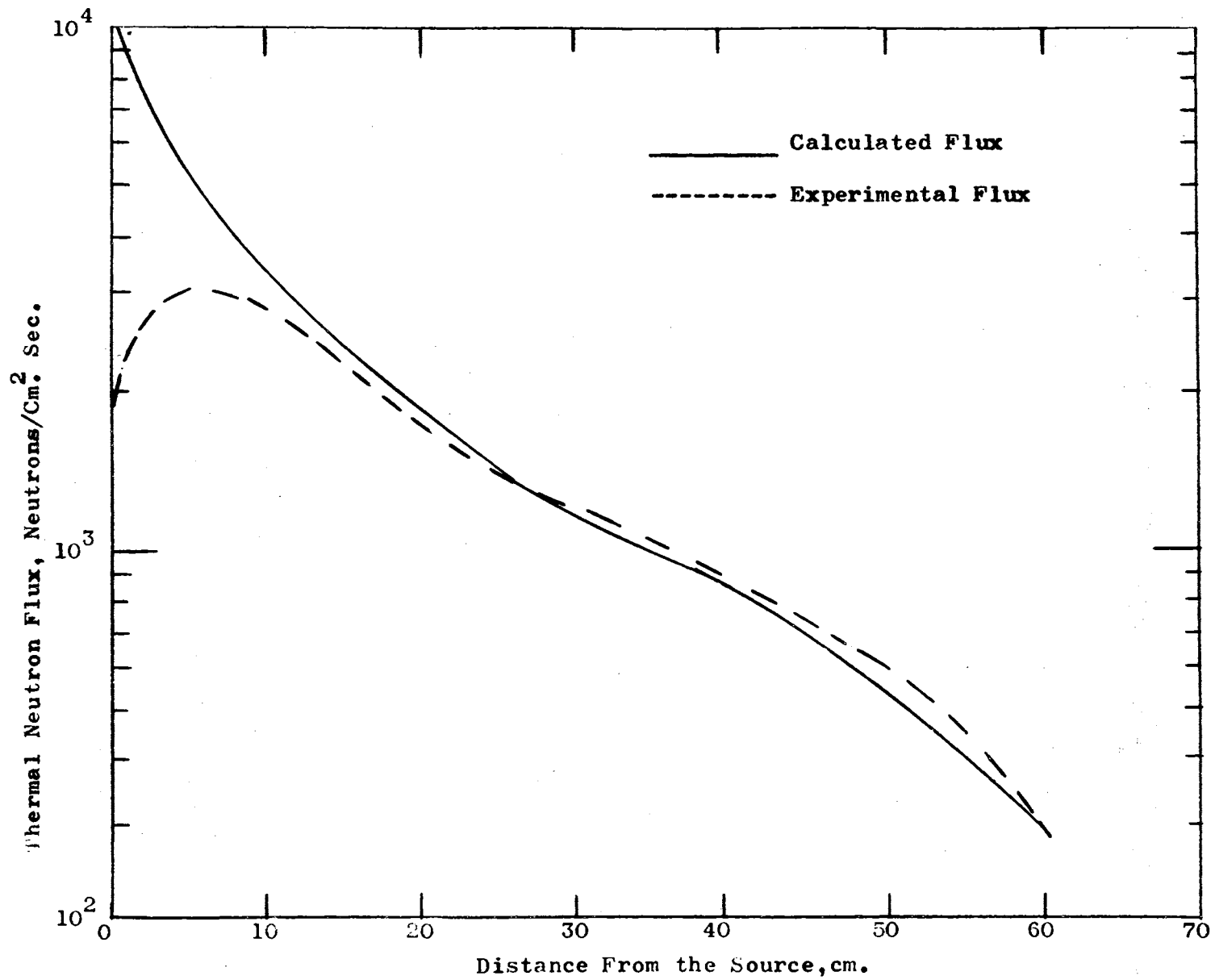
Figure 16. Calculated Neutron Fluxes From a Combination of a Thermal Source Model and a Multi-energetic Fast Source Model.
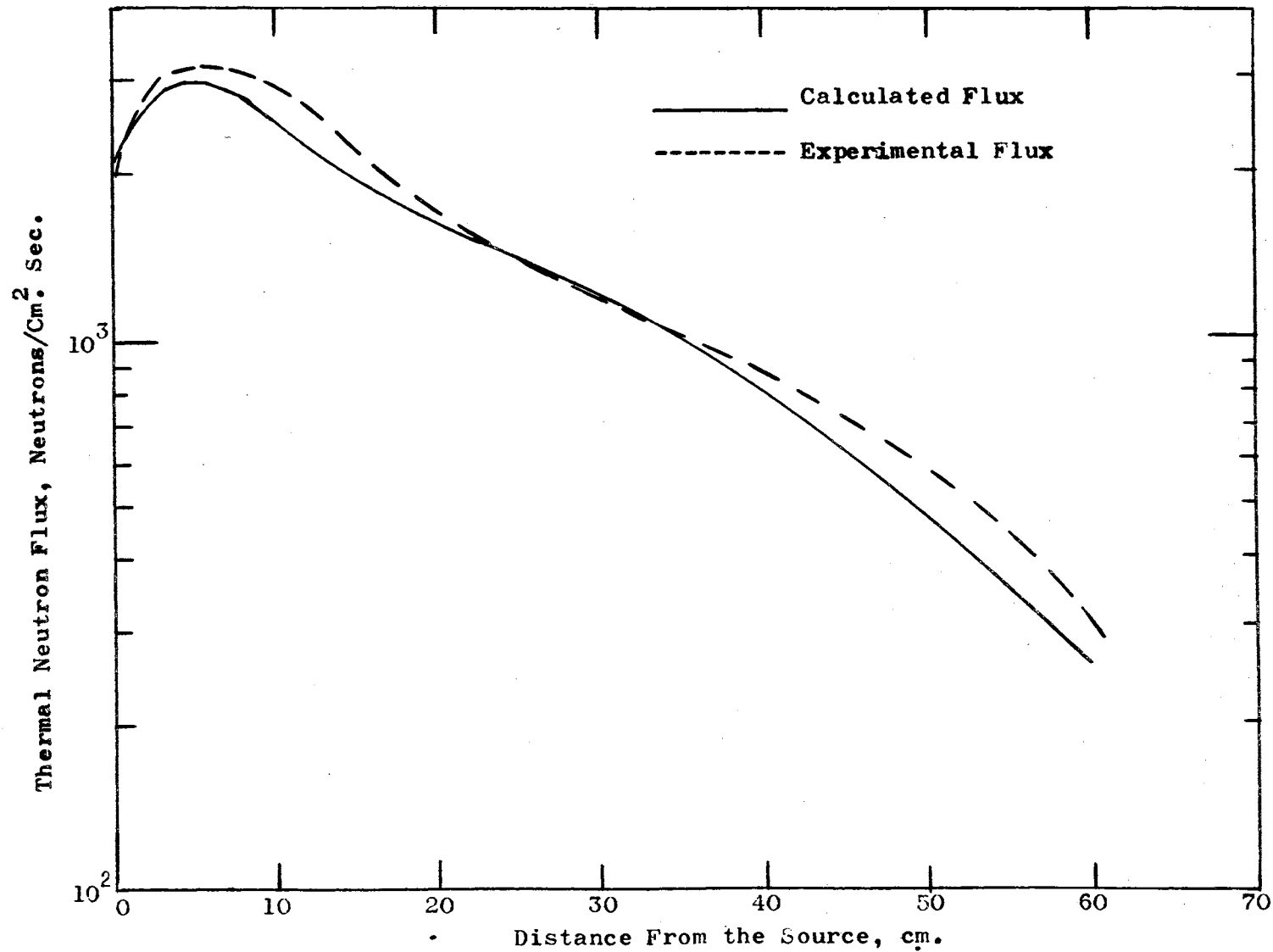
Figure 17. Calculated Neutron Fluxes Showing Flux Depression Due to an Absorber at the Source for a Combination of a Thermal Source Model and a Mono-energetic Fast Source Model.
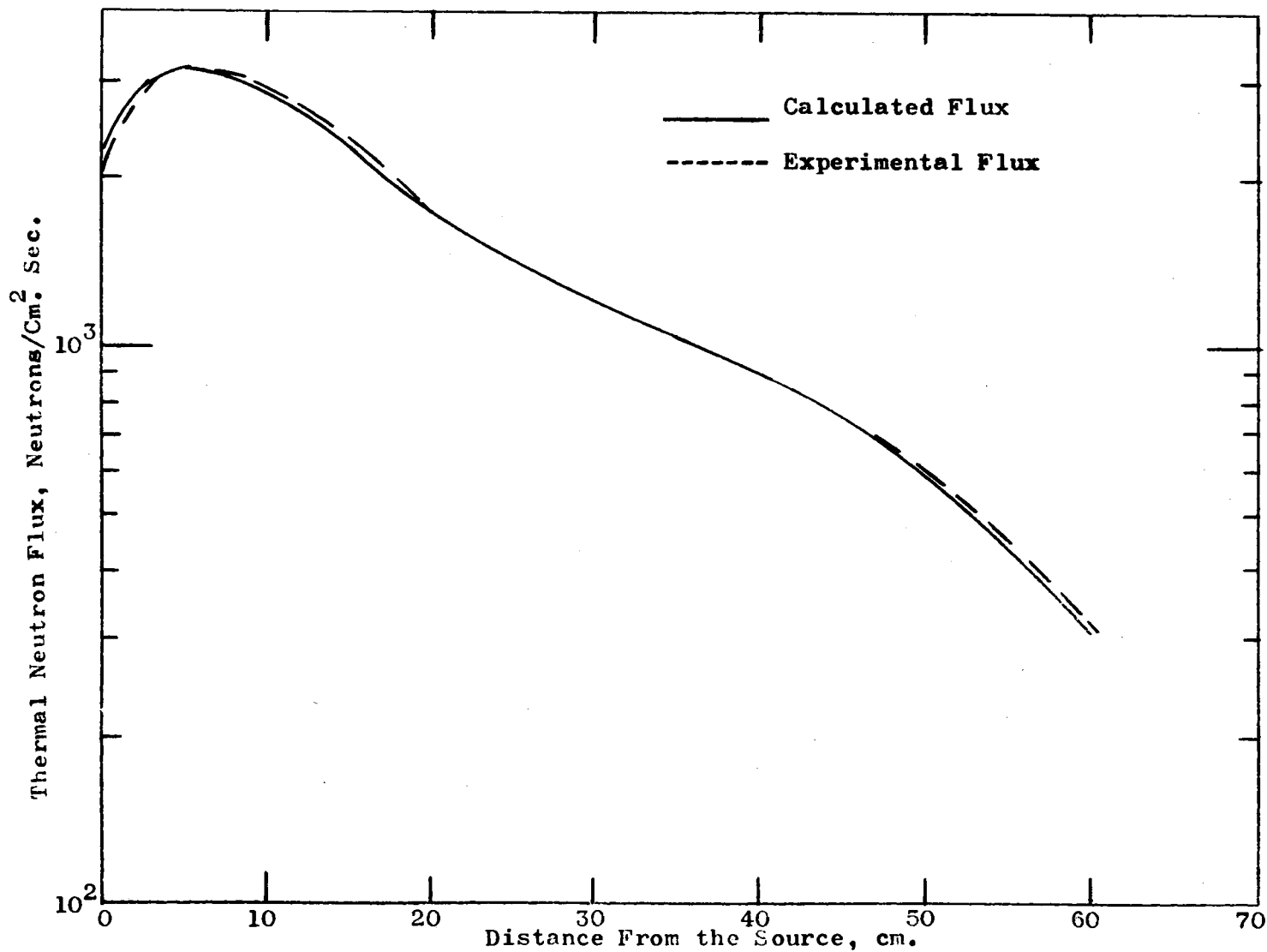
Figure 18. Calculated Neutron Fluxes Showing Flux Depression Due to an Absorber at the Source for a Combination of a Thermal Source Model and a Multi-energetic Fast Source Model.

This combination of the thermal diffusion model and the Age-diffusion model gives an improved fit to the experimental data. Even with this combination, the theoretical curve, as expected, is still inadequate near the source. The experimental value of the flux has a significant depression in the area around the source. In addition to the limitations on the diffusion theory in the area of the source, the reduction in the flux could be due to the presence of the Pu-Be neutron source as an absorber. The source is a strong absorber of neutrons of energies in the thermal range, with an absorption cross-section of approximately 1000 barns. Therefore, to give a value to this depression, a negative source of thermal neutrons is introduced at the origin with the boundary condition that all neutrons from the source which are thermal are absorbed at one-extrapolation distance in the negative z direction. This type of source then becomes only an end correction factor which is multiplied to the thermal flux. The above method of determining the correction due to absorption is known as the image method.

With a correction factor for absorption at the source, the experimental data can be fitted very closely to a combination of a thermal and fast source model. This is noted in Figures 17 and 18.

The theoretical flux predicted from a combination of the thermal point source model with a fast source model incorporating three Gaussian ranges (Figure 18) gives a much improved fit over a combination using only the Fermi age of Pu-Be neutrons in graphite and the thermal source model (Figure 17). The significant differ-
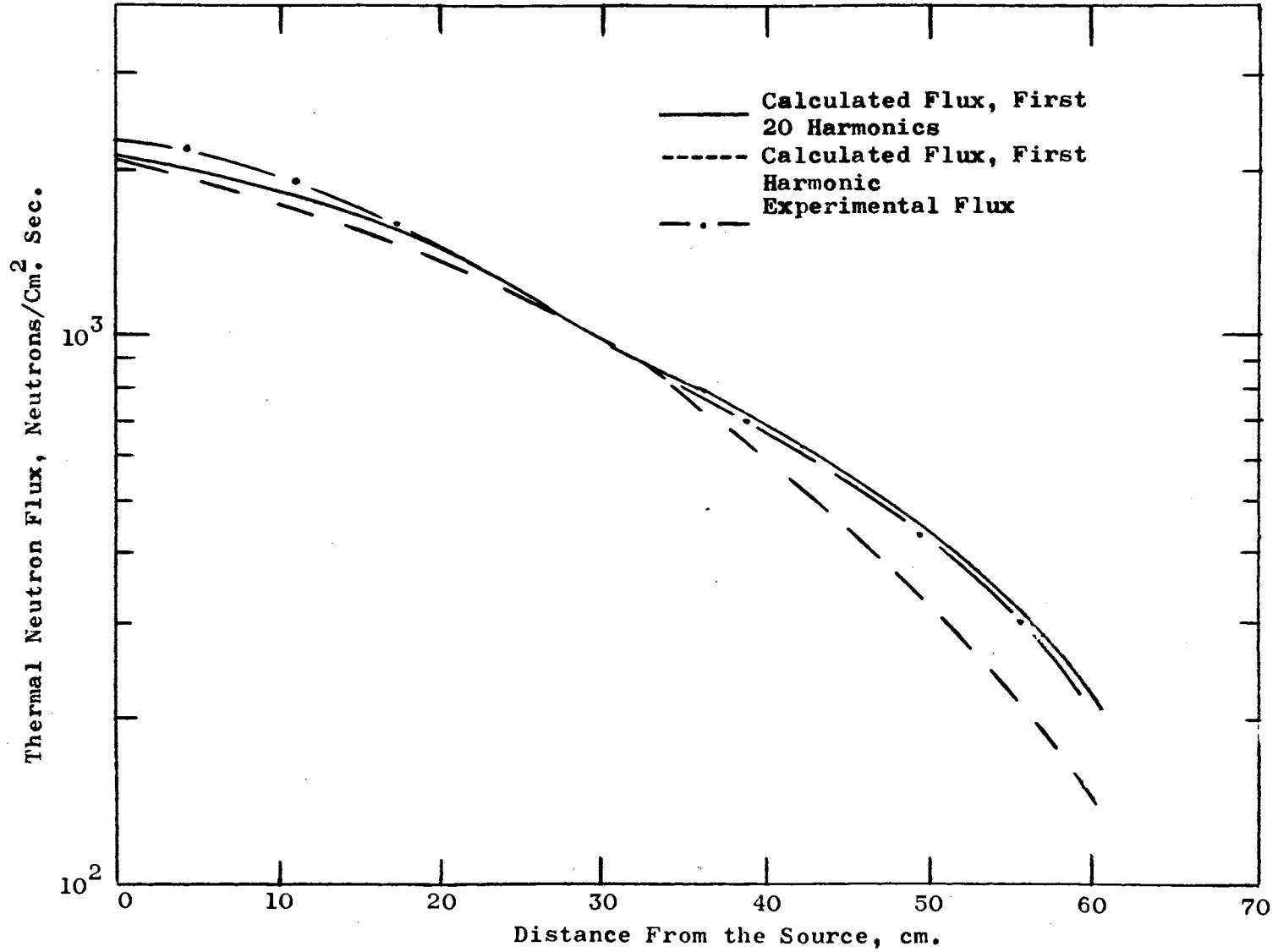
Figure 19. Calculated Neutron Fluxes at $r/R = 0.388$ for Combinations of the Thermal Source Model with the Fast Source Models.
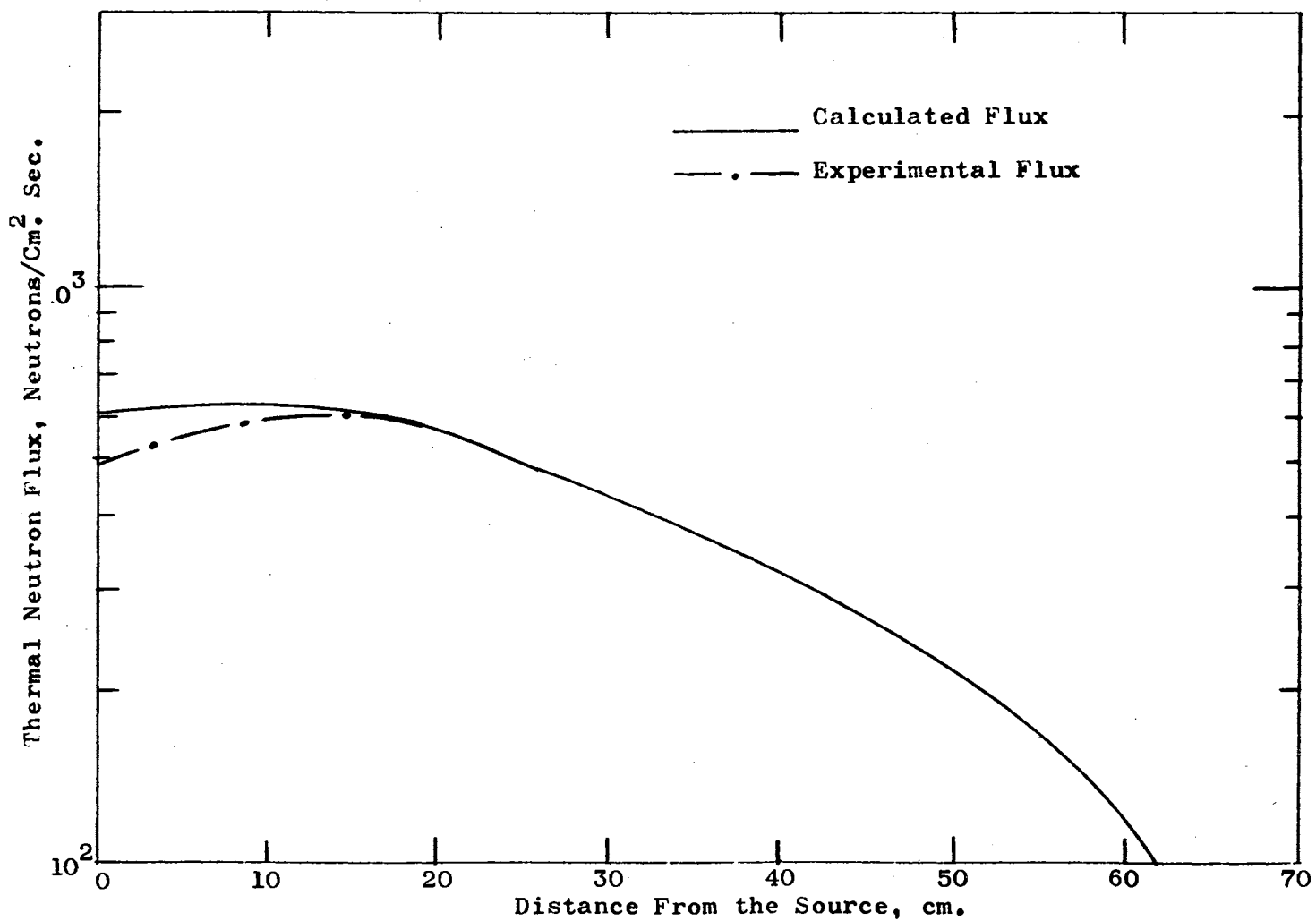
Figure 20.   Calculated Neutron Fluxes at r/R = 0.666 for a combination
of a Thermal Source Model with a Multi-energetic Source Model.
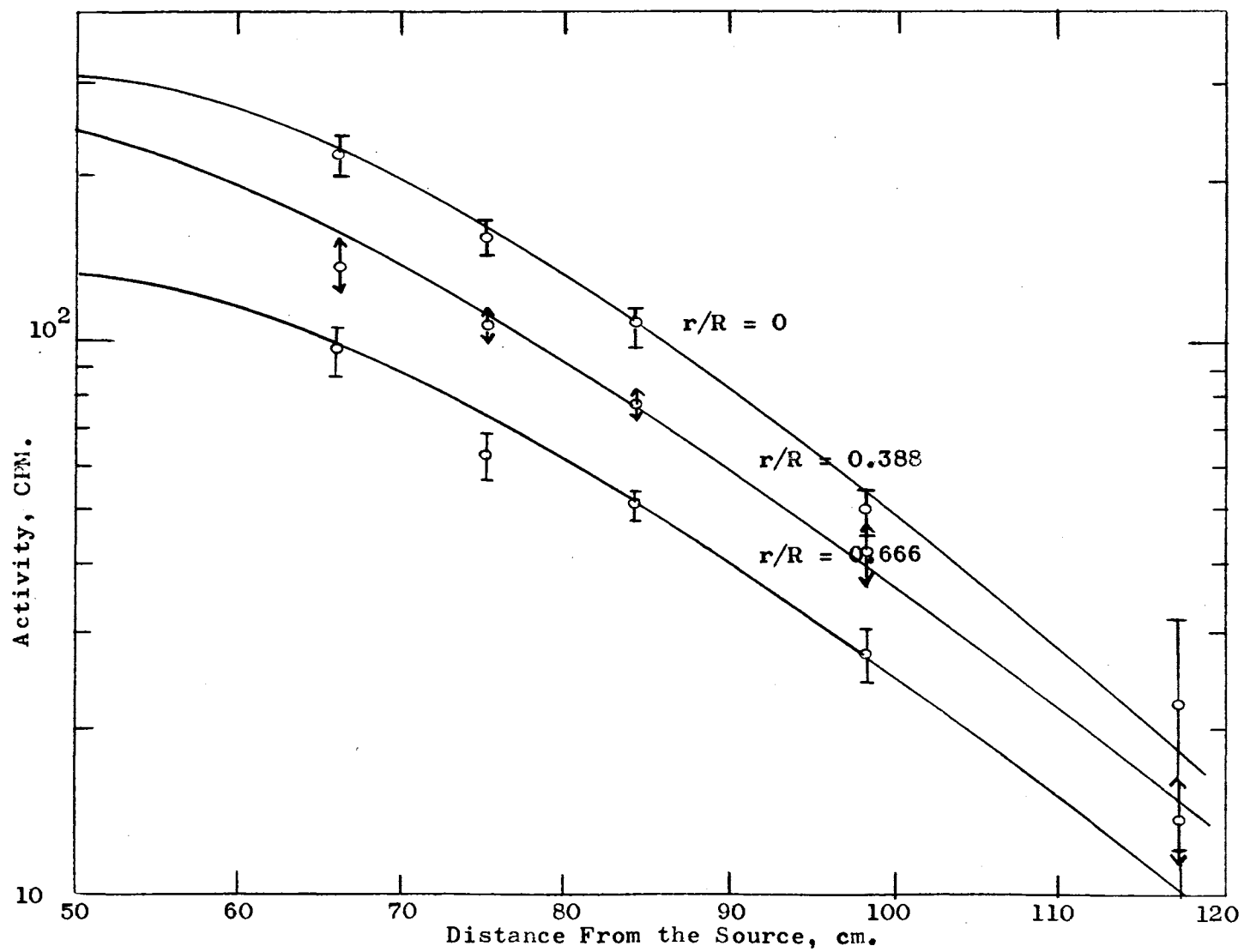
Figure 21.   Experimental Activities of the Bare Indium Foils
Irradiated in the Parallelepiped Section of the
Graphite Pile.
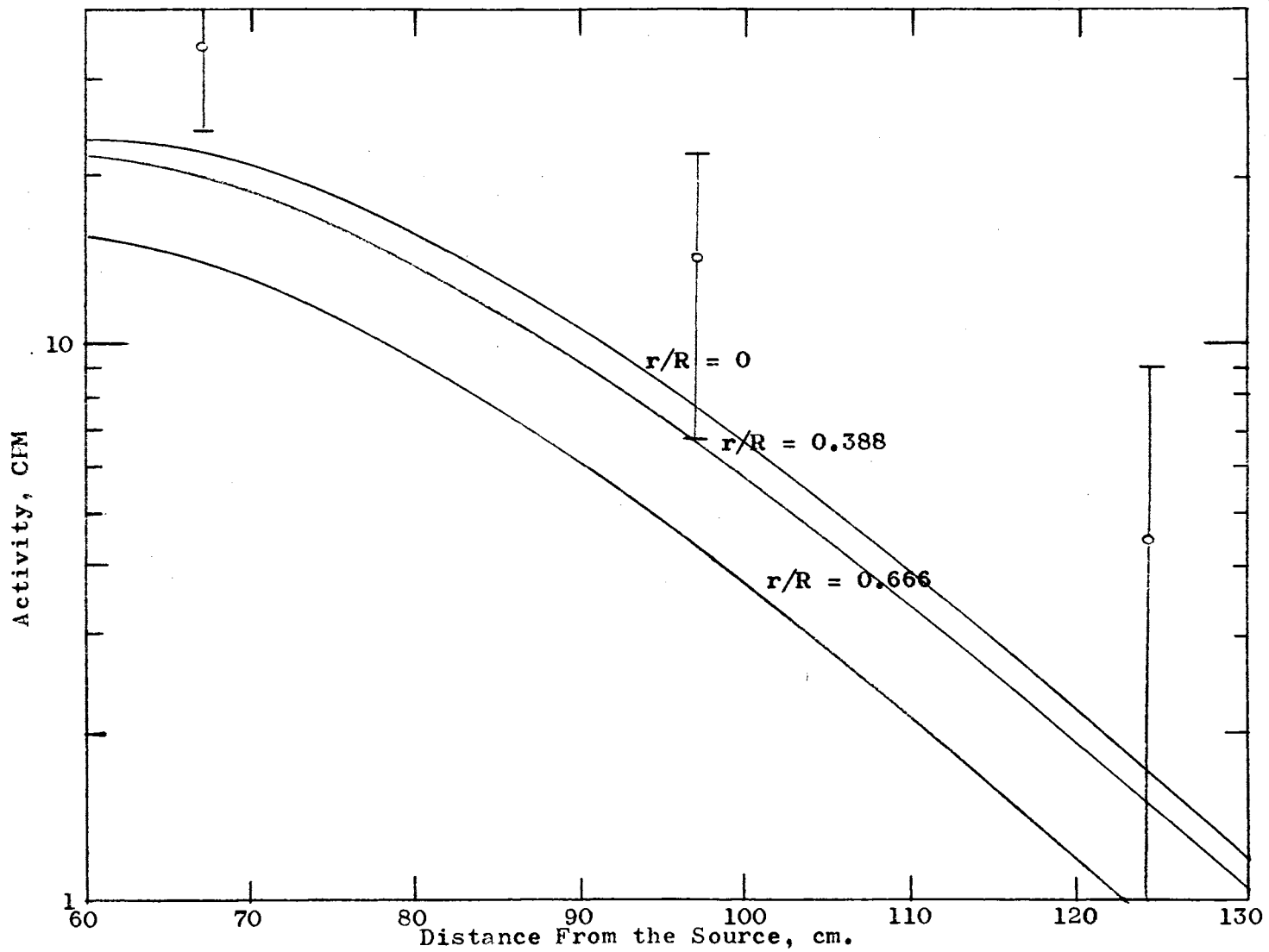
Figure 22.   Corrected Saturation Activities of the Cd Covered
Foils Irradiated in the Parallelepiped Section of
the Graphite Pile.
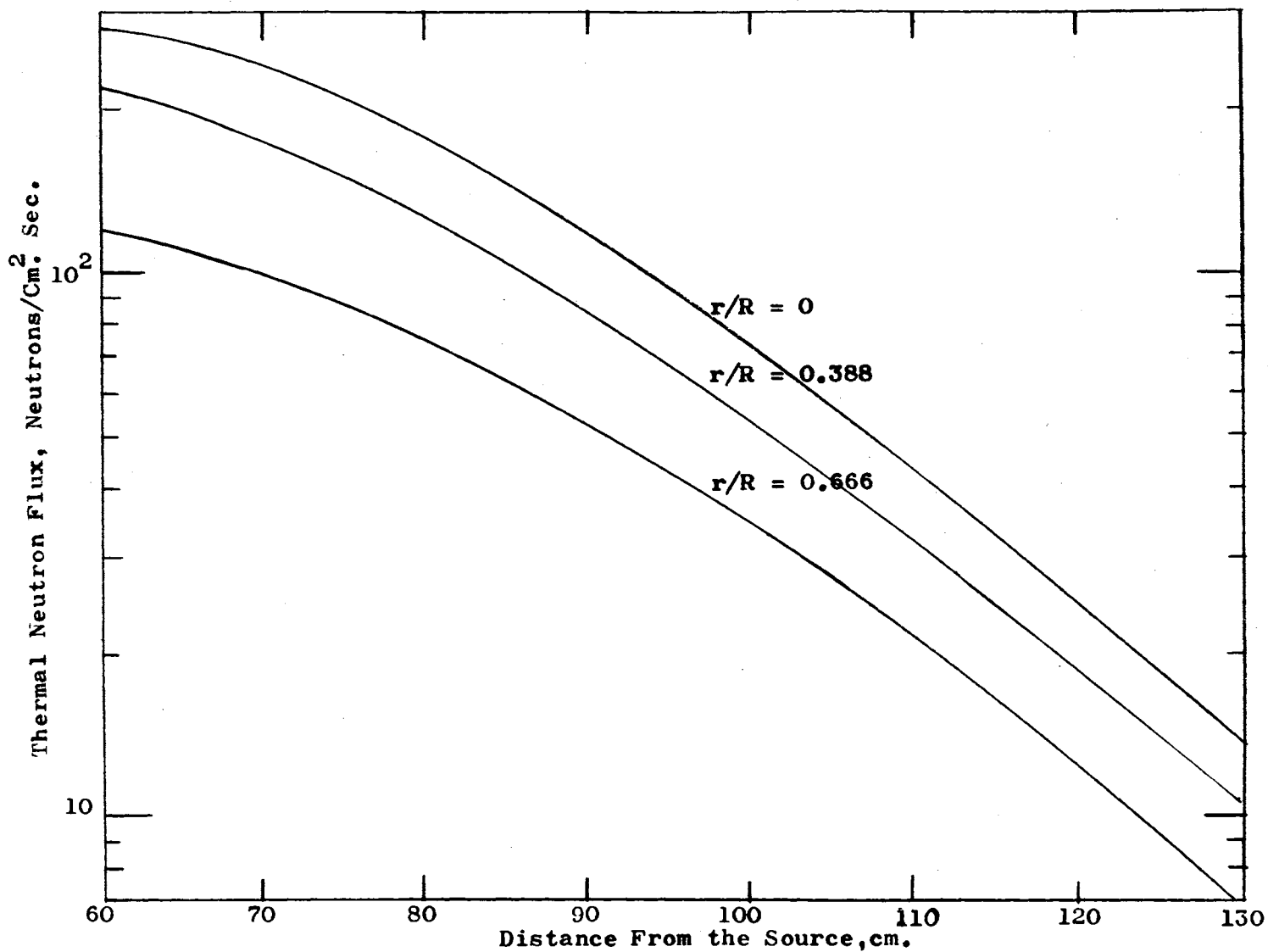
Figure 23.   Thermal Neutron Fluxes in the Parallelepiped
             Section of the Graphite Pile.

ence in the solutions occurs at large distances from the source. Here the second and third Gaussian ranges contribute largely to the slowing - down. Figures 19 and 20 give the comparisons between the experimental data with the theoretical flux at radial distances of r/R equal to 0.338 and 0.666 respectively. The theoretical flux was predicted from the same combination of a thermal point source with a fast source as determined previously for the center rod.

In Figure 19 the theoretical flux using a mono-energetic fast source and a multi-energetic fast source, each in combination with the thermal source, are presented. Figure 20 uses only the theoretical flux from a combination using a fast source of neutrons of three Gaussian ranges and a thermal source.

With the exception of data near the boundary between the cylinder and shield, the experimental data very closely follow the theoretical flux. The depression may arise from the inadequacy of diffusion theory near the boundary between dissimilar materials. It is also seen that at large distances from the source the mono-energetic source deviates somewhat from the experimental data just as it did for the center rod.

Thermal Neutron Flux Distribution in the Parallelpiped Section of the Graphite Pile

The plots of the activities of bare indium foils irradiated in the parallelpiped section are presented in Figure 21. These plots are for rods number one, two and three at radial distances of r/R equal to zero, 0.388 and 0.666 respectively.

Figure 22 presents flux plots of the activities of the cadmium
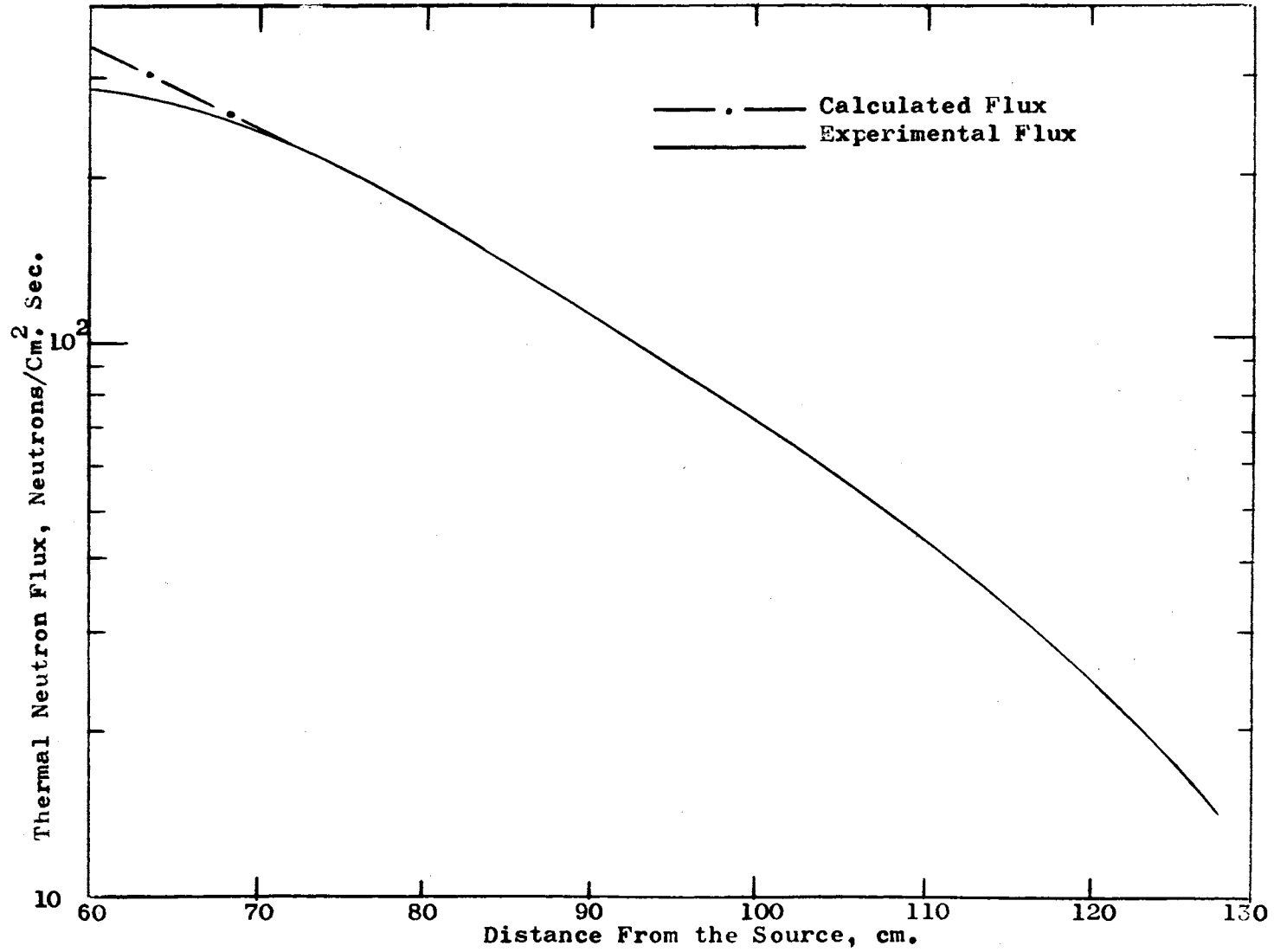
Figure 24.   Calculated Fluxes in the Parallelepiped section of
the Graphite Pile.

covered foils within the parallelpiped section of the pile. The plot for the center rod was made as accurately as possible by determining the statistical deviation of the experimental points. The best curve was then drawn through the points. The plots for the other two rods were assumed to be members of a family of curves to which the plot for the first rod belongs. The activities of the cadmium covered foils were so low that there was a large uncertainty in the measurements for the second and third rod.

Figure 23 presents the thermal neutron flux within the parellelpiped section. Figure 23 was obtained by substracting the epithermal content of the activity of the bare foils of Figure 22 from the total activity of the bare foils presented in Figure 21.

From a comparison of Figure 21 and Figure 23, it is seen that the thermal neutron flux curves are almost parallel to the plot of the activity of the bare indium foils. This was an indication that the cadmium ratio was essentially constant or that the fast neutron contribution is very small in this region of the pile. Assuming this to be true, it was seen that the thermal neutron flux could be fitted with the theoretical flux from a pure thermal neutron source model. Thus the experimental flux was fitted with the theoretical neutron flux from a thermal plane source of neutrons located at the top of the parallelpiped section.

Figure 24 shows that the experimental data taken within the parallelpiped section do follow the theoretical curve very closely. Near the source there is a deviation which is probably due to the source not being entirely a plane source of neutrons at this

point. This is due to the fact that the cylinder does not cover the entire top of the parallelpiped. However, at small distances from the top, the flux will become essentially that for a plane source of neutrons.

Extension to Measurements in the AGN-201 Reactor

Diffusion theory in combination with slowing-down theory was adequate in describing the flux distribution from the Pu-Be neutron source. The theoretical fluxes were extended to experimental measurements in an AGN-201 reactor. This was done by taking the fit of the theoretical curve with the Pu-Be source and applying the derived relationship between the two types of sources, i.e., point and plane. The theoretically predicted fluxes for the plane source were then compared with experimental data from measurements in an AGN-201 reactor.

An axial flux measurement and a radial flux measurement are given in the AGN-201 Reactor Manual (1). These measurements were taken in an AGN-201 reactor thermal column at a reactor power level of 0.1 watt. Chambers, et al., (5) present the axial flux through the core, reflector and thermal column of a five watt AGN-201 reactor. Chambers also gives the axial flux for the case with a lead shield between the thermal column and reflector and the case without the lead shield.

The cross sectional view of an AGN-201 reactor is presented in Figure 25. The core of the reactor is composed of enriched uranium oxide homogeneously dispersed in polyethylene. The polyethylene in the core will moderate the neutrons that are produced

THERMAL COLUMN

WATER SHIELD

LEAD SHIELD

REACTOR CORE
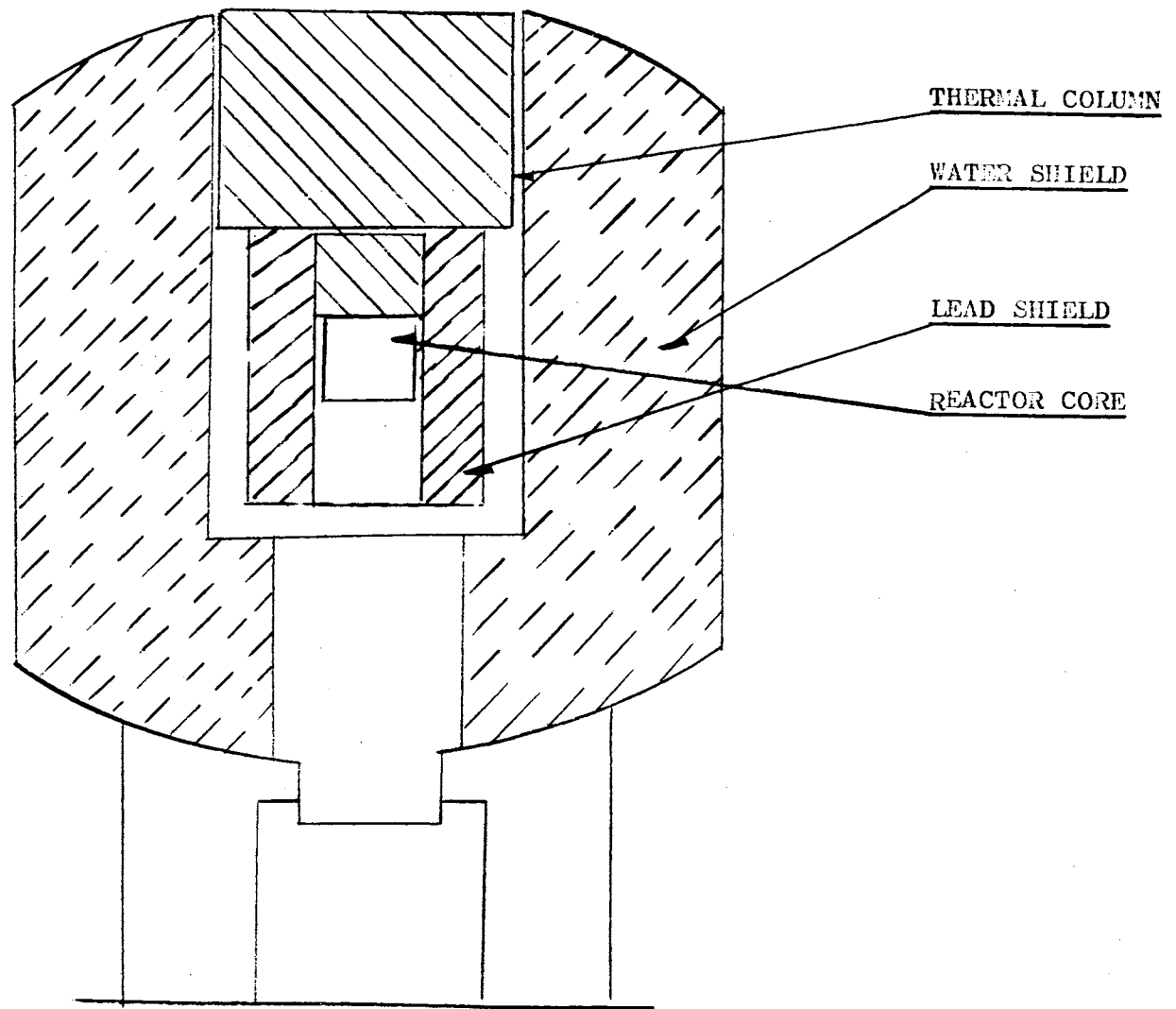
Figure 25.   Cross Section of an AGN-201 Reactor

from fission of the uranium in the same way in which the neutrons

from the Pu-Be neutron source were moderated by the polyethylene

shield. Proof of this can be seen by observing in Figures 26

and 5 the gradient of the flux. In Figure 26, the slope of the

flux curve is much steeper near the core than would be predicted

with a pure fast source. Figure 27 presents a fit of the exper-

imental data with the fast plane source obtained from the mono-

energetic fast source model of neutrons.

The reflector of the reactor is composed of graphite in the

shape of a cylinder. The outer edge of the reflector has a layer

of lead for shielding of the core. With a layer of lead present,

it is impossible to establish theoretically the point where the

radial flux would be extrapolated to zero. The extrapolation

distance is needed to determine the relaxation length, γ , for the

reflector. Figure 26 shows that there is no break in the thermal

neutron flux at the interface between the graphite reflector and

the thermal column. Figure 26 was reproduced from Chambers (5).

This Figure indicates that it can be assumed that the reflector

with the lead shield at the edge will be equivalent to a cylinder

of a radius equal to the radius of the thermal column. If the re-

laxation length did change due to the difference in the radius,

there would be an indication of this change by a change in slope

between the reflector and the thermal column.

The thermal column of the reactor is of graphite in the shape

of a cylinder. In some cases, there is a lead shield between the

thermal column and the reflector. This shield is used to reduce

the gamma radiation from the core. Curve one in Figure 26 is for the case without the lead shield and curve two is for the case with the lead shield.

Measurements reported in the AGN-201 Reactor Manual using cadmium covered foils irradiated in the thermal column indicate that within the thermal column the cadmium ratio is constant. Where this condition exists, it has been shown that the thermal source theory is adequate in predicting the neutron flux (10). Figure 27 shows that within the thermal column the flux is accurately predicted by a thermal source model.

Figure 27 shows also that, within the thermal column, the flux is accurately determined by a mono-energetic fast source located at the top of the core. This is an illustration of the fact cited in Glasstone, et al., (10) that at large distances from a fast source the flux would be almost identical to that from a thermal source.

Since there are no experimental measurements in a parallel-piped section above a cylindrical column available, it was not possible to verify the prediction that the flux from the plane source is a constant times the flux from the point source. However, the following analysis of the available data indicate that this is the expected flux from the reactor. The harmonic content is negligible at the interface between the cylinder and parallelpiped section as can be seen from Figure 9. This, in addition to the above fit of the experimental data in the thermal column to a thermal source model, indicates that the source con-
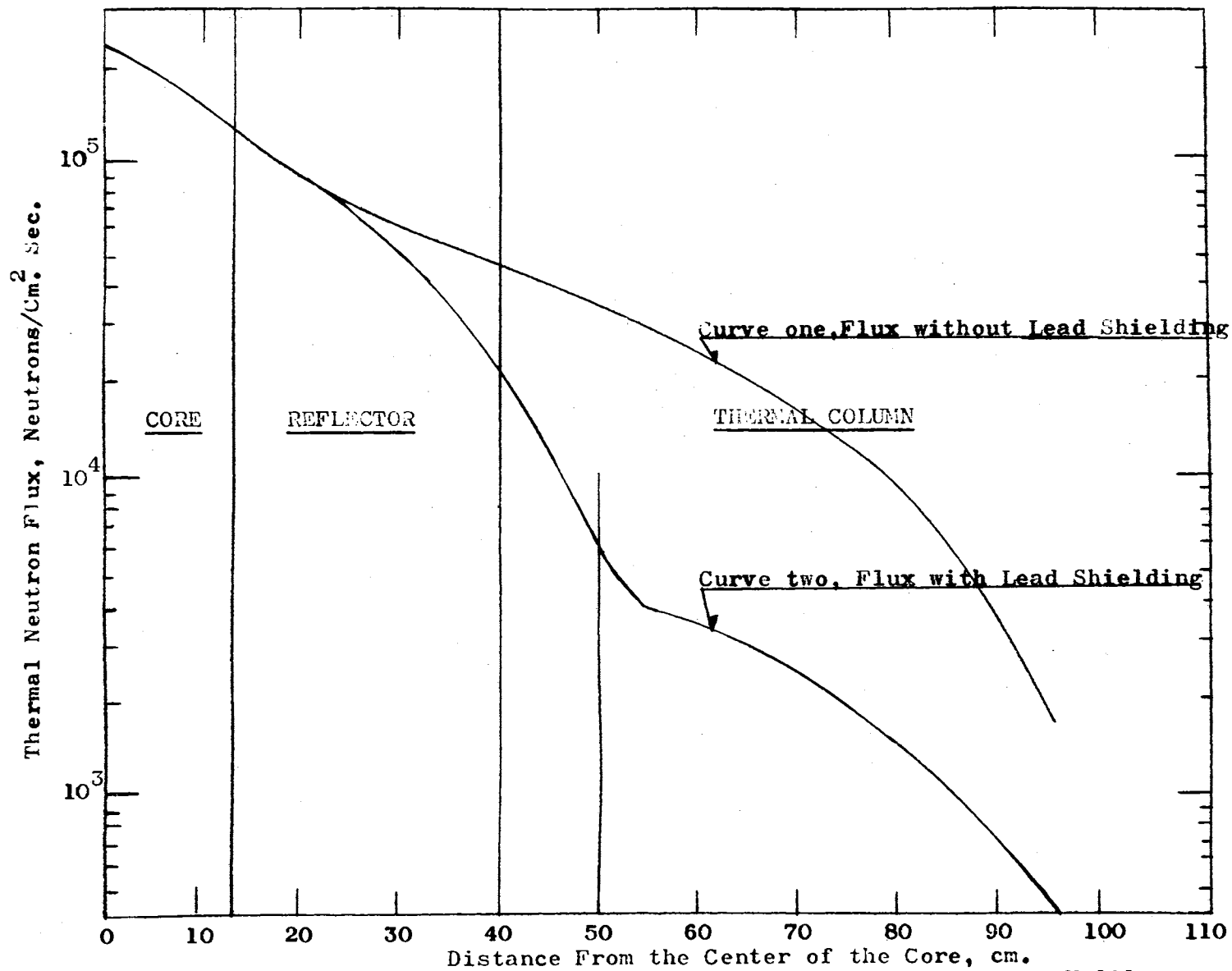
Figure 26. Experimental Fluxes in a Thermal Column of an AGN-201 Reactor.
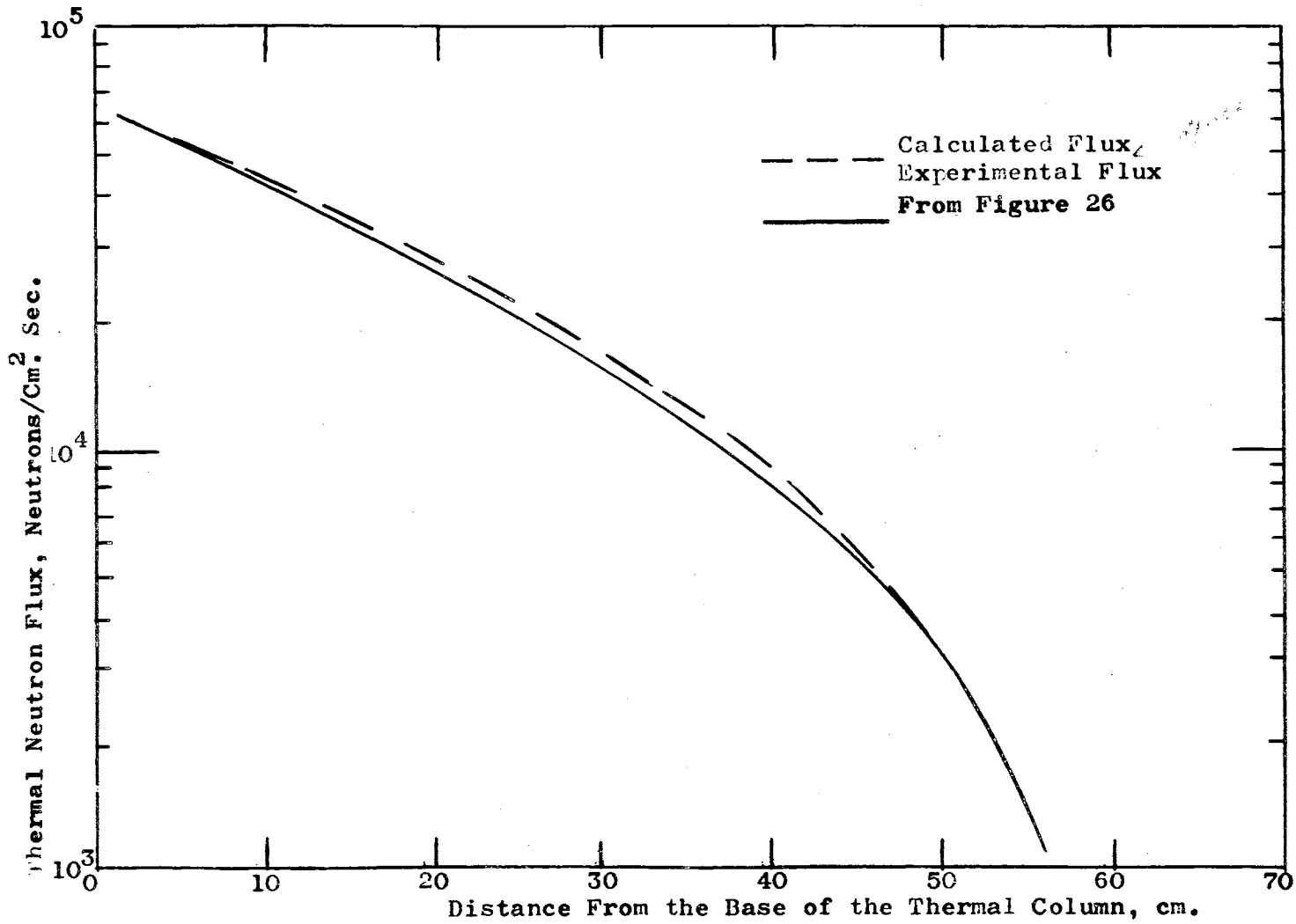
Figure 27.   Calculated Fluxes From a Plane Source of Neutrons.
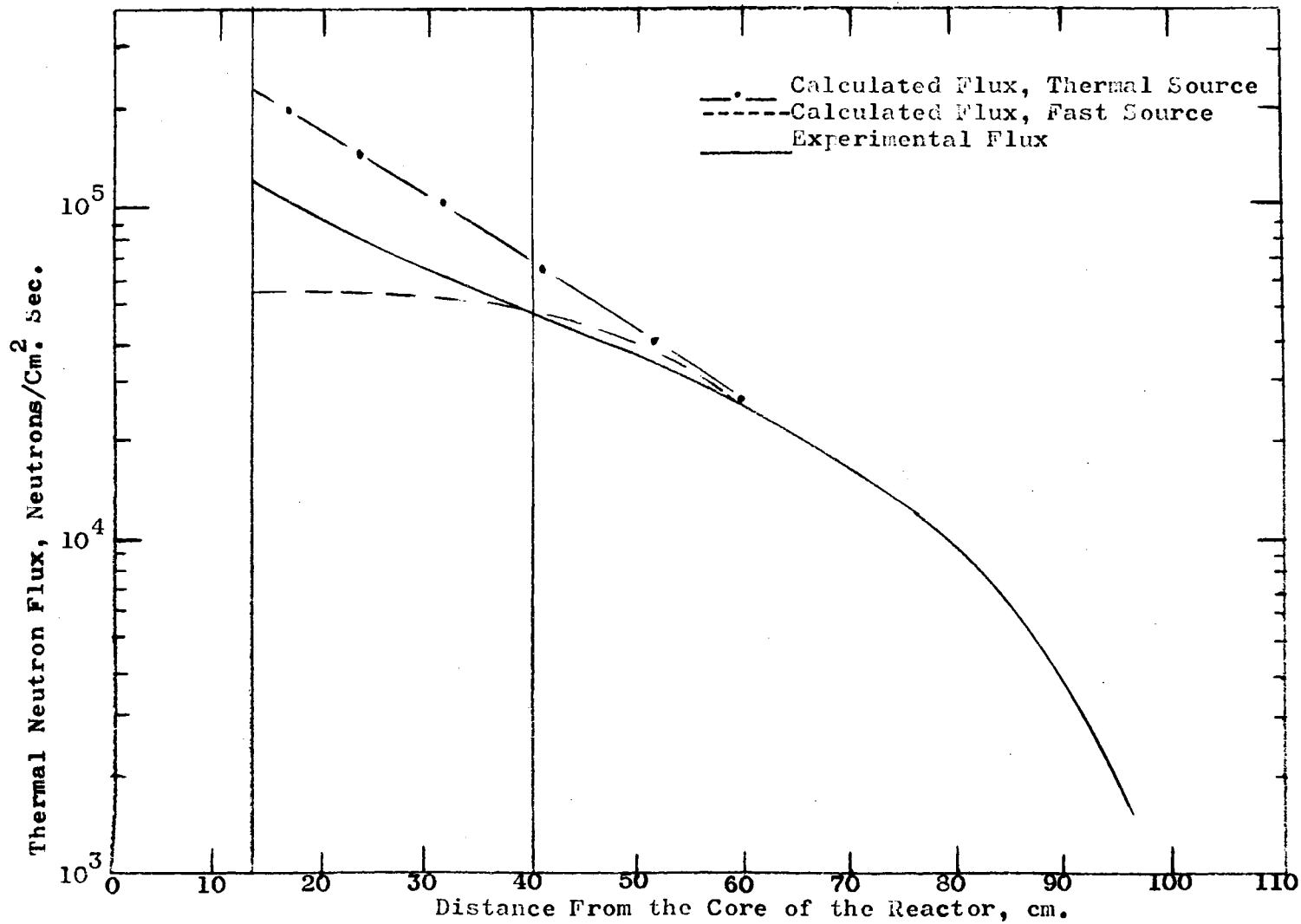
Figure 28. Calculated Neutron Fluxes From Both a Thermal Source and a Mono-energetic Source at the Core of the Reactor.

dition will be that for a thermal source in both cases. The difference will be due to the respective source strengths.

Figure 28 shows that the thermal model extension is very inadequate within the reflector. Since the Fermi age of fission neutrons in graphite is much less than the neutrons from the Pu-Be neutron source, the thermal source model becomes applicable at distances nearer to the source than was true for the Pu-Be source. Figure 28 also shows that within the thermal column the thermal source theory is a very good model.

Figure 28 also shows that the extension of the fast point source model to the AGN-201 reactor is inadequate near the core. Here the fit is very good at large distances from the source. For measurements in the thermal column the extension is very good and is much better than the thermal source extension.

A combination of a plane thermal source and a plane fast source model should be able to determine an accurate fit to the experimental data from an AGN-201 reactor. However, since the fit requires an experimental determination of the contribution to the neutron flux measurements due to the different source models, it is not possible to make a quantitative extension to the axial flux measurements made with the Pu-Be neutron source. Qualitatively the curve is as was predicted from the measurements with the Pu-Be neutron source. Here the flux near the core is rapidly decreasing indicating a thermal component to the flux and then a gradual leveling off indicating the contribution of fast neutrons.

Figure 29 shows the fit of the experimental neutron flux in
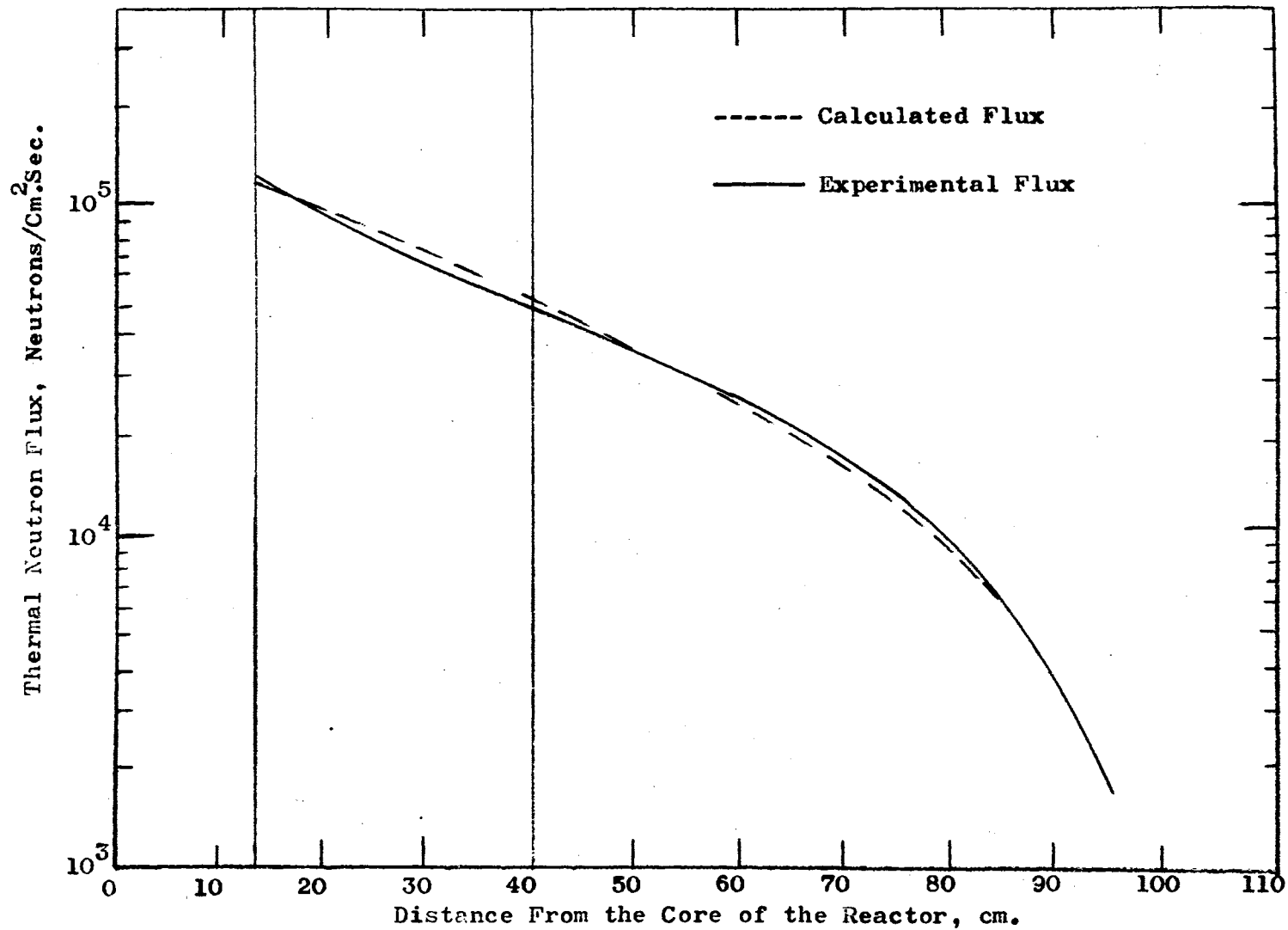
Figure 29. Calculated Neutron Fluxes From a Combination of a Thermal Source and a Mono-energetic Source at the Core of the Reactor.

an AGN-201 reactor with the theoretical combination of the fast

plane source and a thermal source model. The fit was not found by

an extension of the flux from the Pu-Be neutron source but is pre-

sented here to show that the combination of the source models will

describe the flux from an AGN-201 reactor. The contribution of

the different models was found by finding the best fit to the exper-

imental data. The agreement with theory of the experimental data

is very good. There are, however, deviations from the theoretical

curve, but this might be anticipated due to the complicated ar-

rangement of the reactor.

An accurate extension of the flux measurements with the Pu-Be

neutron source to measurements in the AGN-201 reactor could not be

found. However, it was shown that diffusion theory can accurately

predict the flux from both the Pu-Be neutron source and an AGN-201

reactor. Also, it was shown that within the thermal column of the

reactor the extension of the measurements is very good. Although

not experimentally verified, it was shown that the measurements

with the Pu-Be neutron source made in the parallelpiped section of

the graphite pile can be extended to measurements in a similar sec-

tion using an AGN-201 reactor source.

Justification of the Theoretical Combination of the Thermal Model

and Fast Source Model

An attempt was made to justify superpositioning of the sol-

ution for a fast neutron source with the solution for a thermal

source model. It was noted from results in several references (6,

13, 7) that the effect of an additional thermal source was not

evident in any of their measurements with the Pu-De neutron source.
If an analysis of the geometry of the graphite pile is made, it
will be noted that the polyethylene is a hydrogenous material which
will moderate the fast neutrons from the source much faster than
would graphite. Therefore, the increase in the number of neutrons
near the source would have the same effect as that of an addi-
tional thermal source of neutrons.

If a sheet of cadmium is placed between the source and the
graphite pile, the cadmium will absorb all the thermal neutrons
that have been thermalized by the polyethylene. The cadmium sheet
will also absorb neutrons that have been thermalized within the
graphite pile that have been returned to the cadmium by diffusion.
This will create a different boundary condition than had been pre-
viously postulated for the case without the cadmium sheet. This
boundary condition is that the thermal neutron flux must be zero
at the origin where the cadmium is located.

It also will be noted that, previously, boundary conditions
were used such that the flux was zero at $\rho = 0$, where ρ is the
airline distance from a point to the source. Therefore, along the
central z axis, this will be identical to the condition that the
flux be zero at z = 0, since $\rho = \sqrt{z^2 + r^2}$, where for the central
axis r = 0.

With the boundary condition that the neutron flux is zero at
z = 0, a flux peak will occur at some point in the positive z
direction.

The position of the thermal flux peak from the origin is a
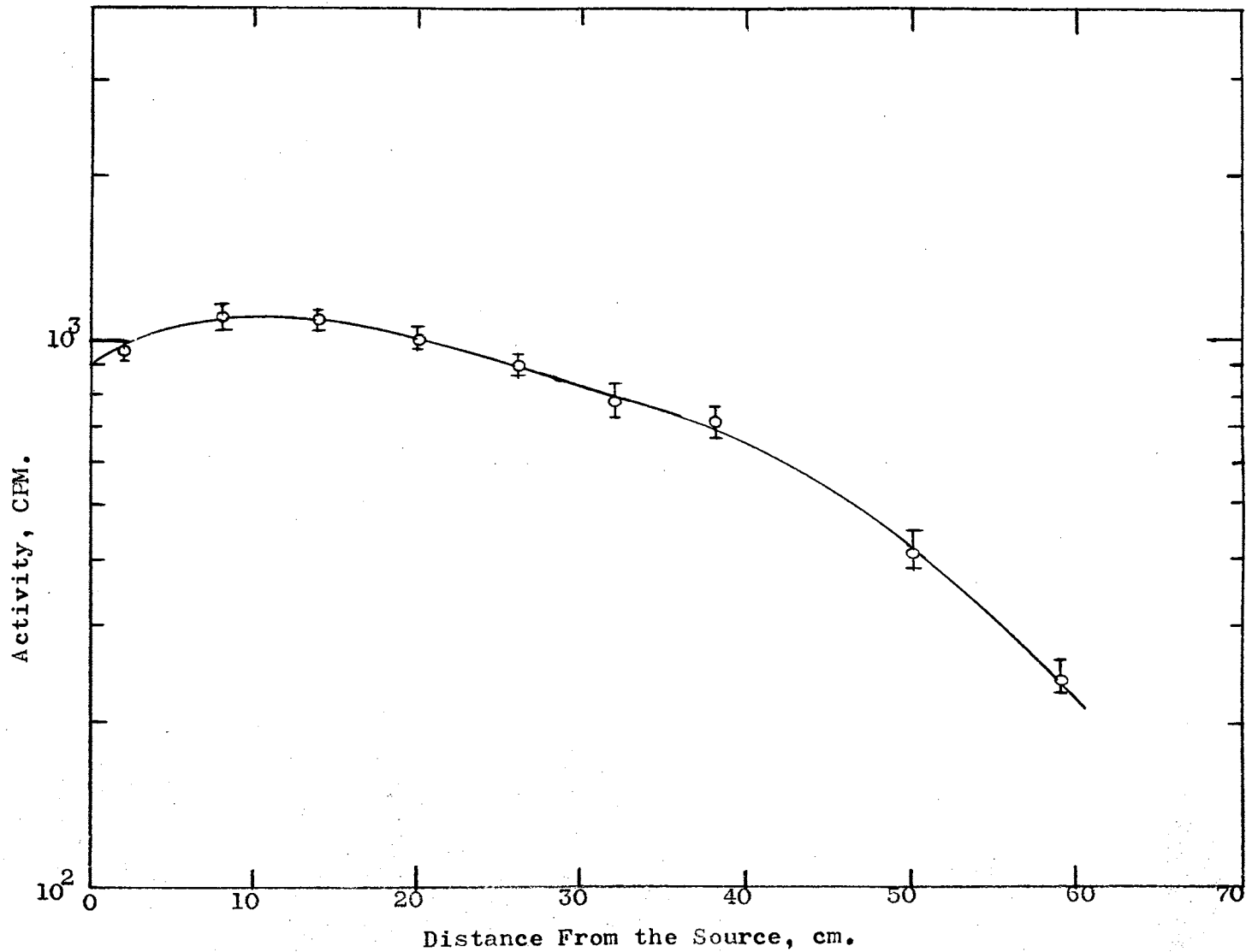
Figure 30. Experimental Activities of Bare Indium Foils Irradiated in the Graphite Cylinder with a Cd Sheet Between the Source and the Cylinder.

measure of the thermal component of the neutron source. This fact comes from the source term of the diffusion equation for the fast source case being dependent on the distance from the source. The source term will in effect decrease the flux gradient. The decrease in the flux gradient will cause a flattening of the flux and delay the peak to larger values of z than would be true for a thermal source.

The width of the peak will also give a measure of the number of thermal neutrons from the source. This also comes from the flux flattening due to the decrease in the flux gradient for the fast source case. From a point source of thermal neutrons a sharp and narrow peak will be present; whereas with a fast point source of neutrons, the peak will be broad and flat.

Figure 30 gives a plot of the experimental activity for bare indium foils obtained with a sheet of cadmium between the source and the graphite pile. Figure 31 is a plot of the corrected activity of the cadmium covered foils with the cadmium sheet present. Figure 31 was obtained from two experimental measurements and the fact that the cadmium sheet should absorb only neutrons below a certain energy. The cadmium foils previously used without the cadmium sheet should also absorb neutrons below the same energy. Therefore, the spectrum of the neutrons above this energy would be unchanged by the presence of the cadmium. The slowing-down density should then be the same for both cases, with and without the cadmium sheet. Taking into account the possibility of reduction of the number of fast neutrons deflected away from the pile
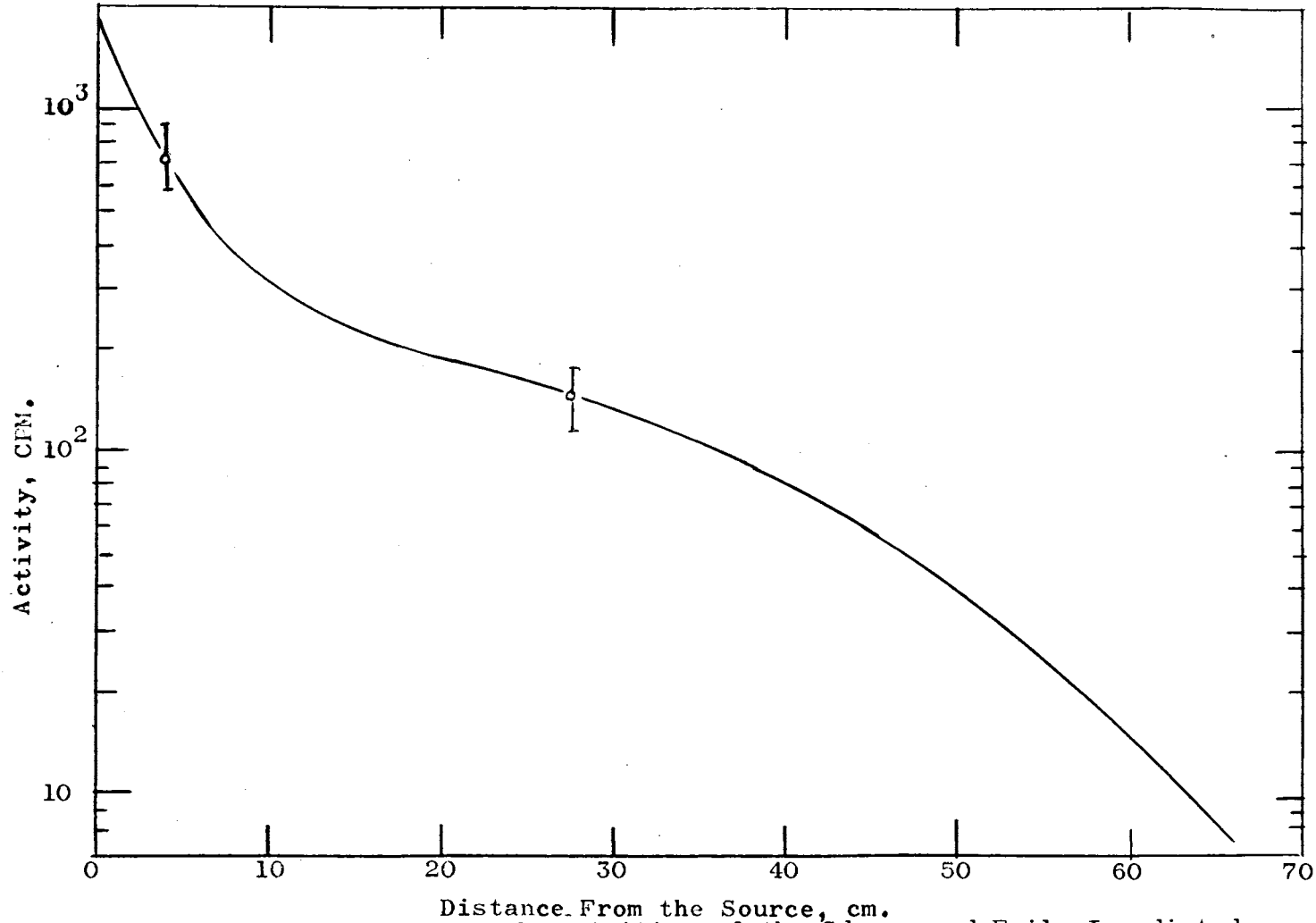
Figure 31. Corrected Activities of the Cd-covered Foils Irradiated
in the Graphite Cylinder with a Cd Sheet Between the
Source and the Cylinder

by the cadmium, the two experimental measurements do fall on the curve previously determined without the cadmium sheet. This curve was accurately determined for the case without the cadmium sheet.

In Figure 32, the activities due only to the thermal neutrons are presented. This thermal activity is found by subtracting the activity of the cadmium covered foils of Figure 31 from the activity of the bare foils in Figure 30. Also in Figure 32 the previously determined thermal flux for the case without the cadmium sheet is presented for a comparison.

From Figure 32, it was evident from the position of the peak that the assumption of a thermal component of the source was valid for the case without the cadmium sheet. The peak for the case without the cadmium is indeed nearer to the source. Also it is seen from the flatness of the curve in the case with the cadmium sheet, as compared with that for the case without the sheet, that the original case without the sheet does have a significant thermal component near the source.

Figures 33 and 34 show a comparison for the fluxes from experimental data with the theoretically predicted curves from a fast point source of neutrons. Figure 33 uses the theoretical flux from a mono-energetic fast source. Figure 34 uses the theoretical flux from a fast source incorporating three Gaussian ranges. Comparison of Figure 33 and Figure 34 further bear out the fact that for the single Pu-Be neutron source the multi-energetic assumption is better than the mono-energetic assumption.
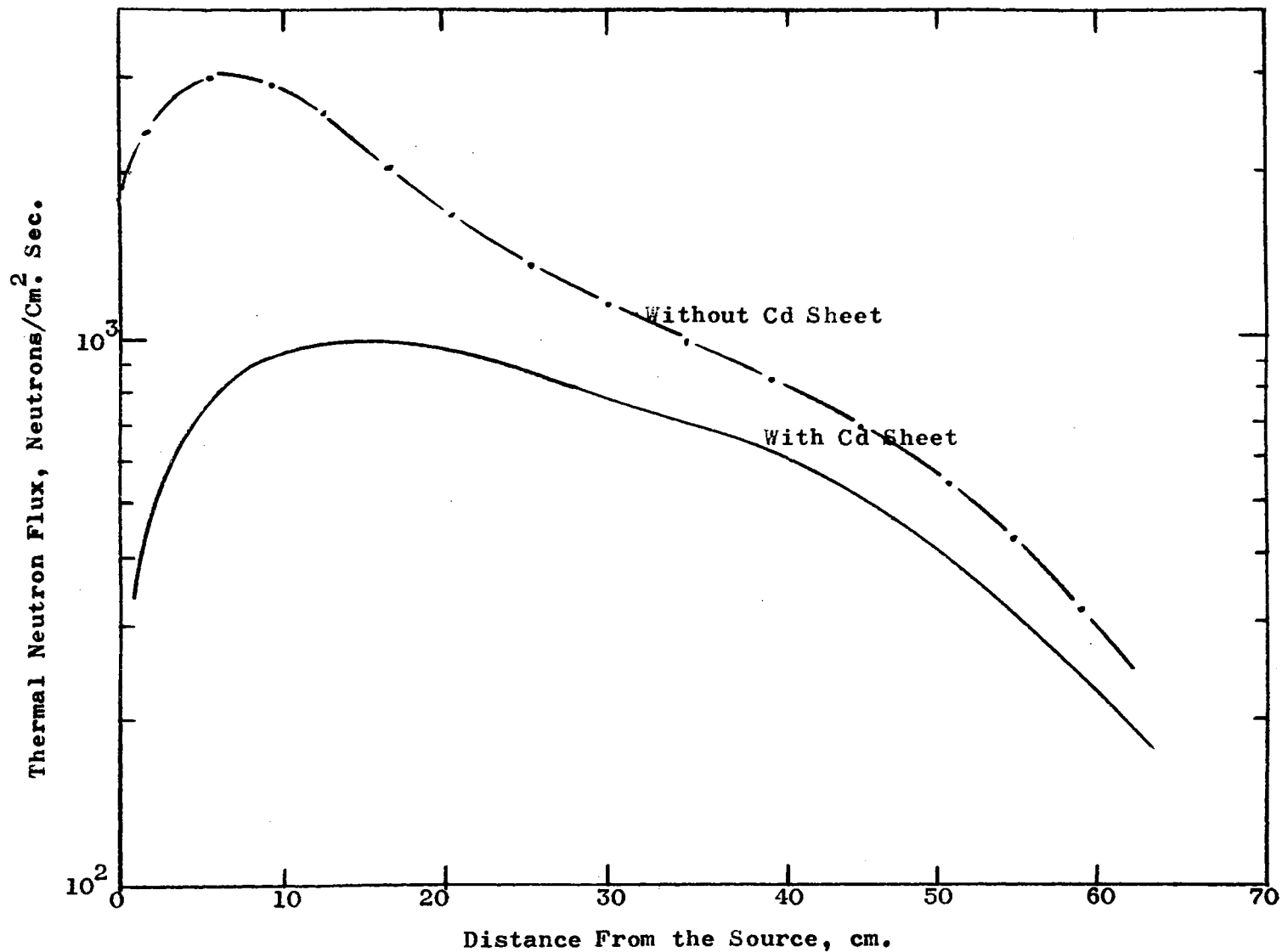
Figure 32. Thermal Neutron Fluxes in the Graphite Cylinder with a Cd Sheet between the Source and Cylinder.
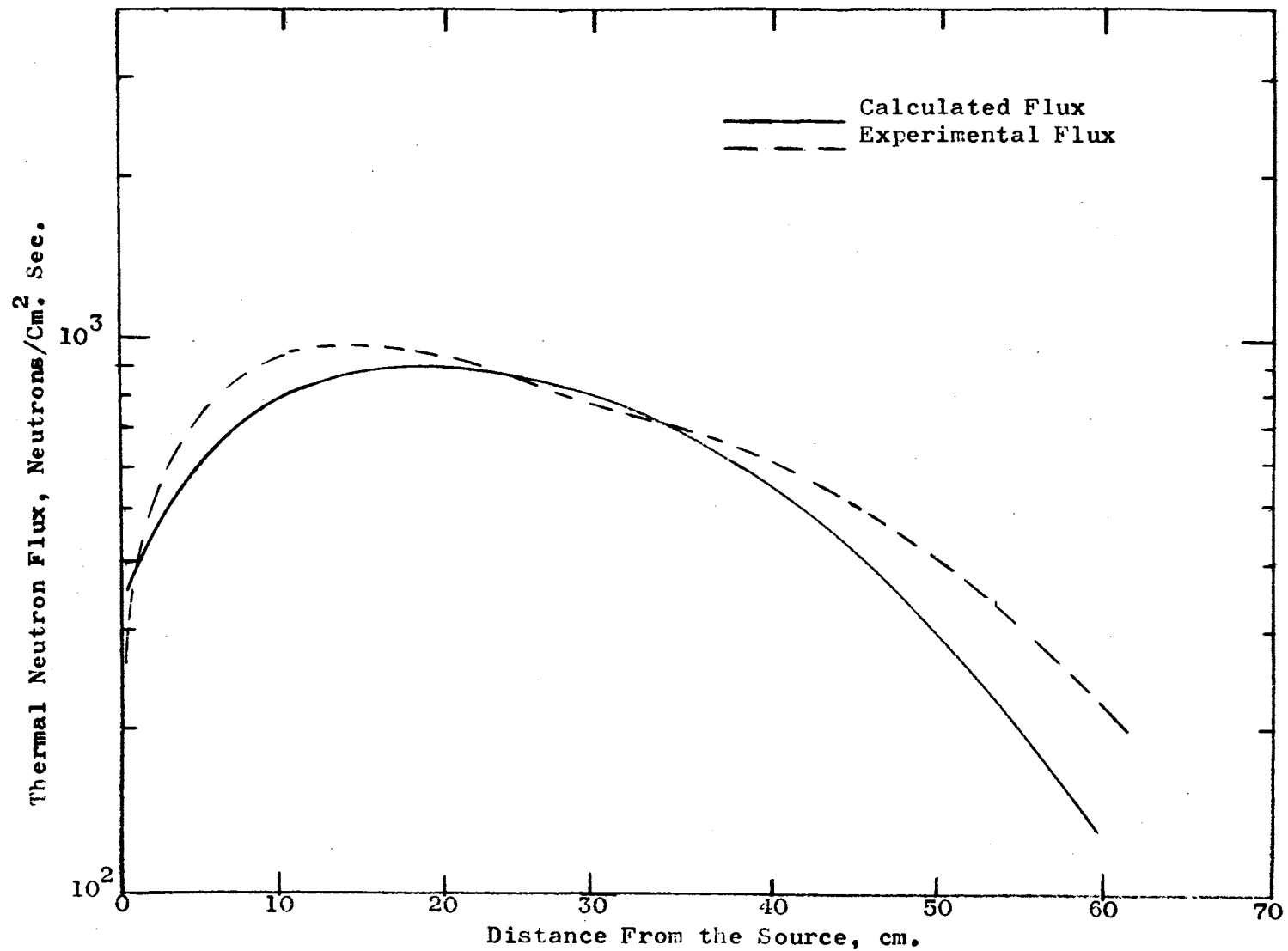
Figure 33. Calculated Neutron Fluxes for a Mono-energetic Source for the Case with a Cd Sheet Between the Source and the Cylinder
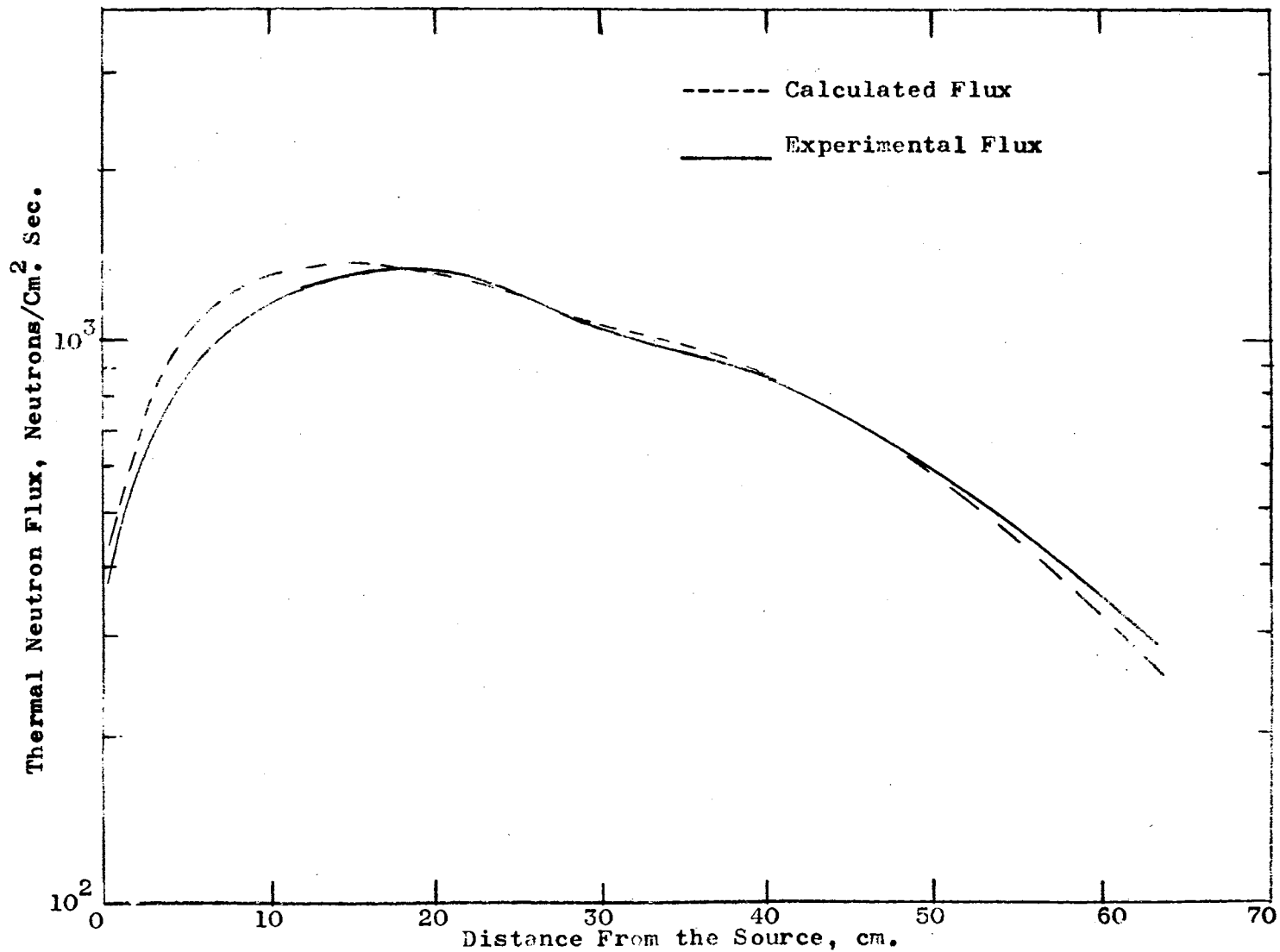
Figure 34. Calculated Neutron Fluxes for a Multi-energetic Source for the Case with a Cd Sheet Between the Source and the Cylinder.

BIBLIOGRAPHY

1. Anonymous, "AGN Reactor Manual", San Ramon, California
      Aerojet General Nucleonics (1957).

2. Anselone, P. M., "Distribution of Thermal Neutrons from Fast
      Sources in Exponential Piles", U. S. AEC Report
      HW-31925 (1954).

3. Baxter, W. V., "IBM-650 Subroutines", U. S. AEC Report
      DP-124 (1955).

4. Bothe, W. Z., Z. Physik, 120, 437-440 (1940).

5. Chamber Jr., F. W., and J. W. Duckworth, "The AGN-201M
      Reactor Thermal Column", Radiology 71, pp 868-870 (1958).

6. Curtis, L. F., An Introduction to Neutron Physics, Trenton,
      New Jersy, D. Van Nostrand Co. (1959).

7. Davenport, D. E., and E. Z. Block, "Variation of Diffusion
      Length with Sigma-Pile Size", U. S. AEC Report
      HW-30422 (1953).

8. Dwight, H. B., Tables of Integrals and Other Mathematical
      Data, New York, New York, The Macmillian Company (1957).

9. Foulke, L. R., "KSU Pile Standardization and Study of Slowing
      Down and Diffusion Models", Kansas State University
      Bulletin 45, 5 (1961).

10. Glasstone, S. and M. C. Edlund, The Elements of Nuclear
      Reactor Theory, New York, New York, D. Van Nostrand
      Co. (1952).

11. Jahnke, E. and F. Emde, Tables of Function with Formulae and
      Curves, New York, New York, Dover Publications (1945).

12. Kaiser, R. E., "Experimental and Theoretical Investigation of
      the Determination of the Diffusion Length of Thermal
      Neutrons in Graphite", Kansas State University Bulletin
      46, 1 (1962).

13. Kimel, W. R., "Proceedings of the University Subcritical
      Assemblies Conference", U. S. AEC Report TID-7619 (1961).

14. Lapp, R. E. and H. L. Andrews, Nuclear Radiation Physics,
      2nd Edition, Englewood Cliffs, New Jersey, Prentice Hall,
      Inc. (1959).

15. Murray, R. L., _Nuclear Reactor Physics_, Englewood Cliffs, New Jersey, Prentice Hall, Inc. (1959).

16. Ritchie, R. H., and H. B. Eldridge, _Nuclear Science and Engineering_ 8, pp 300-311 (1960).

17. Skyrme, T. H. R., "Reduction in Neutron Density Caused by an Absorbing Disc", U. S. AEC Report MS-91 (1951).

18. Tittle, C. W., "Slow-Neutron Detection by Foils", _Nucleonics_ 8, no. 6, pp 5-11 (1951).

19. Weinberg, A. M., and E. P. Wigner, _The Physical Theory of Neutron Chain Reactors_, Chicago, Illinois, The University of Chicago Press (1958).

APPENDIX A

EXPERIMENTAL DATA

Data Reduction

All counting data were corrected for background and reduced to a saturation counting rate. With the exception of the data for the intercalibration of the foils, all counting data were corrected with the computer program presented in Appendix D.

Most measurements of the counting rate of the indium foils were taken over different lengths of time. For a comparison of the activities, the counting rate was then corrected to the activity at removal from the neutron flux. The computer program made this correction with the following equation:

$$A_o = \frac{C_t}{e^{-\lambda t_1} - e^{-\lambda t_2}} \qquad (A - 1)$$

where A_o is the activity at removal, C_t is the total counts due only to the activity of the foil measured between times t_1 and t_2, t_1 is the elapsed time after removal to the start of counting and $t_2 = t_1 +$ (counting time). The decay constant λ is equal to 0.01281/Min.

The foils in most cases had not been irradiated to saturation. The counting rates then had to be corrected to a saturation activity. This correction was made with the following equation:

$$A_o = A_s (1 - e^{-\lambda t}) \qquad\qquad (A - 2)$$

where A_s is the saturation activity and t is the irradiation time.

Table I of the Appendix presents data for the intercalibration of the foils. In this table the counts due to the background have been subtracted. The total number of counts for calibration purposes was 10,000 counts including counts due to background.

The saturation activities of the intercalibration measurements are presented in Table I. From the saturation activities, the intercalibration factors were calculated. The saturation activity of foil number one was used as the standard. These factors are presented in Table II.

Since the raw data were used as input data to the computer program, only the saturation activities from flux plotting are presented in Table III and Table IV. The raw data are presented in Appendix A. It should be noted that in Table IV the activities are for cadmium covered foils; whereas Table III is for bare indium foils.

The activities of the cadmium covered foils were corrected for flux depression due to the presence of the cadmium absorbers. Correction factors were taken from a Graph in Curtis (6). The corrected activities of the cadmium covered foils are presented in Table V.

The activity of the bare foils is due to both fast and thermal neutrons; whereas the activity of the cadmium covered foils, cor-

rected for flux depression, is due only to fast neutrons. The

difference in the two measurements will then be proportional to

the thermal neutron flux.

The determination of the neutron flux from the saturation activ-

ities incorporated Equations 30 and 31 of Chapter three. Since

$\phi = R/\sigma_{act}NA_x$, where R was shown to be C_s/ϵ ; $\phi = KC_s$, where $K = 1/\epsilon \, \sigma_{act}NA_x$.

ϵ was not known; therefore, K was assumed to be equal to one. Thus ϕ

is actually a normilized flux such that $\phi = C_s$.

TABLE I

DATA FOR INTERCALIBRATION OF INDIUM FOILS

$$z = 2 \text{ Cm.}$$

$$r/R = .666$$

Foil	C_B
1	612 ± 7
2	595 ± 7
3	605 ± 7
4	601 ± 7
5	574 ± 7
6	635 ± 7
7	632 ± 7
8	632 ± 7
9	600 ± 7
10	802 ± 7
11	740 ± 7
12	715 ± 7

TABLE II

INTERCALIBRATION FACTORS FOR INDIUM FOILS

Foil	F
1	1.000
2	1.035
3	1.053
4	1.048
5	1.067
6	1.107
7	1.102
8	1.102
9	1.044
10	1.396
11	1.290
12	1.245

TABLE III

SATURATION ACTIVITIES OF BARE INDIUM FOILS

r/R =	0		0.388		0.666	
z,cm.	C_s		C_s		C_s	
2	4496	± 50	2715	± 31	616.1	± 16.4
12	3179	± 35	2072	± 24	685.0	± 12.5
19	2292	± 38	1674	± 25	737.5	± 21.3
20	2034	± 38	1482	± 38	557.5	± 45.6
28	1513	± 20	1210	± 22	557.8	± 13.9
29	1321	± 26	1130	± 27	504.2	± 26.8
37	1204	± 21	861.5	± 11.6	389.3	± 9.4
38	1020	± 24	774.5	± 16.6	369.0	± 13.8
46	807.2	± 10.2	559.4	± 9.6	307.8	± 4.3
47	687.3	± 7.8	543.4	± 6.7	274.8	± 3.6
60	303.2	± 6.5	242.7	± 5.0	137.3	± 3.2
85.2	154.5	± 10.8	105.4	± 7.2	62.10	± 4.04
94.2	109.5	± 8.2	76.79	± 4.25	50.29	± 2.90
108.2	49.16	± 6.68	41.27	± 5.57	26.72	± 3.82
127.2	21.96	± 10.0	13.20	± 18.6	4.92	± .85

TABLE IV

SATURATION ACTIVITIES OF Cd COVERED INDIUM FOILS

$r/R =$	0		0.388		0.666	
z, cm.	C_s		C_s		C_s	
2	-----	------	400	$\pm$ 11	------	------
5	912.0	$\pm$ 35	------	------	79.4	$\pm$ 19
8	540.0	$\pm$ 15	------	------	108	$\pm$ 10
11	-----	------	292.3	$\pm$ 10	------	------
17	-----	------	240	$\pm$ 10	------	------
23	270.0	$\pm$ 9.0	------	------	105	$\pm$ 10
29	204.0	$\pm$ 15	------	------	63.9	$\pm$ 5.9
35	-----	------	105.2	$\pm$ 5.0	------	------
38	-----	------	104	$\pm$ 8.0	------	------
44	96.0	$\pm$ 6.5	------	------	57	$\pm$ 7
59	22.9	$\pm$ 4.3	------	------	12.6	$\pm$ 1.7
65	-----	------	11.5	$\pm$ 1.5	------	------
67.2	35.1	$\pm$ 12.5	7.36	$\pm$ 6.0	15.0	$\pm$ 12
97.2	14.5	$\pm$ 7.5	2.21	$\pm$ 3.0	3.18	$\pm$ 4
124.2	4.7	$\pm$ 4.3	12.9	$\pm$ 13	2.82	$\pm$ 1.8

TABLE V

CORRECTED ACTIVITY OF CADMIUM COVERED
FOILS IRRADIATED IN GRAPHITE PILE

z, cm.	$r/R = 0$ C_s		$r/R = 0.388$ C_s		$r/R = 0.666$ C_s	
2	------	------	427	± 12	------	------
5	975	± 37	------	------	85	± 19.8
8	578	± 16	------	------	117	± 11
11	------	------	314	± 10.5	------	------
17	------	------	257	± 10.2	------	------
23	289	± 9.5	------	------	112	± 10.8
29	218	± 16.0	------	------	68.4	± 6.4
35	------	------	113	± 5.3	------	------
38	------	------	111	± 8.2	------	------
44	103	± 7.0	------	------	61	± 7.8
59	24.5	± 4.8	------	------	13.5	± 1.78
65	------	------	12.3	± 1.6	------	------
67.2	37.6	± 13.2	7.9	± 6.6	16.0	± 12.2
97.2	15.5	± 8.0	2.35	± 3.2	4.06	± 4.9
124.2	5.0	± 4.7	13.8	± 14.0	3.02	± 2.0
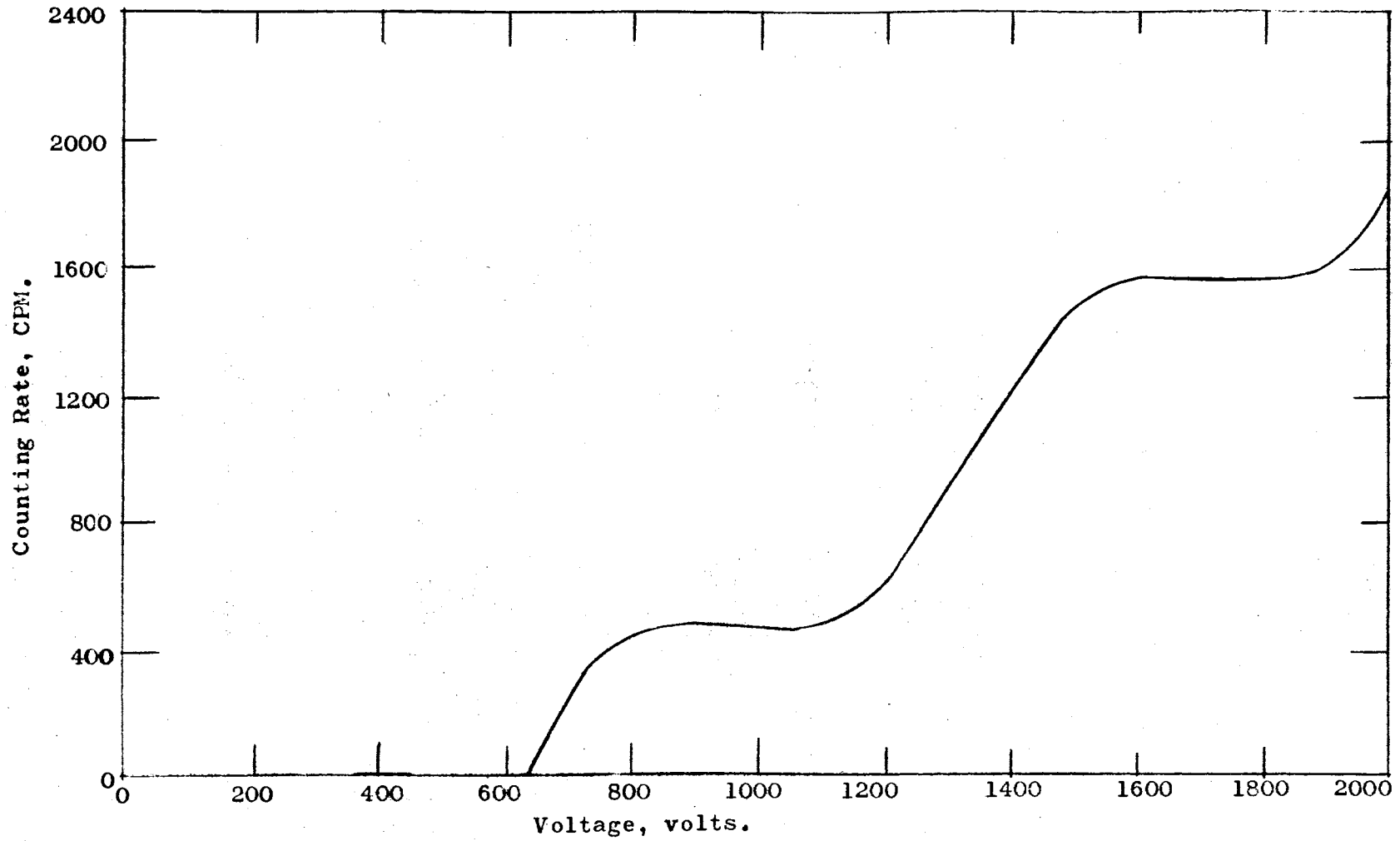
Figure 35.   Count-rate Vs Voltage for the Gas Flow Counter.

THERMAL DIFFUSION MODEL

Derivation of the Flux Distribution in Cylindrical Coordinates

Neglecting the source term due to slowing-down of fast neutrons, the diffusion equation for mono-energetic neutrons in a moderator may be written:

$$D \nabla^2 \phi - \Sigma_a \phi = 0 \qquad (A - 3)$$

or

$$\nabla^2 \phi - \frac{\Sigma_a}{D} \phi = 0 \qquad (A - 4)$$

K^2 is then substituted for the quantity Σ_a/D, where

$$\frac{\Sigma_a}{D} = \frac{1}{L^2} = K^2 \qquad (A - 5)$$

The diffusion equation then becomes:

$$\nabla^2 \phi - K^2 \phi = 0 \qquad (A - 6)$$

Using the definition of the operator ∇^2 in cylindrical coordinates, the diffusion equation becomes:

$$\frac{\partial^2 \phi}{\partial r^2} + \frac{1}{r} \frac{\partial \phi}{\partial r} + \frac{\partial^2 \phi}{\partial z^2} - K^2 \phi = 0 \qquad (A - 7)$$

This partial differential equation can be solved by the method of separation of variables. It is assumed that the flux is separable into a function of z alone and a function of r alone. Thus,

$$\phi = F(r)Z(z) \qquad\qquad (A - 8)$$

Making this substitution into the diffusion equation, the following equation is obtained:

$$\frac{1}{F}\frac{d^2F}{dr^2} + \frac{1}{Fr}\frac{dF}{dr} + \frac{1}{Z}\frac{d^2Z}{dz^2} - K^2 = 0 \qquad\qquad (A - 9)$$

From an analysis of Equation (A - 9), it is seen that the sum of the first two terms is a constant as is the third term. The first two terms are functions of r alone and the third is a function of z alone. Taking each component separately the following equations are obtained.

$$\frac{1}{F}\frac{d^2F}{dr^2} + \left(\frac{1}{Fr}\right)\frac{dF}{dr} + B_r^2 = 0 \qquad\qquad (A - 10)$$

$$\frac{1}{Z}\frac{d^2Z}{dz^2} - \gamma^2 = 0 \qquad\qquad (A - 11)$$

where B_r and γ are constants which are defined in the following manner:

$$B_r^2 + \gamma^2 = K^2 \qquad\qquad (A - 12)$$

Equation (A - 10) has the form of a Bessel's equation and the following solution:

$$F(r) = A \ J_0 \ (B_r \ r) + C \ Y_0 \ (B_r \ r) \qquad (A - 13)$$

The following boundary conditions were used to evaluate the constants;

1. $F = 0$ at $r = R$, where R is the extrapolated boundary of the cylinder.

2. F is finite at $r = 0$.

From these boundary conditions, it is seen that C must be zero and $B_r = j_n/R$, where j_n is the n'th zero of the Bessel function, J_0, for $n = 1, 2, 3, 4, \ldots \infty$

Therefore Equation (A - 10) becomes:

$$F(r) = A \ J_0 \ (\ j_n \frac{r}{R} \ ) \qquad (A - 14)$$

Equation (A - 11) has the following solution:

$$Z = C_1 \ \text{Sinh} \ (\gamma z) + C_2 \ \text{Cosh} \ (\gamma z) \qquad (A - 15)$$

The boundary condition, that $Z = 0$ at $z = c$, was used to evaluate the constants. Using this boundary condition:

$$0 = C_1 \ \text{Sinh} \ (\gamma c) + C_2 \ \text{Cosh} \ (\gamma c) \qquad (A - 16)$$

Then

$$C_1 = -C_2 \ \text{Coth} \ (\gamma c) \qquad (A - 17)$$

and

$$Z = C_2 \ \text{Cosh} \ (\gamma z) - C_2 \ \text{Coth} \ (\gamma c) \ \text{Sinh} \ (\gamma z) \qquad (A - 18)$$

or

$$Z = \frac{C_2}{\text{Sinh } (\gamma c)} \quad \text{Sinh } (\gamma c) \text{ Cosh } (\gamma z) -$$

$$\text{Cosh } (\gamma c) \text{ Sinh } (\gamma z) \qquad (A - 19)$$

Simplifying by using the identity, $\text{Sinh } (x - y) = \text{Sinh } x \text{ Cosh } y - \text{Cosh } x \text{ Sinh } y$:

$$Z = C_3 \text{ Sinh } \gamma (c - z) \qquad (A - 20)$$

where:

$$C_3 = \frac{C_2}{\text{Sinh } (\gamma c)} \qquad (A - 21)$$

Therefore:

$$\phi_n(r,z) = A_n J_0 \left(j_n \frac{r}{R} \right) \text{Sinh } \gamma_n (c - z) \qquad (A - 22)$$

where A_n is a combination of constants.

It is also seen that $\phi (r,z)$ must be the sum of all possible solutions of the equation for $n = 1, 2, 3, 4, \ldots \infty$
Thus:

$$\phi (r,z) = \sum_{n=1}^{\infty} A_n J_0 \left(j_n \frac{r}{R} \right) \text{Sinh } \gamma_n (c - z) \qquad (A - 23)$$

where A_n is a constant determined by the value of n.

For an evaluation of A_n, the flux at $z = 0$ was taken to be $\phi (r,0)$. Thus:

$$\phi (r,0) = \sum_{n=1}^{\infty} A'_n J_0 \left(j_n \frac{r}{R} \right) \text{Sinh}(\gamma_n c) \qquad (A - 24)$$

where $A'_n = A_n \sinh(\gamma_n c)$.

For evaluation of A_n, a point source of thermal neutrons was considered at the origin of the coordinate system emitting S neutonrs per second. A source of this kind can be represented $S\,\delta(r)$ at $Z = 0$. The Dirac delta function, $\delta(r)$, is defined to be zero everywhere except at r and z equal zero. At r and z equal zero it has the value of unity (10).

Glasstone gives the following conditions that are true for the Dirac delta function:

at $z = 0$
$$\delta(r)\ dr = 1 \qquad\qquad (A - 25)$$

where r is some variable. And

$$S \int \delta(r)\ dr = S \qquad\qquad S\,\delta(r)\ dr \qquad (A - 26)$$

Also

$$F(r) \int \delta(r)dr = F(o) \qquad\qquad (A - 27)$$

$\delta(r)$ satisfying the above conditions between $-\infty$ and $+\infty$ becomes $\delta(r)/r$.

Thus Equation A - 24 becomes:

$$S(r)\ \frac{\delta(r)}{r} = \sum_{n=1}^{\infty} J_o\left(j_n \frac{r}{R}\right) \sinh(\gamma_n C) \qquad (A - 28)$$

where $S(r)$ is a measure of the source strength.

The Bessel function J_o forms a complete orthogonal set in the interval $0 \le r \le R$ (10). Thus multiplying both sides of Equation

(A - 28) by $(j_n/R)^2 r\, J_0(j_n/R)$ and integrating between $r = 0$

and $r = R$, the extrapolated boundary of the cylinder, all terms

vanish except where $j_n = j_m$. Therefore:

$$S \int_0^R (\frac{j_n}{R})^2 \; J_0 \; (\; j_n \frac{r}{R} \;) \mathcal{E}(r) \; dr =$$

$$(S_n) \text{Sinh}(\gamma_n C) \int_0^R (\frac{j_n}{R})^2 r\, J_0^2 \; (\; j_n \frac{r}{R} \;) \; dr \qquad\qquad \text{(A - 29)}$$

From the definition of the Dirac delta function, the left side of

Equation (A - 29) becomes $S(\; j_n/R)^2$. The right side after integra-

tion becomes:

$$(\frac{j_n}{2})^2 \; S_n \; J_1^2 \; (j_n) \; \text{Sinh} \; (\gamma_n C) \qquad\qquad \text{(A - 30)}$$

Therefore, S_n is given by:

$$\frac{S/2}{R^2 J_1^2(j_n) \; \text{Sinh}(\gamma_n C)} \qquad\qquad \text{(A - 31)}$$

From a definition of the neutron current:

$$J_n = -D \; \frac{\partial \phi_n}{\partial z} \qquad\qquad \text{(A - 32)}$$

At $z = 0$, it is seen that this is half the number of neutrons

emitted by the source in the n'th mode which is S_n. Glasstone, et.

al., note that due to lack of symmetry the fraction is not one-half.

Combining the two equations:

$$J_n = -D \; \frac{\partial \phi_n}{\partial z} \; {}_{(z=0)} = DA_n \gamma_n J_0 \; (j_n \frac{r}{R}) \; \text{Cosh}(\gamma_n C) \quad \text{(A - 33)}$$

Thus:

$$A_n = \frac{1}{2} \, \frac{S}{R^2 \, J_1^{\,2} \, (j_n) \, D \, \gamma_n} \, \tanh(\gamma_n c) \qquad (A - 34)$$

This is the Fourier constant for the point source of thermal neutrons at the origin.

For an evaluation of A_n for a plane source, the source of thermal neutrons is taken at the origin. For a plane source the Dirac delta is not considered. Only $\phi(r,0)$ is considered which is seen to be equal to S. Following the same procedure as for the point source but with the above noted modifications:

$$S \int_0^R \left(\frac{j_n}{R}\right)^2 r \, J_0 \, (j_n \tfrac{r}{R}) \, dr =$$

$$\frac{j_n^2}{2} \, S_n \, J_1^{\,2} \, (j_n) \mathrm{Sinh} \, (\gamma_n C) \qquad (A - 35)$$

Integrating:

$$S \, j_n \, J_1 \, (j_n) = \frac{j_n^2}{2} \, S_n \, J_1^{\,2} \, (j_n) \, \mathrm{Sinh}(\gamma_n C) \qquad (A - 36)$$

Then

$$S_n = \frac{2S}{j_n \, J_1 \, (j_n) \mathrm{Sinh} \, (\gamma_n C)} \qquad (A - 37)$$

The neutron current at z = 0 then is:

$$J_n' = -D \, A_n \, \gamma_n \, J_0 \, (j_n \tfrac{r}{R}) \mathrm{Cosh} \, \gamma_n \, (c - z) \qquad (A - 38)$$

Thus

$$A_n = \frac{2S \, \tanh \, \gamma_n C}{j_n \, J_1 \, (j_n) \, D \, \gamma_n} \qquad (A - 39)$$

or

$$\frac{A_n \text{ (plane)}}{A_n \text{ (point)}} = C \, \frac{J_1 \, (\, j_n)}{j_n} \qquad\qquad (A - 40)$$

where C is a constant determined from the ratio of source strengths.

APPENDIX C

THERMAL DIFFUSION INCORPORATING A FAST SOURCE

As shown previously, the slowing-down density, q, is equal to the source term for thermal neutrons that result from slowing-down of fast neutrons. Thus the diffusion equation incorporating this type of source is:

$$\nabla^2 \phi - K^2 \phi + \frac{q}{D} = 0 \qquad (A - 41)$$

And from the Fermi age theory:

$$\nabla^2 q = \frac{\partial q}{\partial \tau} \qquad (A - 42)$$

Solution of Fermi age equation: The slowing-down density q is assumed to be separable into a function of r, τ and z, ie,

$$q = F(r) \, \Theta(\tau) \, Z(z) \qquad (A - 43)$$

The terms in Equation A - 42 now become:

$$\nabla^2 q = \Theta Z \frac{d^2 F}{dr^2} + \frac{\Theta Z}{r} \frac{dF}{dr} + \Theta F \frac{d^2 F}{dz^2} \qquad (A - 44)$$

and

$$\frac{\partial q}{\partial \tau} = F Z \frac{d\Theta}{d\tau} \qquad (A - 45)$$

Then the Fermi age equation becomes:

$$\frac{1}{F}\frac{d^2F}{dr^2} + \frac{1}{Fr}\frac{dF}{dr} + \frac{1}{Z}\frac{d^2Z}{dz^2} = \frac{1}{\Theta}\frac{d\Theta}{d\mathcal{T}} \qquad (A - 46)$$

The left side is only a spatial distribution and the right side is only an energy function. Therefore, each side is equal to a constant $(-\alpha^2)$.

Thus:

$$\frac{1}{F}\frac{d^2F}{dr^2} + \frac{1}{Fr}\frac{dF}{dr} + \frac{1}{Z}\frac{d^2Z}{dz^2} = -\alpha^2 \qquad (A - 47)$$

and

$$\frac{1}{\Theta}\frac{d\Theta}{d\mathcal{T}} = -\alpha^2 \qquad (A - 48)$$

Taking only the r function, Equation A - 47 becomes:

$$\frac{1}{F}\frac{d^2F}{dr^2} + \frac{1}{Fr}\frac{dF}{dr} = \alpha_r^2 \qquad (A - 49)$$

which has the solution:

$$F = J_o(\alpha_r r) \qquad (A - 50)$$

where F must always be finite. It also must satisfy the following boundary condition at r = R, F = 0. Thus:

$$F = J_o\left(j_n\frac{r}{R}\right) \qquad (A - 51)$$

where j_n is the n'th zero of J_o. Then:

$$\alpha^2 = \frac{1}{Z}\frac{d^2Z}{dz^2} - \left(\frac{j_n}{R}\right)^2 \qquad (A - 52)$$

Then the Fermi age equation becomes:

$$\frac{1}{Z} \frac{d^2 Z}{dz^2} - \left(\frac{j_n}{R}\right)^2 = \frac{1}{\Theta} \frac{d\Theta}{d\tau} \qquad (A - 53)$$

Multiplying by $q(z, \tau)$ which is equal to ΘZ:

$$\Theta \frac{d^2 Z}{dz^2} - \left(\frac{j_n}{R}\right)^2 q(z, \tau) = Z \frac{d\Theta}{d\tau} \qquad (A - 54)$$

Therefore:

$$\frac{\partial^2 q}{\partial z^2} - \left(\frac{j_n}{R}\right)^2 q = \frac{\partial q}{\partial \tau} \qquad (A - 55)$$

Introducing a substitution:

$$V \exp \left[- \left(\frac{j_n}{R}\right)^2 \tau \right] = q \qquad (A - 56)$$

and

$$\frac{\partial^2 q}{\partial \tau^2} = \frac{\partial^2 V}{\partial z^2} \exp \left[- \left(\frac{j_n}{R}\right)^2 \tau \right] \qquad (A - 57)$$

and

$$\frac{\partial q}{\partial \tau} = \frac{\partial V}{\partial \tau} \exp \left[\left(\frac{j_n}{R}\right)^2 \tau \right] - V \left(\frac{j_n}{R}\right)^2$$
$$\exp \left[- \left(\frac{j_n}{R}\right)^2 \tau \right] \qquad (A - 58)$$

Equation A - 55 with these substitutions becomes:

$$\frac{\partial^2 V}{\partial z^2} \exp \left[- \left(\frac{j_n}{R}\right)^2 \tau \right] - V \left(\frac{j_n}{R}\right)^2 \exp \left[- \left(\frac{j_n}{R}\right)^2 \right] =$$
$$\frac{\partial V}{\partial \tau} \exp \left[- \left(\frac{j_n}{R}\right)^2 \right] - V \left(\frac{j_n}{R}\right)^2 \exp \left[- \left(\frac{j_n}{R}\right)^2 \tau \right]$$

$$(A - 59)$$

which reduces to:

$$\frac{\partial^2 V}{\partial z^2} = \frac{\partial V}{\partial \mathcal{T}}$$ (A - 60)

Assuming that V is separable into a function of z and $\mathcal{T}$,

Equation (A-60) becomes:

$$\frac{1}{X(z)} \frac{d^2 X(z)}{dz^2} = \frac{1}{T(\mathcal{T})} \frac{dT(\mathcal{T})}{d\mathcal{T}}$$ (A - 61)

The left side is a function of z alone and the right is a

function of $\mathcal{T}$ alone. Therefore each side is equal to a constant

$-B^2$. Then:

$$\frac{1}{X} \frac{d^2 X}{dz^2} = -B^2 \quad \text{and} \quad \frac{1}{T} \frac{dT}{d\mathcal{T}} = -B^2$$ (A - 62)

which have the solutions:

$$X = A \text{ Cos } (Bz) + C \text{ Sin } (Bz)$$ (A - 63)

and

$$T = Fe^{-B^2 \mathcal{T}}$$ (A - 64)

Thus:

$$V = e^{-B^2 \mathcal{T}} \left[A' \text{ Cos } (Bz) + C' \text{ Sin } (Bz) \right]$$ (A - 65)

where A' and C' are combinations of constants. Following the

procedure in Glasstone, et al:

$$V = K' \exp \frac{-z^2}{4\mathcal{T}}$$ (A - 66)

for both a point and plane source, where K' determines whether a

plane or point source.

Therefore:

$$q(r,z,\mathcal{T}) = \sum_{n=1}^{\infty} K_{n\mathcal{T}} \exp\left(\frac{-z^2}{4\mathcal{T}}\right)\left[J_0\left(j_n \frac{r}{R}\right)\right] \tag{A - 67}$$

where $K_{n\mathcal{T}}$ incorporates the constants.

Solution of the Diffusion Equation

A solution similar to the solution for the thermal source is assumed, i.e.,

$$\phi(r,z) = \sum_{n=1}^{\infty} Z_n(z) A_n J_0\left(j_n \frac{r}{R}\right) \tag{A - 68}$$

$\phi(r,z)$ is again assumed to be separable into a function of r and a function of z viz.,

$$\phi(r,z) = F(r) Z(z) \tag{A - 69}$$

The gradient of the flux then becomes:

$$\nabla^2\phi = F\frac{d^2Z}{dz^2} + Z\frac{d^2F}{dr^2} + \frac{Z}{r}\frac{dF}{dr} \tag{A - 70}$$

or

$$\nabla^2\phi = FZ\left[\frac{1}{F}\frac{d^2F}{dr^2} + \frac{1}{Fr}\frac{dF}{dr} + \frac{1}{Z}\frac{d^2Z}{dz^2}\right] \tag{A - 71}$$

Substituting this into the diffusion equation and noting that:

$$\frac{1}{F}\frac{d^2F}{dr^2} + \frac{1}{Fr}\frac{dF}{dr} = \left(\frac{j_n}{R}\right)^2 \tag{A - 72}$$

when $F = J_0(j_n r/R)$.

The diffusion equation then becomes:

$$F \, Z \left[\frac{j^2}{R^2} \right] + F \, Z \left[\frac{1}{Z} \frac{d^2 Z}{dz^2} \right] - K^2 \, F \, Z = - \quad q_n \qquad (A - 73)$$

where $q_n = K'_n \exp \left(-z^2/4 \, T \right)$, Equation (A - 73) becomes:

$$Z''_n \, (z) + \gamma^2_n \, Z_n \, (z) = C \exp \frac{-z^2}{4T} \qquad (A - 74)$$

For a solution of Equation (A - 74), the following general equation was solved:

$$Z'' + \gamma^2 \, Z = \exp \frac{-z^2}{4T} \qquad (A - 75)$$

The general solution to Equation (A - 75) is:

$$Z = C_1 \, e^{\gamma z} + C_2 \, e^{-\gamma z} \qquad (A - 76)$$

C_1 and C_2 are arbitrary constants which may be functions of z. Thus using the method of variation of the parameters:

$$Z' = \quad C_1 \, e^{\gamma z} - \quad C_2 \, e^{-\gamma z} + C'_1 \, e^{\gamma z} + C'_2 \, e^{-\gamma z}$$

$$(A - 77)$$

Letting $C'_1 \, e^{\gamma t} + C'_2 \, e^{-\gamma z} = 0$, Z'' becomes

$$Z'' = \gamma^2 \, C_1 \, e^{\gamma z} + \gamma^2 \, C_2 \, e^{-\gamma z} + \quad C'_1 \, e^{\gamma z} -$$

$$C'_2 \, e^{-\gamma z} \qquad (A - 78)$$

Z'' and Z are substituted into Equation (A - 75). Thus:

$$C'_1 \, e^{\gamma z} - \quad C'_2 \, e^{-\gamma z} = \frac{e^{-z^2}}{4T} \qquad (A - 79)$$

Equations (A - 77) and (A - 79) are solved simultaneously. C'_1 and

$C_2^!$ become:

$$C_1^! = \frac{1}{2\gamma} \exp\left(\frac{-z^2}{4T} - \gamma z\right)$$

and

$$C_2^! = \frac{1}{2\gamma} \exp\left(\frac{-z^2}{4T} + \gamma z\right) \qquad (A-80)$$

Integrating between $z = 0$ and $z = z$ to obtain C_1 and C_2:

$$C_1 = \frac{1}{2\gamma} \int_0^z \exp\left[\frac{-z^2}{4T} - \gamma z\right] dz + G \qquad (A-81)$$

and

$$C_2 = \frac{1}{2\gamma} \int_0^z \exp\left[\frac{-z^2}{4T} + \gamma z\right] dz + G \qquad (A-82)$$

The change in the value of the lower limit to other than zero will only change the value of G.

Letting $z = u$, and completing the square on the exponential under the integral sign, Equation(A-81) becomes:

$$C_1 = \frac{1}{2\gamma} e^{\gamma^2 T} \int_0^u \exp\left[- \frac{u}{2\sqrt{T}} + \gamma\sqrt{T}\right]^2 du + G \qquad (A-83)$$

and Equation(A-82) becomes:

$$C_2 = \frac{1}{2\gamma} e^{\gamma^2 T} \int_0^u \exp\left[\frac{u}{2\sqrt{T}} + \gamma T\right]^2 du + G \qquad (A-84)$$

Letting $n^2 = (u/2\sqrt{T} + \gamma\sqrt{T})^2$, du becomes:

$$du = \frac{dn}{2\sqrt{T}} \qquad (A-85)$$

C_1 then becomes:

$$C_1 = \frac{\pi \tau}{2\gamma} \; e^{\gamma^2 \tau} \; \frac{2}{\pi} \; \int_0^n e^{-n^2} \, dn + G \qquad (A - 86)$$

Thus:

$$C_1 = A_1 \; e^{\gamma^2 \tau} \; \text{erf (n)} + G \qquad (A - 87)$$

where A_1 equals $\pi \tau / 2\gamma$. Thus C_1 becomes:

$$C_1 = A_1 \; e^{\gamma^2 \tau} \; \text{erf} \left[\frac{z}{2\sqrt{\tau}} + \gamma \sqrt{\tau} \right] + G \qquad (A - 88)$$

Likewise C_2 becomes:

$$C_2 = -A_1 \; e^{\gamma^2 \tau} \; \text{erf} \left[\frac{z}{2\sqrt{\tau}} - \gamma \sqrt{\tau} \right] + G \qquad (A - 89)$$

Substituting C_1 and C_2 into Equation(A - 79), Z becomes:

$$Z = A \; e^{\gamma^2 \tau} \quad - e^{-\gamma z} \; \text{erf} \left[\frac{z}{2\sqrt{\tau}} - \gamma \sqrt{\tau} \right] +$$

$$e^{\gamma z} \; \text{erf} \left[\frac{z}{2\sqrt{\tau}} + \gamma \sqrt{\tau} \right] + C \; \text{Sinh} \; (\gamma z)$$

$$(A - 90)$$

where C equals G/2.

To evaluate C the boundary condition for $\tau = 0$, the value for thermal neutrons, Z becomes identical to Equation(A - 24). From this, it is seen that C = 2A. Thus Z becomes:

$$Z = e^{\gamma^2 \tau} \left\{ e^{-\gamma z} \left[1 + \text{erf} \left(\frac{z}{2\sqrt{\tau}} - \gamma \sqrt{\tau} \right) \right] + e^{\gamma z} \left[1 - \text{erf} \left(\frac{z}{2\sqrt{\tau}} + \gamma \sqrt{\tau} \right) \right] \right\} \qquad (A - 91)$$

For each value of n there is a different value of A. The complete solution then must be the sum of all solutions for n =

$1, 2, 3, 4, \ldots \infty$

The flux distribution then becomes:

$$\phi(r,z) = \sum_{n=1} A_n \, e^{\gamma^2_n} \left\{ e^{-\gamma_n z} \left[1 + \mathrm{erf}\left(\frac{z}{2\sqrt{T}} - \gamma\sqrt{T} \right) \right] \right.$$

$$\left. + e^{\gamma_n z} \left[1 - \mathrm{erf}\left(\frac{z}{2\sqrt{T}} + \gamma_n T \right) \right] \right\} \quad J_0 \left(j_n \frac{r}{R} \right)$$

$$(A - 92)$$

F_{nz} is then defined as:

$$F_{nz} = e^{\gamma^2_n} \, e^{-\gamma_n z} \left[1 + \mathrm{erf}\left(\frac{z}{2\sqrt{T}} - \gamma_n\sqrt{T} \right) \right] +$$

$$e^{\gamma_n z} \left[1 - \mathrm{erf}\left(\frac{z}{2\sqrt{T}} + \gamma_n\sqrt{T} \right) \right] \qquad (A - 93)$$

$\phi(r,z)$ then becomes:

$$\phi(r,z) = \sum_{n=1}^{\infty} F_{nz} \, A_n \, J_0 \left(j_n \frac{r}{R} \right) \qquad (A - 94)$$

This is the result for an infinite cylinder. The result is modified for a finite cylinder by multiplying by the following end correction:

$$C_E = 1 - e^{-2\gamma_n(c - z)} \qquad (A - 95)$$

Using the same procedure and superpositioning the solutions, the following result is found for N number of Gaussian ranges:

$$\phi(r,z) = \sum_{i=1}^{N} \sum_{n=1}^{\infty} f_i \, F_{niz} \, A_n \, J_0 \left(j_n \frac{r}{R} \right) \qquad (A - 96)$$

where F_{niz} is dependent on n, i, and z; and f_i is the fraction of neutrons in the i'th range.

APPENDIX D

IBM 650 COMPUTER PROGRAM FOR REDUCTION OF DATA

This computer program was written to obtain the saturation activity of each indium foil from the experimental data. The saturation activities from this program have been standardized to a standard foil activity by intercalibration.

The program was written in IBM 650 Fortran language. A print out of the program is presented in Table VI.

The program calculated the solution for the following equation:

$$A_s = \frac{C_T \; \lambda \; \frac{1}{F}}{(1 - e^{-\lambda t}) \, (e^{-\lambda t} - e^{-\lambda t_2})} \qquad (A - 97)$$

where F is the intercalibration factor obtained by comparing the saturation activities of all foils irradiated at one foil location. The other symbols are those as previously defined.
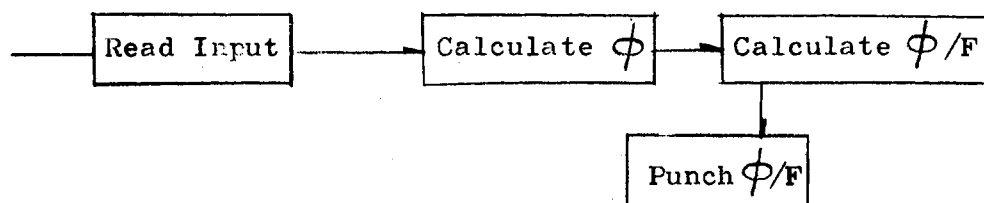
Figure 36. Flow Diagram for the IBM 650 Program for Data Reduction.

Table VI

IBM 650 FORTRAN Program for Data Reduction

```
10 Read,Z,RR,T,TA,TB,C,F

   G=0.01281
   A=EXPEF(-G*T)
   B=EXPEF(-G*TA)
   D=EXPEF(-G*TB)
20 AO=((C+(TA-TB)*63.2)*G)
21 /((1.0-A)*(B-D))

   AO=AO/F

   PUNCH,AO,Z,RR

   IF(Z) 100,1,1
1000 END
```

APPENDIX E

IBM 650 COMPUTER PROGRAM FOR FLUX DISTRIBUTION

This computer program was written in IBM 650 Fortran language. The program predicts the theoretical thermal flux from four different source models, ie, plane thermal source model, point source model, point fast source and plane fast source. The program obtained the solution for the Equation:

$$\phi(r,z) = \sum_{n=1}^{\infty} A_n F_{nz} J_0\left(j_n \frac{r}{R}\right) \qquad (A - 98)$$

For a point source:

$$A_n = \frac{1}{2} \frac{S \text{ Tanh }(\gamma_n C)}{R^2 J_1^2(j_n) D \gamma_n} \qquad (A - 99)$$

For a plane source:

$$A_n = \frac{2S \text{ Tanh }(\gamma_n C)}{j_n J_1(j_n) D \gamma_n} \qquad (A - 100)$$

For a thermal source:

$$F_{nz} = \text{Sinh } \gamma_n (c - z) \qquad (A - 101)$$

And for a fast source:

-114-

$$F_{nz} = e^{\gamma^2 T} \left\{ e^{-\gamma} \left[1 + \mathrm{erf} \left(\frac{z}{2 T} - \gamma_n T \right) \right] \right.$$

$$\left. + e^{\gamma z} \left[1 - \mathrm{erf} \left(\frac{z}{2 T} + \gamma_n T \right) \right] \right\} \qquad (A - 102)$$

The Fortran program is presented in Table VII and the flow chart is presented in Figure 37.

The value of the Bessel's function is obtained from a subroutine incorporated in the program. The program makes use of a convergent series approximation for the Bessel's function. The Bessel's function was obtained from the following equation taken from DP - 124 (3):

$$F = A \ (x) \ G \ (x) \qquad (A - 103)$$

where F is the function, G (x) is the sum of an infinite series and $A \ (x) = X^n / 2^n \ n!$ where n is the order of the Bessel's function.

For a Bessel's function of order n, ie, $J_n(x)$:

$$Gx = \sum_{i=0}^{\infty} G_i \qquad (A - 104)$$

where $G_o = 1$ and $G_i = -(x/2)^2 \ G_{i-1} \ / \ r_i \ (r_i + n)$
Also r_i and $\nabla r = 1$ and $r_i = r_{i-1} + \nabla r$.

The G (x) series was considered complete when G_i was less than 10^{-4}. G (x) was a very rapidly convergent series for values of x less than 5.29.

For values of x greater than 5.29, the following asymptotic solution (8) for the Bessel's function was used.

$$J_0(x) = \sqrt{\frac{2}{\pi x}} \quad P_0(x) \, \cos(x - \frac{1}{4}) \; - $$

$$Q_0(x) \, \sin(x - \frac{1}{4}) \hspace{3cm} (A - 105)$$

where for large values of x, $P_0 = 1$ and $Q_0 = 1/8x$. P_0 and Q_0 are series functions of x.

The value of the error function was obtained by using the first two terms of Taylor's series,

$$F(x \pm h) = F(x) \pm hF'(x) \hspace{2cm} (A - 106)$$

Taylor's series was used as an interpolation formula between given values of the error function. Several values of the error function at different values of x were provided in the program.

The program uses an interative process with h set equal to 0.01. A new F(x) was calculated from the Taylor's series. This F(x) then was substituted into the series to obtain still another value of F(x). When the difference in the argument of the series and the required value of the argument was less than 0.01, h was changed to the difference to give an F(x) at the required argument.

The hyperbolic sine was calculated from its definition:

$$\text{Sinh } \gamma_n(c - z) = e^{\gamma_n c} \left\{ e^{-\gamma_n z} \left[1 - e^{-2\gamma_n(c - z)} \right] \right\} \hspace{1cm} (A - 107)$$

This FORTRAN program computes the theoretical flux up to a z of sixty cm. at increments of ten cm.. At z equal sixty cm.,an increment of 1.96 was added to find the flux at 61.96 cm. the

interface between the cylinder and parallelpiped. In the radial direction the flux was calculated up to the extrapolated distance of R in increments of r/R or 0.1 starting at r/R equal zero.
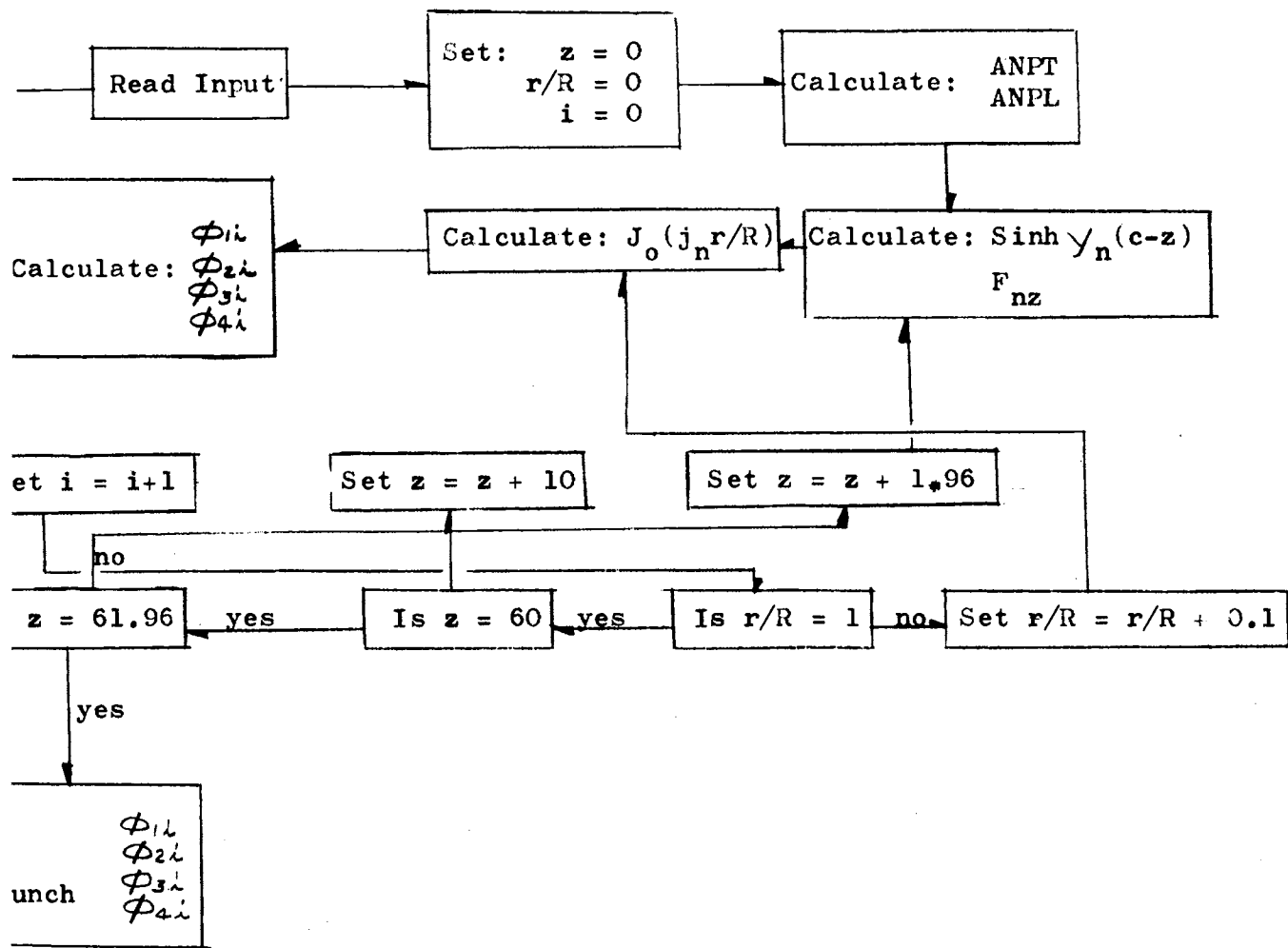
Figure 37. Flow Diagram for the IBM 650 Program for Flux distribution.

TABLE VI

650 FORTRAN STATEMENTS FOR FLUX CALCULATION

```
100  0  DIMENSION FN(88),FP(88),
100  1  CFP(88),ERX(2),CFN(88)
        J=0
        READ,C,T
  1  0  READ,Z,R
        I=1
  2  0  GMS=.000387+((Z/45.2)**2)
  3  0  GAM= EXPF((LOGF(GMS))/2.0)
  4  0  ANPL=1.0/(GAM*R*Z)
  5  0  ANPT= ANPL*(Z/R)
  6  0  ZE= 0.0
  7  0  IF((2.0*GAM*(C-ZE))-40.0)   92,
  7  1  93,93
 92  0  ECOR= EXPEF(-2.0*GAM*(C-ZE))
        GO TO 94
 93  0  ECOR= 0.0
 94  0  SHN=(EXPEF(-GAM*ZE))*(
 94  1  1.0-ECOR)
  8  0  RR= 0.0
 29  0  EP=(ZE/(2.0*T))+(GAM*
 29  1  20.54)
 30  0  EM=(ZE/(2.0*T))-(GAM*
 30  1  20.54)
        L= 1
 31  0  IF (EP-1.0) 35,32,39
 32  0  ERO=0.8427
 33  0  E=1.0
 34  0  GO TO 50
 24  0  ERO= 0.0
 25  0  E= 0.0
 26  0  GO TO 50
 35  0  IF(EP) 36,24,24
 36  0  EP= -EP
 37  0  J= 1
 38  0  GO TO 31
 39  0  IF (EP-1.5) 32,40,43
 40  0  ERO= 0.9611
 41  0  E= 1.5
 42  0  GO TO 50
 43  0  IF (EP-2.0) 40,44,47
 44  0  ERO=0.99532
 45  0  E= 2.0
 46  0  GO TO 50
 47  0  IF (EP-2.5) 44,48,88
 48  0  ERO=0.99959
```

TABLE VI (Continued)

```
 49 0 E= 2.5
 50 0 H=0.01
 51 0 DRO=(2.0/1.772)*(EXPEF(-E*E))
 53 0 IF ((E)-EP) 56,58,54
 54 0 H= EP-E
 55 0 GO TO 56
 56 0 E= E+H
 52 0 ERA= ERO+(H*DRO)
      ERO= ERA
      ERA=1.0-ERA
 57 0 GO TO 51
 88 0 IF (EP-4.0) 48,89,104
 89 0 ERO= 1.5417258E-8
      E= 4.0
102 0 DRO= (2.0/1.772)*(EXPEF(-E*E))
      H= 0.1
      IF((E)-EP) 101,58,103
103 0 H= EP-E
101 0 E= E+H
      ERA= ERO-(H*DRO)
      ERO= ERA
      GO TO 102
104 0 IF(EP-6.0) 89,105,106
105 0 ERO=2.1519737E-17
      E=6.0
      GO TO 102
106 0 IF (EP-8.0) 105,107,107
107 0 ERA= 0.0
 58 0 IF (J-1) 60,59,60
 59 0 ERA=-ERA+2.0
      J=0
      EP= -EP
 60 0 ERX(L)=ERA
 61 0 IF (EP-EM) 6s,65,62
 62 0 EP= EM
 63 0 L= 2
 64 0 GO TO 31
 65 0 GZ= GAM*ZE
      ERX(2)= - .0+ERX(2)
 66 0 FNZ=
 66 1 (ERX(1)*EXPEF(GZ)-(ERX(2)*
 66 2 EXPEF(-GZ)))/SHN
  9 0 IF (Z-3.0) 90,99,99
 90 0 CFN(I)= 0.0
      CFP(I)= 0.0
      FN(I)= 0.0
      FP(I)= 0.0
 99 0 BAR=Z*RR
 10 0 IF(BAR-7.29) 11,22,22
```

TABLE VI (Continued)

```
11 0 AJX= 1.0
12 0 ON= 1.0
13 0 BSE= 1.0
14 0 TER= -((BAR-7.29)
14 1 (ON*ON)
15 0 IF(ABSF(TER)-(1.E-4)) 20,20,16
16 0 ON= ON+1.0
17 0 BSE= BSE+ TER
18 0 AJX= TER
19 0 GO TO 14
20 0 BSE= BSE+ TER
21 0 GO TO 27
22 0 BSE= (0.125*(SINF(BAR-0.7854))
22 1 /BAR)+(COSF(BAR-0.7854))
23 0 D=EXPEF((LOGEF(2.0/(3.1416*
23 1 BAR)))/2.0)
       BSE= BSE*D
27 0 FN(I)= (ANPL*BSE*SHN
27 1 )+FN(I)
28 0 FP(I)= (ANPT*BSE*SHN
28 1 )+FP(I)
67 0 CFN(I)= FNZ*(ANPL*BSE*SHN
67 1 )*((1.0-ECOR)**2)+CFN(I)
68 0 CFP(I)=FNZ*(ANPT*BSE*SHN
68 1 )*((1.0-ECOR)**2)+CFP(I)
69 0 I= I+1
70 0 IF(RR-1.0) 71,73,73
71 0 RR= RR+0.1
72 0 GO TO 9
73 0 IF(ZE-60.0) 74,76,78
74 0 ZE=ZE+10.0
75 0 GO TO 7
76 0 ZE=ZE+0.96
77 0 GO TO 7
78 0 IF(Z-62.) 1,79,79
79 0 PUNCH, FN
80 0 PUNCH, FP
81 0 PUNCH, CFN
82 0 PUNCH,CFP
86 0 CONTINUE
87 0 END
```

APPENDIX F

IBM 650 FORTRAN PROGRAM FOR THE FLUX DISTRIBUTION

FROM A MULTI-ENERGETIC FAST SOURCE OF NEUTRONS

This computer program was written in IBM 650 Fortran Language. The program uses the solutions of the flux from Appendix E for different values of the Gaussian ranges. The program combines the values of the flux according to the following equation:

$$A_1 \phi_1 + A_2 \phi_2 + A_3 \phi_3 = \phi \qquad (A - 108)$$

where the ϕ's are fluxes, the A's are the weighting factors and the subscripts denote the Gaussian range.

It is seen that the above equation weights the flux from each of the Gaussian ranges and sums the weighted results to obtain the flux from the multi-energetic fast source. This is in effect super-positioning the solutions. The Fortran Statements are presented in Table VIII.

TABLE VIII

IBM 650 Fortran Program for Flux Weighting

```
100 0 DIMENSION D(364), (364)
100 1 , B(364),C(364)
      READ,A
      READ,B
      READ,C
      I=1
      READ,E,F,G
  1 0 D(I) = A(I)*E + B(I)*F + C(I)*G
      IF(I-364) 3,2,2
  3 0 I=I+1
      GO TO 1
  2 0 PUNCH D
      END
```


Where:

$A = \phi_1$

$B = \phi_2$

$C = \phi_3$

$D = \phi$

VITA

Lemuel Carter Allison

Candidate for the Degree of

Master of Science

Thesis: DIFFUSION OF NEUTRONS FROM POINT AND PLANE SOURCES

Major Field: Nuclear Engineering

Biographical:

Personal data: Born at Gould, Oklahoma, March 11, 1938,
the son of Joe C. and Fern M. Allison; married,
May 28, 1961, to Barbara Ann Jones.

Education: Attended grade school in Gould, Oklahoma;
graduated from Gould High School in 1956; received
the Bachelor of Science degree from Oklahoma State
University, with a major in chemical engineering,
in May 1960; completed the requirements for the
Master of Science degree in May, 1965

Experience: Employed as a Research Engineer at Atomics
International, Canoga Park, California, during
summers of 1960 and 1961; presently employed by
Atomics International, Canoga Park, California.

Honorary organizations: Sigma Tau, 1958.

Honors and awards: Graduate teaching assistant, Chemistry
department, Oklahoma State University, 1960 - 1961.